Applied Catalysis B: Environmental 342 (2024) 123401

Contents lists available at ScienceDirect

Applied Catalysis B: Environmental

journal homepage: www.elsevier.com/locate/apcatb

Recent advances in the applications of encapsulated transition-metal nanoparticles in advanced oxidation processes for degradation of organic pollutants: A critical review

Ting Yu [a,1], Hong Chen [c,1], Tong Hu [a], Jing Feng [b], Wenle Xing [d], Lin Tang [a], Wangwang Tang [a,*]

[a] College of Environmental Science and Engineering and Key Laboratory of Environmental Biology and Pollution Control (Ministry of Education), Hunan University, Changsha 410082, China
[b] PowerChina Zhongnan Engineering Corporation Limited, Changsha 410014, China
[c] Key Laboratory of Dongting Lake Aquatic Eco-Environmental Control and Restoration of Hunan Province, School of Hydraulic and Environmental Engineering, Changsha University of Science & Technology, Changsha 410114, China
[d] School of Resources and Environment, Hunan University of Technology and Business, Changsha 410205, China

ARTICLE INFO

Keywords:
Advanced oxidation processes
Transition-metal nanoparticles
Encapsulated structure
Organic pollutants

ABSTRACT

Advanced oxidation processes are widely recognized as effective techniques for the removal of organic pollutants from water. In recent years, encapsulated transition-metal nanoparticle catalysts have exhibited excellent performance in inducing AOPs for elimination of organic contaminants due to their unique physicochemical properties. Taking advantage of the synergy between transition-metal nanoparticles and encapsulation materials, the catalytic activity, stability and selectivity of the catalysts can be adjusted and improved. Particularly, the carbon shell might benefit pollutant enrichment, accelerate charge transfer, enable confinement effect, and protect the transition-metal core from aggregation or deterioration. This review presents recent advances in the applications of encapsulated transition-metal nanoparticle catalysts for AOPs to degrade organic pollutants. Firstly, the structure and composition types of encapsulated transition-metal nanoparticle catalysts were introduced and then the synthetic methods of the catalysts were described. Subsequently, the applications of encapsulated transition-metal nanoparticles as heterogeneous catalysts to degrade organic pollutants in AOPs, including Fenton reactions, photocatalysis, persulfate activation, etc., were discussed with the underlying reaction mechanisms revealed. Finally, the article concludes by highlighting the major challenges and opportunities associated with encapsulated transition-metal nanoparticle catalysts in these AOPs, providing valuable insights for future research and development.

1. Introduction

With the rapid growth of industrialization and human population, the problems of environmental security and sustainable development caused by water pollution have attracted widespread attention from countries around the world [1–4]. Various refractory organic pollutants in the water environment could directly or indirectly affect ecosystem and human health because of their high resistance to degradation and high toxicity [5–7]. For example, herbicides like atrazine could inhibit photosynthesis in plants, and interfere with endocrine hormone metabolism and cause cancer in human beings [8–11]. Pharmaceuticals like chloramphenicol might cause severe harmful effects towards humans

Abbreviations: AOPs, Advanced oxidation processes; CB, Conduction band; CDs, Carbon dots; CNTs, Carbon nanotubes; CVD, Chemical vapor deposition; e^--h^+, Electron-hole; g-C_3N_4, Graphitized carbon nitride; GDE, Gas diffusion electrodes; HEF, Heterogeneous electro-Fenton; HoMS, Hollow multi-shell; IME-Fenton, Internal micro-electronics with Fenton-like process; MOFs, Metal-organic frameworks; ORR, Oxygen reduction reaction; PAA, Peracetic acid; PF, Photo-Fenton; PI, Periodate; PMS, Peroxymonosulfate; PS, Persulfate; ROS, Reactive oxygen species; SMSI, Strong metal-support interactions; SMSMPR, Submerged magnetic separation membrane photocatalytic reactor; S_v, Sulfur vacancy; TMCs, Transition-metal carbides; TMNs, Transition-metal nitrides; TMOs, Transition-metal oxides; TMPs, Transition-metal phosphides; TMSs, Transition-metal sulfides; VB, Valence band; VDW, Van Der Waals; V_o, Oxygen vacancy; V_n, Nitrogen vacancy.

* Corresponding author.
E-mail address: wtang@hnu.edu.cn (W. Tang).
[1] These authors contribute equally to this article.

https://doi.org/10.1016/j.apcatb.2023.123401
Received 15 July 2023; Received in revised form 27 September 2023; Accepted 16 October 2023
Available online 18 October 2023

such as aplastic anemia and genotoxic carcinogenicity [12–15]. Water or wastewater treatment by degrading or removing these pollutants is undoubtedly of great significance. As for biological treatment method, it is not effective because the refractory organic pollutants are highly resistant to biodegradation and could inhibit the growth of active microorganisms. Other common treatment methods such as membrane separation process and adsorption process do not destruct the pollutants, and dealing with the membrane concentrate or desorption solution is still a great challenge. This lack of efficiency of the traditional treatment methods prompts the research interest for other novel techniques.

Advanced oxidation processes (AOPs), including Fenton reactions, photocatalysis, persulfate activation etc., have drawn increasing interest and have been regarded as an efficient and promising method to degrade refractory organic contaminants in water or wastewater [6,16–19]. AOPs are defined as the oxidation processes primarily involving the generation of highly reactive radical species such as hydroxyl radicals and sulfate radicals [20–23]. Nowadays, AOPs have been extended to certain non-radical pathways [24–26]. Generally, AOPs can be divided into homogeneous AOPs and heterogeneous AOPs. Homogeneous AOPs have several drawbacks such as narrow working pH range and potential production of a large amount of metal-containing sludge, which limits their practical applications [27–30]. Heterogeneous AOPs can overcome the above-mentioned shortcomings of homogeneous AOPs [30–32]. Heterogeneous AOPs usually take advantage of solid catalysts combined with H_2O_2, light, electricity, or persulfate to remove organic contaminants [17,33,34]. Finding heterogeneous AOPs catalysts possessing outstanding catalytic activity and stability is critical to guarantee the effective elimination of refractory organic pollutants.

Over the past decades, transition-metal nanomaterials have been increasingly used as heterogeneous catalysts for AOPs because of their remarkable physico-chemical characteristics like abundant reaction sites and impressive catalytic activity [35]. However, there are a series of issues when transition-metal nanomaterials are applied in AOPs, such as unsatisfactory mass transport, easy aggregation, and poor recyclability [36,37]. In order to deal with these problems, Bao et al. proposed the concept of "chainmail" catalyst, which is colloquially an armer-like shield over the transition metal [38,39]. This means that transition-metal nanoparticles are encapsulated in nano-shells,

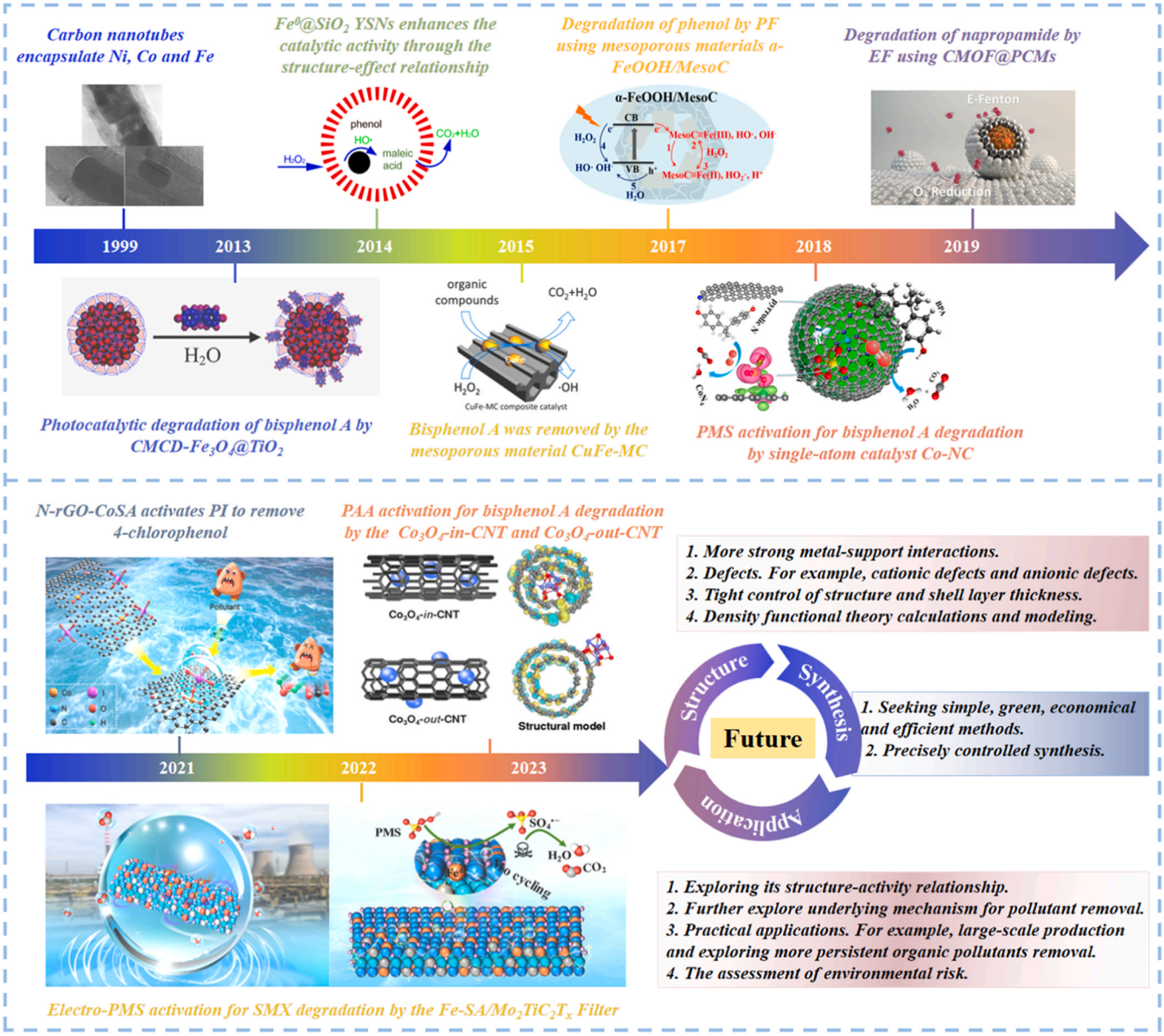

Fig. 1. A timeline for the origin and development of encapsulated transition-metal nanoparticle catalysts applied in AOPs. The adopted sub-graphs came from references of [52–61].

nano-pores or nano-layers. Such encapsulation structure exhibits unique features and advantages. For example, it can improve the catalytic activity of conventional transition-metal nanoparticles by adjusting the catalytic properties (e.g., enabling electron transfer from encapsulated metals to the chain-mail layer and stimulating unique catalytic activity on the outer surface) and inducing confined catalytic behaviors [40]. Additionally, such encapsulation structure is capable of preventing the contact between the reaction medium and the active metal cores, protecting the active transition-metal core from aggregation or deterioration, thereby improving the catalytic stability [41]. Another important advantage of encapsulated transition-metal nanoparticle catalysts is the potentially enhanced selectivity towards target pollutant [42]. The encapsulated layer materials can act as sieves for molecules, and the functional groups on the surface of the encapsulated layer material can selectively complex with certain specific pollutants, thereby facilitating the selective pollutant removal.

The past decade has witnessed a rapid development of encapsulated transition-metal nanoparticle catalysts in the applications of AOPs (see Fig. 1), and the development of this kind of catalyst has alleviated the environmental problems caused by refractory organic pollutants to a large extent [43,44]. Some works have reviewed certain aspects of encapsulated-metal nanoparticle catalysts previously, such as biosensors [45], supercapacitors [46,47], batteries [46,47], CO_2 conversion [40], fuel cells [45], water splitting [48], organic synthesis [49], and steam reforming [50]. The application of encapsulated-metal nanoparticle catalysts in environmental catalysis has been also reviewed by Zhao et al. [51], but this review only focused on NH_3-selective catalytic reduction, elimination of volatile organic compounds and sulfate-based AOPs, and the review content is rough. To the best of our knowledge, there is no comprehensive review about encapsulated transition-metal nanoparticle catalysts for various AOPs applications in treatment of aqueous organic pollutants. Therefore, this review is intended to cover this topic and fill the knowledge gap. Firstly, the structural and composition types of encapsulated transition-metal nanoparticle catalysts were introduced. Secondly, the various synthetic methods of encapsulated transition-metal nanoparticle catalysts of different architectures were described, including the hydrothermal/solvothermal method, thermal synthesis, chemical vapor deposition, template-based method, self-assembly strategy, and the combined methods. Thirdly, the versatile applications of encapsulated transition-metal nanoparticle catalysts in AOPs for environmental remediation were summarized and discussed with the underlying reaction mechanisms revealed. Lastly, the remaining challenges and our understandings of the future research trend on this topic were presented.

2. Structure and composition of encapsulated transition-metal nanoparticle catalysts

2.1. Structure types

The encapsulated transition-metal nanoparticle catalysts mainly have four types of structures: core-shell structure, yolk-shell structure, mesoporous structure and layered structure (Fig. 2). The catalyst formed by coating a functional shell on the surface of transition-metal nanoparticles is called core-shell catalyst. In practical applications, the confined environment provided by core-shell catalysts is beneficial to the dispersion of active metals and the prevention of metal aggregation [50,62–64], laying a solid foundation for its infinite possibilities in many application fields. Generally, the core-shell structure implies that the core is in close contact with the shell without movable interior space. In order to obtain encapsulated catalysts with more versatile functions, scholars developed a new structure with internal space on the basis of core-shell structure by partially shifting the shell or core, which was called yolk-shell structure and can be described as the structure of active metal core@void@shell. Due to the cavity of yolk-shell structure between the core and shell, the cavity greatly exposes the outer surface of the active metal core, leading to a large number of accessible active sites, which in turn may make the yolk-shell structure catalysts more active than the equivalent core-shell catalysts. Compared with core-shell structures, yolk-shell structures have lower density, larger internal space, higher specific surface area, and higher loading capacity [62,65,66]. In addition, the encapsulated catalyst with mesoporous structure limits the active metal core to mesoporous materials. This type of catalyst has the characteristics of relatively high specific surface area, variable pore shape, and diverse skeleton composition [67,68]. Another layered structure encapsulated catalyst embeds active metal core in the middle layer of the layered material. This structural encapsulated catalyst is often used in the field of photocatalysis because the active metal core and the layered material often form heterojunction, and the electron migration rate between the layered materials is fast [69,70].

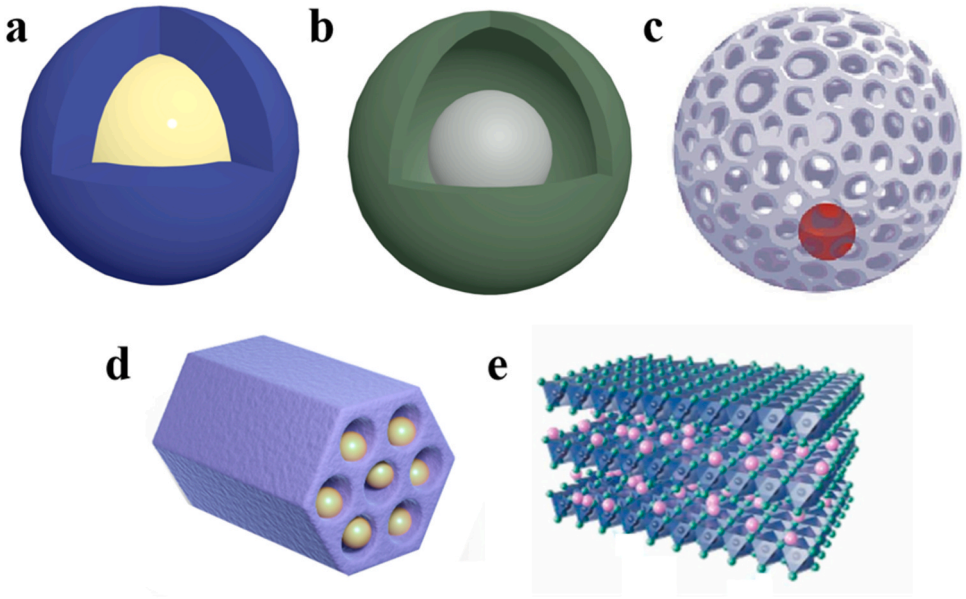

Fig. 2. (a) Core-shell structure, (b, c) yolk-shell structure, (d) mesoporous structure, and (e) layered structure.

2.2. Composition types

The catalyst is mainly composed of transition-metal nanoparticles and encapsulated materials. Among them, not only the composition of transition-metal nanoparticles can be diverse, but also the encapsulated materials have many different choices. The flexible combination of different transition-metal nanoparticles and encapsulated materials greatly enriches the research on encapsulated transition-metal catalysts.

2.2.1. Types of transition metals

In the initial studies of encapsulated transition-metal nanoparticle catalysts, the active cores were mostly metallic transition-metal nanoparticles, such as Fe@C-BN [71], Co@N-C, Ni@N-C [72], etc. Subsequently, researchers found that synergistic interactions between bimetallic or polymetallic nanoparticles enable the enhancement of the catalytic activity and stability, because transition-metal alloying provides an efficient way to regulate the chemical, electronic and even magnetic characteristics between different metallic components, such as FeMn@CNTs [73], FeMn@NC [74], FeCo@NC [75], etc. Single-atom metal catalyst with atomically dispersed active sites has also become one promising catalytic material due to the metal atom utilization, high catalytic activity and stability [76,77]. For example, the turnover frequency of Co single-atom catalysts anchored on tetrapyridine macrocycles was reported to be 2-4 orders of magnitude higher than that of the benchmark homogeneous catalysts (Co^{2+}) and Co_3O_4 nanoparticles [76]. On these basis, the embedding of heteroatoms can optimize the distance between metal lattice and metal atoms, and further improve the stability and catalytic performance of the material [78]. Therefore, in recent years, new transition-metal based catalysts have been developed and applied to various catalytic processes, including transition-metal oxides (TMOs), transition-metal carbides (TMCs), transition-metal nitrides (TMNs), transition-metal phosphides (TMPs), and transition-metal sulfides (TMSs). TMOs have been used extensively in AOPs for the removal of contaminants from wastewater due to their advantages of low cost and good durability. Iron oxide and cobalt oxide are two of the most common transition-metal based active cores, such as FeO [79], Fe_3O_4 [80–83], Co_3O_4 [84]. TMCs are a interstitial compound composed of transition metal and carbon [85]. It is considered that the incorporation of carbon atom would lead to the expansion of metal lattice, which also leads to the contraction of metal d-band, resulting in the special Pt-like catalytic properties of transition-metal carbide materials. Compared with TMOs, TMCs have better thermal and chemical stability as well as better conductivity. TMNs are also a kind of interstitial compound and have similar physical and chemical properties to TMCs [86]. TMSs are widely distributed in nature in the form of minerals with various structural types, and have been widely studied for various applications, such as CO_2 reduction reaction, energy storage [87,88]. In view of the strong covalent metal-metallic bond and metalloid-metalloid bond, TMSs have properties of high energy density and high stability. TMPs have a spherical triangular prismatic unit structure, which results in a higher surface active density and better catalytic activity than TMSs by exposing more complex-unsaturated surface atomic numbers [89–92].

2.2.2. Types of encapsulated layer

Carbonaceous materials, including graphene, carbon nanotubes, graphitized carbon nitride, MXenes, metal-organic frameworks (MOFs) derived carbon and amorphous carbon, are dominant types of encapsulated layer due to their unique properties. Graphene is a robust and flexible two-dimensional sheet material with good chemical stability and electrical conductivity, in which carbon atoms are connected with the surrounding carbon atoms in the way of sp^2 hybridization, forming a honeycomb structure with a six-membered ring as the basic unit [93–95]. Carbon nanotubes (CNTs) can be viewed as one-dimensional carbon nanomaterials formed by the curling of graphene. Graphitized carbon nitride (g-C_3N_4) has a two-dimensional sheet-like structure similar to graphene, and has a relatively narrow energy bandgap as well as good solar absorption capability. In addition, the intrinsic moieties and vacancies along with the sp^2-hybridized carbon network benefit the production and transportation of delocalized electrons. Due to these properties, g-C_3N_4 has been widely used to degrade organic pollutants in AOPs, especially in photocatalysis [18,48,94]. MXenes, a group of two-dimensional transition metal carbides and nitrides, own a layered graphene-like structure, good chemical stability, excellent electrical conductivity and abundant surface terminations [96–98]. Transition-metal nanoparticles encapsulated by MOFs-derived carbon shell can be easily obtained via direct pyrolysis of the transition-metal nanoparticles and/or metal salts encapsulated in MOFs under an inert atmosphere [99–101]. Transition-metal nanoparticles encapsulated by amorphous carbon can be facily fabricated by coating a polymer on transition-metal nanoparticles and then transforming the polymer to an amorphous carbon shell [102]. Apart from carbonaceous materials, other materials can also act as encapsulated layer for transition-metal nanoparticles. Silica (SiO_2) can maintain the integrity of its structure and morphology under thermal conditions, thus ensuring that the size and catalytic performance of encapsulated transition-metal nanoparticles do not change [102]. TiO_2 hollow spheres could serve as an excellent photocatalyst for photoelectron-hole generation and its inner shell surface could provide a good support for transition-metal nanoparticle deposition [102,103]. Transition-metal nanoparticles can also be encapsulated in MOFs [104–108]. The advantages of using MOF as coating layer are multifaceted, such as large surface area, adjustable cavity size and chemical composition, and well-positioned metal sites.

3. Synthetic methods of encapsulated transition-metal nanoparticle catalysts

There are many synthetic routes for encapsulated transition-metal nanoparticle catalysts. In general, catalysts of different structural types require different synthetic routes. In this section, we will introduce the various synthetic strategies for encapsulated transition-metal nanoparticle catalysts, including the hydrothermal/solvothermal method, thermal synthesis, chemical vapor deposition (CVD), template-based method, self-assembly strategy, and the combined methods. The advantages and disadvantages of these synthetic strategies are summarized in Table 1.

Table 1
Advantages and disadvantages of different methods for synthesizing encapsulated transition-metal nanoparticle catalysts.

Method	Advantages	Disadvantages	Ref.
Solvothermal/ hydrothermal synthesis	High crystallinity, easily controllable synthesis condition	Consuming many solvents and hazardous chemicals; difficult to observe crystal growth	[94,109]
Thermal synthesis	Low requirements on instruments, suitable for mass production	Energy-intensive; high cost	[57,73, 110]
Chemical vapor deposition	Uniformity and thickness of the shell are controlled precisely	High reaction temperature and many toxic by-products	[47,94, 111]
Template-based method	Controllable morphology and structure, simple operation	The more complex the target product, the more complex the experimental process	[112–114]
Self-assembly strategy	Simple operation and flexible design, and the synthesis of encapsulated catalyst can be controlled precisely	Long preparation time; easy to lead to sedimentation fluid cross infection	[48,113]

3.1. Hydrothermal/solvothermal method

Hydrothermal/solvothermal synthesis is the chemical synthesis in water/solvent medium under the specified temperature and pressure, and is often used to prepare catalysts with core-shell structure. The catalyst prepared by this method has high degree of crystallinity, small strength and uniform distribution [94,115]. Compared with other synthetic methods, the catalyst prepared by hydrothermal/solvothermal synthesis in its closed environment has higher purity, which can effectively avoid crystal defects in the preparation of nanomaterials and has a better crystal growth environment [94,109].

The main control parameters of hydrothermal/solvothermal synthesis are reaction temperature, precursor volume, reaction time and pH of solution. The reaction temperature and time affect the crystallinity and morphology of the material, and then affect the activity of the catalyst. For instance, when the reaction time in the autoclave was shortened from 6 h to 3 h while the concentration of the precursor kept unchanged, the morphology of Pd@Fe_3O_4@MOF changed from yolk-shell structure to core-shell structure (Fig. 3a) [116]. In addition, the amount of precursor will affect the activity of reaction nucleation, and if the amount of precursor is excessive, the active core is easy to gather, leading to the reduction of catalytic activity. For example, Xia et al. prepared dendritic Fe^0@Fe_3O_4 with polar carbon groups [117]. The structure, composition and catalytic activity of the catalyst were affected by the use of volume ratios of ethanol and ultrapure water. As shown in Fig. 3b-c, as the ethanol content increased, the catalyst changed from Fe_3O_4@Fe_2O_3 to Fe^0@Fe_3O_4, and the particle-like feature became dendritic structure, which had outstanding catalytic ability towards phenol degradation.

Due to the potential use of stabilizers, surfactants and organic solvents, hydrothermal/solvothermal methods cannot yield high-quality encapsulated structures [45]. In order to further improve the interaction between transition-metal active core and shell, many scholars have combined hydrothermal/solvothermal processes with calcination steps to prepare high-quality encapsulated catalysts [118,119]. For example, Mn_3O_4/C composite had regular nanocube morphology and many mesoporous structure, whose miscrostucture and morphology could be adjusted by changing the synthesis temperature and the ratio of precursor [120]. As the synthesis temperature rose to 400℃ and 600℃, it could be observed from Fig. 3e that the porosity was reduced. As the precursor glucose ratio increased, the dimension of the nanocube got a bit smaller, and the edges and corners got rounder along with a smaller specific surface area (Fig. 3f), thereby unfavorable to the catalytic activity. In addition, Zhou et al. [121] obtained zero-valent Co-Fe dodecahedral catalysts wrapped in nitrogen-containing carbon nanoparticles by hydrothermal and calcination (Fig. 3d). The degree of graphitization of carbon shell can be adjusted by changing the proportion of Co^{2+} in ZIF-67 and Co in $CoFe_2O_4$. When the molar ratio was 30, the catalyst had abundant defects, which was conducive to improving the electron acceptor/donor capacity in the catalytic process.

3.2. Thermal synthesis

Thermal synthesis is an efficient method to fabricate core-shell catalysts, whose mechanism is to convert precursors into nanomaterials with specific encapsulated structures based on the use of thermal energy. The process involved in thermal synthesis is simple and easy to achieve large-scale preparation. In recent years, encapsulated catalysts synthesized via thermal synthesis based on transition-metal nanoparticles [71,122,123], TMNs [124], TMSs [125–127], TMCs [26,128–130], and TMOs [131–133] have been widely used in the degradation of pollutants in the AOPs field.

Compared with other synthesis methods, the influencing factors of thermal synthesis are relatively simple, mainly including type and

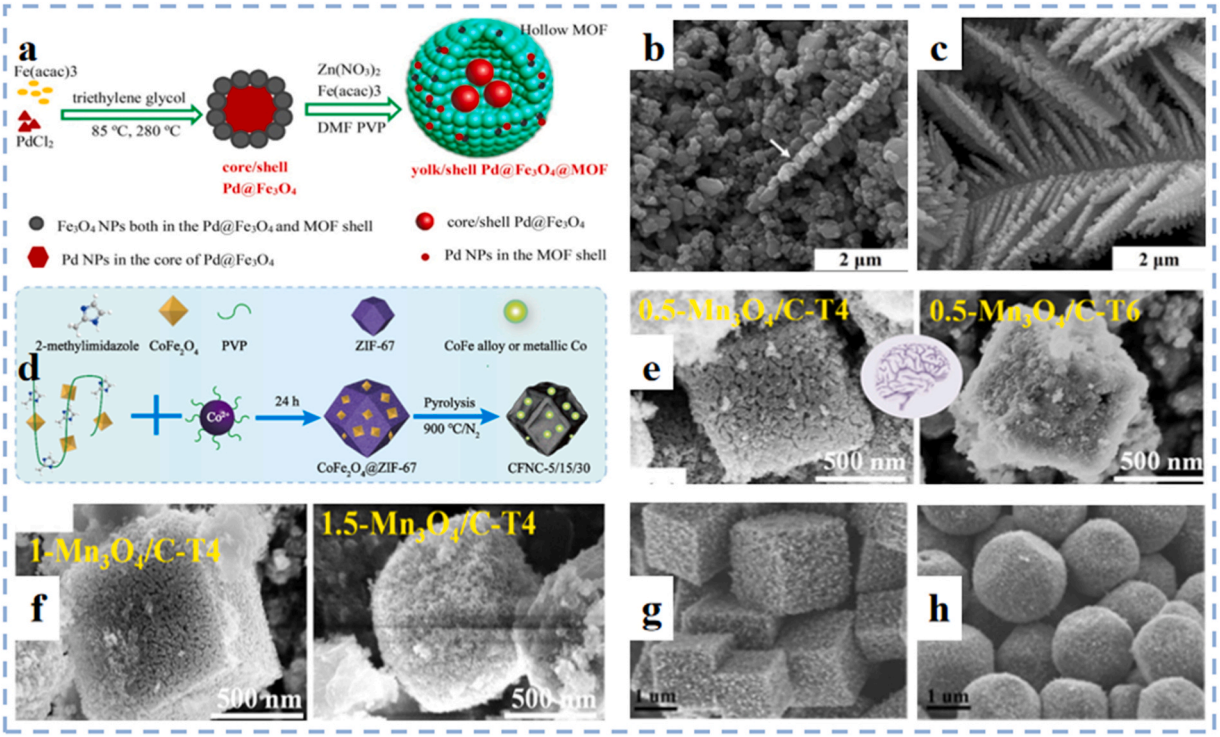

Fig. 3. (a) Illustration of the yolk/shell Pd@Fe_3O_4@MOFs nanocomposites synthesis procedure. Reproduced with permission from Ref. [138]. Copyright 2018 Elsevier. SEM images of E50 (b) and E100 (c). E50 and E100 represent that the volume ratios of ethanol and ultrapure water during material preparation were 100:0 and 50:50, respectively. Reproduced with permission from Ref. [117], Copyright 2018 Elsevier. (d) Preparation process of zero-valent Co-Fe encapsulated in nitrogen-containing carbon nanoparticles. Reproduced with permission from Ref. [121]. Copyright 2020 Elsevier. SEM images of catalysts prepared at different reaction temperatures (e) and precursor ratios (f). Reproduced with permission from Ref. [120]. Copyright 2020 American Chemical Society. FESEM images of $Fe_1Mn_5Co_4$-N@C (g) and $Fe_5Mn_1Co_4$-N@C (h). Reproduced with permission from Ref. [134]. Copyright 2016 American Chemical Society.

proportion of precursors, reaction temperature. The structure of encapsulated catalyst is affected by different precursor types and different precursor proportions, which might further influence the catalytic activity [73,110]. For instance, through thermal decomposition of MOF precursor Mn_yFe_{1-y}-Co Prussian blue analogues under nitrogen atmosphere, graphene-encapsulated transition-metal nitrides ($Fe_xMn_{6-x}Co_4$-N@C) could be synthesized with controllable shape by varying the content of Mn (Fig. 3g-h) [134]. And the catalytic efficiency of the $Fe_xMn_{6-x}Co_4$-N@C via peroxymonosulfate (PMS) activation for degrading bisphenol A improved with the increase in Mn content. Another example is CoS_x@nitrogen-sulfur-oxygen co-doped carbon catalyst (CoS_x@N-S-O-C) as PMS activator for sulfamethoxazole degradation [125]. The use of different sulfur precursors as well as different sulfur/cobalt molar ratios had a great impact on the structual property of the catalyst. Only when the sulfur precursor was benzyl disulfide and the sulfur/cobalt molar ratio was 5:1, CoS_x@N-S-O-C catalyst had a clear layered structure. In addition to type and proportion of precursors, the influence factor reaction temperature will also affect the surface morphology of encapsulated catalysts [135,136]. Zhang et al. found that the carbon shell of the synthesized graphene encapsulated zero-valent iron nanoparticles gradually became rough with the increase of reaction temperature, and when the temperature rose to 700℃, the synthesized catalyst presented a three-dimensional network structure [137].

3.3. Chemical vapor deposition

CVD acts as a general nanocatalyst gas-phase synthesis technique. CVD is a technology that gaseous precusors react chemically under gaseous conditions to generate a new substance and deposit on the surface of a heated substrate to form solid materials [47]. Despite the complex chemical system, CVD can control the crystal structure, surface morphology, graphitization degree of carbon components, and produce high-density and pure materials. Hence, it has been widely used in the preparation of core-shell structure catalysts for photocatalysis and photoelectrocatalysis [94,111,139].

The CVD process is mainly split into three steps: 1) diffusion of the reaction gases to the surface of substrate; 2) adsorption of the reaction gases on the surface of the substrate; 3) reaction takes place on the substrate surface, resulting in the formation of solid deposits and the generation of gaseous by-products [140]. By adjusting the parameters such as reaction gas, reaction temperature and precursor volume, the uniformity of encapsulated catalyst and the thickness of shell can be well controlled [141]. For example, Park et al. coated g-C_3N_4 nanoflakes on ZnO nanorod arrays by CVD. In the first step, ZnO nanorods grew on the glass substrate coated with fluorine-doped tin oxide via seed mediated growth; In the second step, melamine was polymerized in the air at 520℃, then forming a thin g-C_3N_4 coating on the ZnO nanorods surface. As the amount of melamine increased in the process, g-C_3N_4 gradually agglomerated on the top of ZnO nanorods, promoting visible-light absorption and photocatalytic activity [142].

3.4. Template-based method

Template-based method is often used to prepare yolk-shell/mesoporous structure encapsulated catalysts. The special difference between template-based method and other methods is that template with nanostructure needs to be introduced in advance, which can effectively control the size, morphology and structure of the reaction material. The key factor of template-based method is the selection of template, which determines the formation of structure, while the structure of encapsulated catalyst often determines its catalytic activity and stability [112,113]. There are two types of templates according to their characteristics and different confinement effects: soft template and hard template. Generally, the surfactant aggregate is used as the soft template, and the rigid material maintained by the covalent bond is used as the hard template [112–114,143]. Common to both is that they can provide a limited reaction space. The difference is that the cavity wall of soft template allows substances to diffuse in and out, while hard template only allows substances to enter the pore from the opening of the template.

Generally, the synthesis process of hard template method mainly involves the following steps: 1) constructing template with specific shape, and common hard templates include SiO_2 [144–146], carbon and polymers [147]; 2) template surface functionalization; 3) template can be removed by selective etching or heat treatment according to the material characteristics [148]. The size, shell thickness, shell number and pore size of the encapsulated catalyst could be regulated by changing the template size, precursor content, coating times of target product and sacrificial layer, reaction temperature and reaction time [114]. For example, the iron single atom catalyst deposited on nitrogen-doped hollow mesoporous carbon spheres (Fe-NC HMCS) was synthesized by in-situ hard template method (Fig. 4a) [149]. Specifically, the SiO_2 nuclei formed by hydrolysis of ethylsilicate was condensed with polydopamine (PDA)-Fe^{3+} to form SiO_2@PDA-Fe^{3+} with core-shell structure. And then SiO_2@Fe-NC was formed by pyrolysis at 800℃. Finally, HF etching was used to remove SiO_2 and iron-containing clusters, and the Fe-NC HMCS catalyst was synthesized (Fig. 4b-c).

Unlike the hard template method, the soft template uses micelles, vesicles and lotion formed by surfactants in solution as templates to induce the formation of encapsulated catalysts [113,114,143]. For instance, in the preparation of Cu_2O/Cu/rGO@carbon nanomaterial [150], firstly, sodium alginate chain was cross-linked to hydrogel by Cu^{2+}; secondly, rGO nanosheets were assembled and Cu^{2+} was precipitated on the hydrogel template; and finally Cu_2O/Cu/rGO@carbon nanomaterial photocatalyst was obtained by carbonization at 1100℃ (Fig. 4d). Interestingly, it could be clearly observed from Fig. 4e-f that an increase in rGO proportion led to a gradual decrease in Cu_2O content, which indicated that the presence of rGO was conducive to regulating the particle size of Cu_2O. However, although the soft template method requires relatively mild conditions to avoid the destruction of the catalyst's structure during the template removal process, soft template (e.g., micelles, vesicles and lotion) has uncertain morphology and it is difficult to achieve accurate control of products. Therefore, soft templates can be used for the synthesis of chemically and thermodynamically unstable materials [113,114].

3.5. Self-assembly strategy

Self-assembly can transform disordered molecular units into ordered composite structures [113]. Self-assembly strategy is a simple and common method for preparing encapsulated catalysts, especially photocatalysts. The self-assembly method is based on other methods, and its preparation steps are as follows: 1) nanoparticles are prepared by conventional methods; 2) nanoparticles are bonded to the shell through chemical adsorption, electrostatic force and Van Der Waals force to obtain encapsulated catalyst. The method is simple in operation and flexible in design, and can control the synthesis of encapsulated catalyst more accurately [48].

In general, there are many applications in the self-assembly process through the electrostatic interaction between the shell and the active transition-metal core, such as SiO_2@C-doped TiO_2 hollow sphere [151], SiO_2-Ag@TiO_2 hollow sphere [152], SiO_2-Fe_2O_3@TiO_2 hollow sphere [44], etc. In the synthesis process of SiO_2-Fe_2O_3@TiO_2 hollow sphere, the synthesis steps were mainly divided into five steps: 1) cationic polystyrene sphere (CPS) @SiO_2 was formed by electrostatic interaction between CPS and SiO_2; 2) due to electrostatic interaction, CPS@SiO_2 particles were used as templates to adsorb Fe^{3+}; 3) ultra-thin CPS layer was coated on CPS@SiO_2-Fe^{3+} surface; 4) TiO_2 layer deposited onto CPS@SiO_2-Fe^{3+}@CPS surface; 5) SiO_2-Fe_2O_3@TiO_2 hollow spheres were obtained by calcination (Fig. 4g). As shown in Fig. 4h-i, it could be

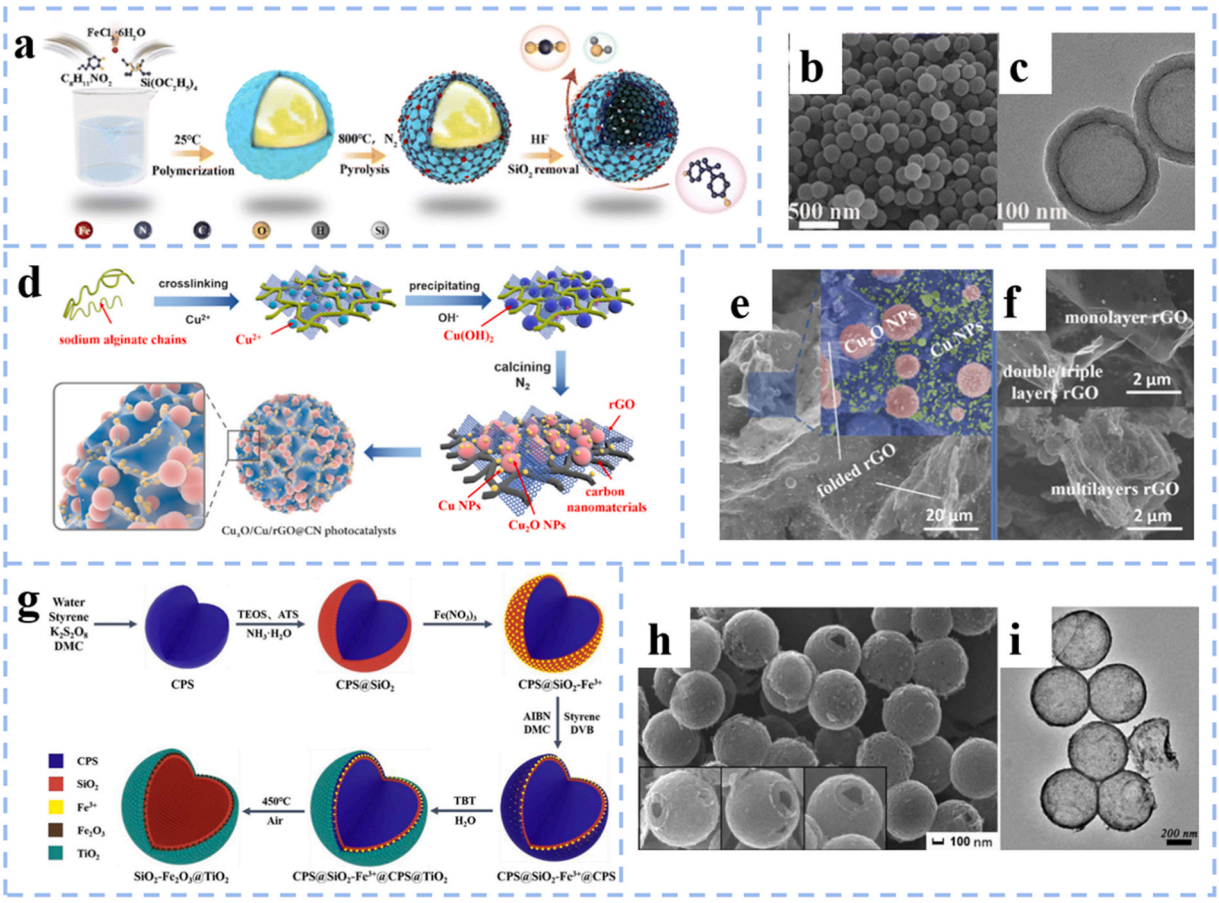

Fig. 4. (a) Synthetic process of the Fe-NC HMCS. SEM image (b) and TEM image (c) of Fe-NC HMCS. Reproduced with permission from Ref. [149]. Copyright 2022 The Royal Society of Chemistry. (d) Schematic for preparation of Cu_2O/Cu/rGO@ carbon nanomaterial. SEM images of Cu_2O/Cu/rGO@carbon nanomaterial (e) and rGO (f). Reproduced with permission from Ref. [150]. Copyright 2019 Elsevier. (g) Illustration of design and fabrication process of SiO_2-Fe_2O_3@TiO_2 hollow spheres. SEM (h) and TEM (i) image of SiO_2-Fe_2O_3@TiO_2 hollow spheres. Reproduced with permission from Ref. [44]. Copyright 2020 Elsevier.

seen that SiO_2-Fe_2O_3@TiO_2 was a sphere with high uniformity and integrity as well as with a layered hollow structure.

3.6. Combined methods

In addition to a single synthesis method, the combination of two or more methods is becoming a mainstream method for preparing such catalysts because it helps to construct structurally diverse and more complex encapsulated transition-metal nanoparticle catalysts. Specifically, the coupling of hydrothermal method and thermal synthesis can further improve the crystallinity of encapsulated transition-metal nanoparticle catalysts, thereby improving their catalytic activity [84, 153]. A good example is the work reported by Lyu and his group, who constructed hierarchical nano-vesicle catalysts ($FeCu_{1.5}O_3$@NV) through two hydrothermal crystallizations with assisted calcination, i.e., hollow sphere structure assembled from hollow sphere units (Fig. 5a-c) [153]. In addition, the sol-gel method-assisted calcination enables the finely controlled synthesis of multilayer core-shell structured catalysts [154].

However, when the target encapsulated transition-metal catalysts are more complex, the combination of the two methods is difficult to meet the needs of the research, so it is necessary for researchers to combine more methods. In the synthesis process of a typical micro-nano reactor (Co-Fe/NC@GCS), it can be divided into the following steps: 1) preparation of nano ZIF-67 dodecahedra by chemical deposition method; 2) ZIF@PBA was obtained by cation exchange method; 3) conversion to nitrogen-doped graphitic carbon Co-Fe alloy (Co-Fe/NC) by thermal synthesis under N_2 atmosphere; 4) Co-Fe/NC was encapsulated in chitosan microspheres by emulsification cross-linking method (Fig. 5d-e) [155]. Noteworthily, in the process of preparing encapsulated transition-metal catalysts, an appropriate preparation method should be selected according to actual needs, and an overly complicated method should not be blindly pursued.

The previously discussed encapsulation pathways exhibit different advantages and disadvantages. Since the performance of encapsulated transition-metal catalysts is greatly influenced by their form, structure and composition, the synthesis strategy plays a critical role in obtaining the optimized catalyst form, structure and composition to enhance catalytic activity, stability and selectivity. In general, the preparation procedure involves the preparation of an active transition-metal core, which is later encapsulated by various methods. In the current and foreseeable future, the targeted applications of encapsulated transition-metal catalysts may drive the appropriate use of synthesis strategies, i.e., the selection of suitable preparation methods according to the needs of practical applications. And the research focus will be prioritized on optimizing and regulating the relationship between key synthesis conditions and parameters to prepare the target encapsulated transition-metal catalysts in a controlled manner. For example, if the target encapsulated transition-metal catalyst requires high crystallinity, the hydrothermal/solvothermal method can be chosen; if large quantities of catalysts with controllable thickness of the encapsulated layer need to be prepared, the CVD technique can be chosen; if yolk-shell nanoreactors need to be prepared, the template-based method and self-assembly method are the preferred choices.

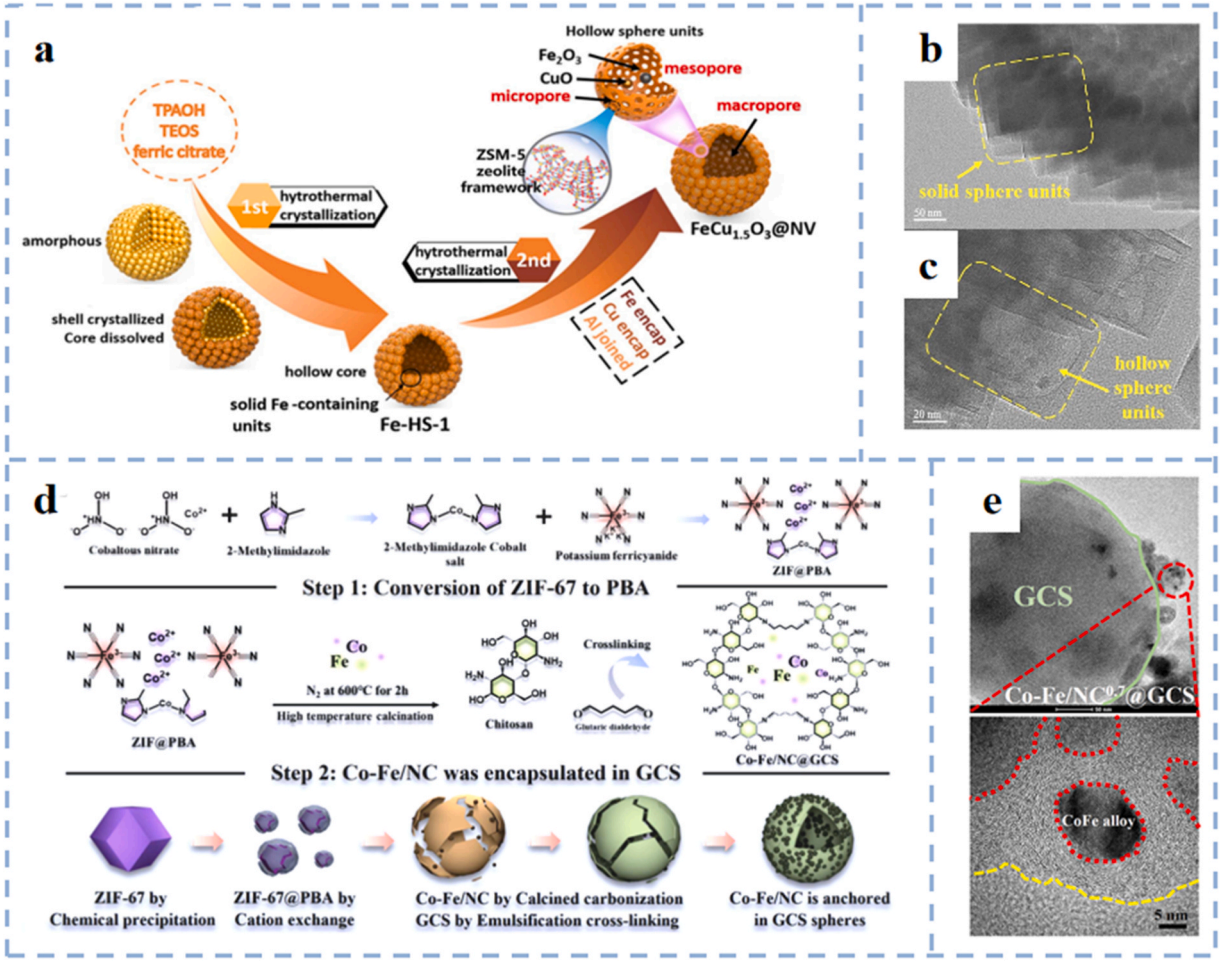

Fig. 5. (a) Synthetic process of the $FeCu_{1.5}O_3$@NV. (b) TEM images of Fe-HS-1. (c) HRTEM images of $FeCu_{1.5}O_3$@NV. Reproduced with permission from Ref. [153]. Copyright 2022 Elsevier. (d) Synthetic process of the Co-Fe/$NC^{0.7}$@GCS micro-nano reactor. (e) HRTEM images of Co-Fe/$NC^{0.7}$@GCS micro-nano reactor. Reproduced with permission from Ref. [155]. Copyright 2022 Elsevier.

4. Applications of encapsulated transition-metal nanoparticle catalysts in advanced oxidation processes

Due to the interaction between transition-metal nanoparticles and coating layer, encapsulated transition-metal nanocatalysts might possess high catalytic activity, stability and selectivity, which can meet the requirements of specific AOPs. AOPs are considered to be promising techniques for degrading organic pollutants due to its ability to generate reactive oxygen species (ROS) in situ. In this section, the recent progress of encapsulated transition-metal nanoparticle catalysts applied in various AOPs for treatment of aqueous organic pollutants will be reviewed, including Fenton reaction, photocatalysis, persulfate activation and so on.

4.1. Fenton reaction

4.1.1. Fenton-like process

Fenton reaction is considered as one effective method for removal of aqueous organic pollutants. Nevertheless, the application of traditional Fenton reactions is often limited by the narrow range of operating pH values and poor reusability [32]. The heterogeneous Fenton-like process can generate •OH using solid catalysts instead of dissolved Fe^{2+} [156]. In Fenton-like systems, the oxidation ability of Fenton-like systems is greatly affected by pH, H_2O_2 dosage, and encapsulated transition-metal catalyst dosage. Studies have shown that the optimal pH of Fenton-like systems is around 3 [80,157–159], although a considerable portion of studies have shown that good degradation efficiency of pollutants can be also obtained under neutral (or even alkaline) conditions [160–162]. This is mainly because the decomposition of H_2O_2 tends to produce O_2 rather than •OH as the pH increases [159,160]. When the concentration of H_2O_2 changes, the degradation efficiency of pollutants generally shows a trend of increase and a subsequent decrease. This is because the increased H_2O_2 can decompose to produce more •OH, while excessive H_2O_2 can lead to the self-scavenging of •OH radicals with the activation of the encapsulated catalyst [158–160,163]. When the dosage of encapsulated transition-metal catalyst is changed, the trend of degradation efficiency of pollutants is similar to that of H_2O_2 mentioned above. This is mainly because more active sites can be used for Fenton-like reaction, while excessive encapsulated catalyst might cause transition-metal agglomeration and elimination of •OH [160,163,164].

Noteworthily, the heterogeneous Fenton-like reaction still has a rate-limiting step for metals from the oxidized state to the reduced state [161, 165–168]. It has been reported that constructing dual reaction centers with uneven electron distribution in encapsulated catalysts through lattice doping or surface compaction methods is crucial to overcoming the above-mentioned problems [161,169]. Electron transfer is a particularly important process in the cation-π interaction of transition-metal ions [167]. Recently, building special bond bridges to enhance cation-π interactions has become an attractive strategy to promote uneven distribution of electrons on the surface of encapsulated catalysts, such as C-O-Cu bond bridges [161,167], C-O-Fe bond bridges [162,170,171], and Fe-O-Mn bond bridges [168]. Specifically, Lai et al.

[161] prepared Cu-MP NCs catalyst with special aromatic structure (π-electron) for the first time. As shown in Fig. 6a, the interaction of π→cations and C-O-Cu bridges inhibited the peroxidation of H_2O_2, further accelerating the electron transfer cycle from electron-poor centers to electron-rich centers. Considering the extended transport distance and transport resistance caused by vibrating or roating chemical bonds, Zhang et al. constructed short C-M bonds to transport electrons from one reaction center to another, and prepared Fe/Fe_3C@NCNTs-CL catalyst [172]. In the Fe/Fe_3C@NCNTs-CL/H_2O_2/norfloxacin system, the adsorption of norfloxacin antibiotic and its intermediates occurred on the NCNTs surface, with electrons being transferred to the benzene ring of NCNTs via π-π stacking. Subsequently, the C-Fe bond bridge facilitated the reduction of Fe^{3+} to Fe^{2+}, resulting in the formation of electron-rich Fe centers and electron-poor carbon centers (Fig. 6b-d).

Combining internal micro-electronics with Fenton-like process (IME-Fenton) can also effectively solve the above-mentioned rate-limiting steps and selectively decompose H_2O_2 into •OH, such as Fe-Pd@C [110], Fe^0@CNTs(x) [174], and Fe@C-MMT [175] and nZVI@Ti_3C_2 [70]. In He et al.'s studies [110], they found that the core-shell structure of Fe-Pd@C promoted TME-Fenton because the galvanic corrosion of Fe^0 anode released Fe^{2+}, triggering the H_2O_2 decomposition into •OH, while the trace of Pd contributed to maintaining the reducibility of Fe^0 and facilitating the conversion of Fe^{3+} to Fe^{2+}. And the core-shell structure of Fe-Pd@C could avoid Fe inactivation and terminate Fe-C IME and prolong its service life (Fig. 7a). In order to explore more economical and efficient Fenton-like systems, the in-situ production of H_2O_2 by activating oxygen through the IME system has become a research hotspot. Xu's team has prepared a series of catalysts, including 3D-GN@Cu^0 [176], 3D-GN@nZVI [157], 3D-GN@Fe/a-Al [177] and 3D-rGO@nZVI/MnO_2 [178]. In the 3D-GN@Fe/a-Al–DO/chloramphenicol system, GN matrix acted as an electrical conductor, while nZVI acted as electron donor, forming abundant microscopic galvanic corrosion cells. Moreover, it promotes Fe(II)/Fe(III) redox cycle for the production of $^1O_2$. Interestingly, Al^{3+}-promoted single electron transfer also promotes the generation of $^1O_2$ (Fig. 7b).

4.1.2. Photo-Fenton process

The heterogeneous photo-Fenton (PF) system can promote the reuse of metal catalysts and the activation of H_2O_2 via the synergy between photocatalysis and Fenton-like reaction. The mechanism of action mainly involves: 1) the active electrons generated by photoexcited encapsulated transition-metal catalysts directly or indirectly participate in H_2O_2 activation; 2) the separation of the optimized electron-hole (e^--h^+) pair can effectively consume photogenerated electrons while release highly oxidizing holes to promote the mineralization of pollutants [179–181]. However, the recombination of photogenerated electrons and holes in the photocatalyst restricts the delocalization and transfer of electrons, thereby inhibiting the PF catalytic efficiency [182]. Therefore, finding photocatalysts that can rapidly separate photogenerated electrons and holes is crucial for the PF system to degrade pollutants. In terms of this issue, optimization strategies such as morphology control, element doping, defect engineering, heterogeneous structure construction and coupling with other processes have been applied to PF systems.

Improving charge carrier separation by changing the morphology of encapsulated catalysts can enhance the catalytic efficiency of PF because the morphology of encapsulated catalysts affects specific surface area, active sites, and electron transfer efficiency [183]. Given that PF primarily takes place on the surface of encapsulated transition-metal catalysts, the most direct and effective approach to enhance PF catalytic activity lies in the control of the encapsulated catalysts' morphology. Firstly, in order to control the morphological size of photocatalysts, including 0D (quantum dots), 1D (micro/nanorods), 2D

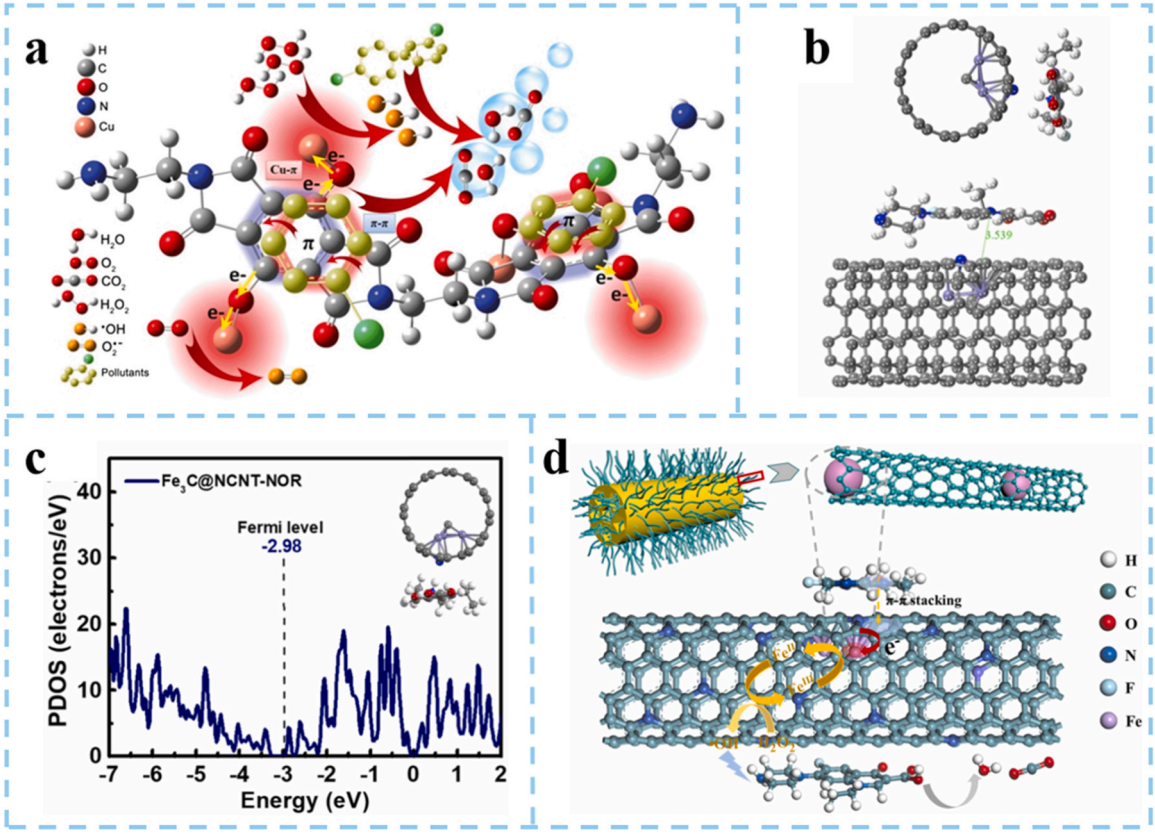

Fig. 6. (a) Mechanism of the degradation of ciprofloxacin in Cu-MP NCs/H_2O_2 system. (b) Model of norfloxacin adsorbed on Fe_3C@NCNT surface. Reproduced with permission from Ref. [161]. Copyright 2019 The Royal Society of Chemistry. (c) The projected density of states of Fe_3C@NCNT-norfloxacin. (d) Mechanism of the degradation of norfloxacin in the Fe/Fe_3C@NCNTs-CL-800/H_2O_2 system. Reproduced with permission from ref. [173]. Copyright 2022 Elsevier.

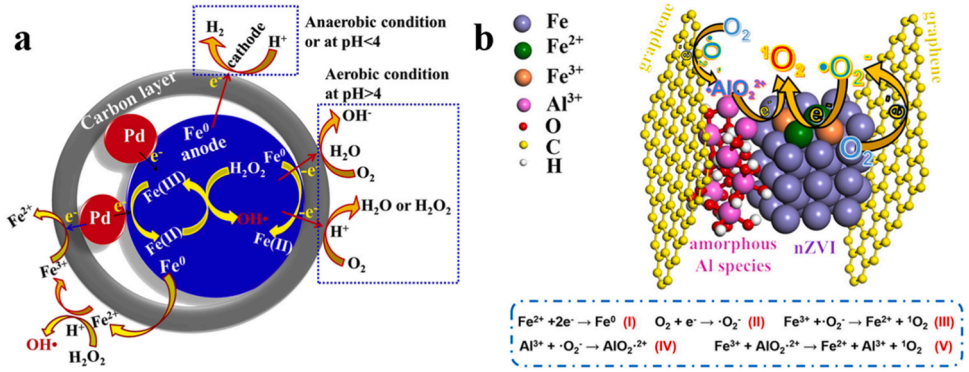

Fig. 7. (a) Reaction mechanisms of IME-Fenton on Fe–Pd@C surface. Reproduced with permission from Ref. [110]. Copyright 2019 Elsevier. (b) Likely degradation mechanism of chloramphenicol in the 3D-GN@Fe/a-Al-DO system. Reproduced with permission from Ref. [177]. Copyright 2021 Elsevier.

(micro/nanoplates) and 3D (powders, thin films and bulk crystals), the development of diverse photocatalysts for pollutant degradation in PF system has been broadly researched. Studies have shown that 1D structural morphology engineering could increase the exposure of active centers and serve as highway for electron transfer [184]. Specifically, Zhang et al. prepared tubular core-shell Cu-HNCN catalysts with highly dispersed CuN_x sites [181]. It could be seen from Fig. 8a-b that the Cu(II) N_x on CuN_x sites could trap electrons with resultant reduction to Cu(I) N_x, achieving the efficient separation of charges. Based on the quantum confinement effect, the decrease in dimension of semiconductor materials could enhance the quantization along the confinement direction, which would promote the directional migration of electrons. Mechanism exploration revealed that the outstanding catalytic ability was ascribed to the characteristics of nanotubes, which facilitated the production,

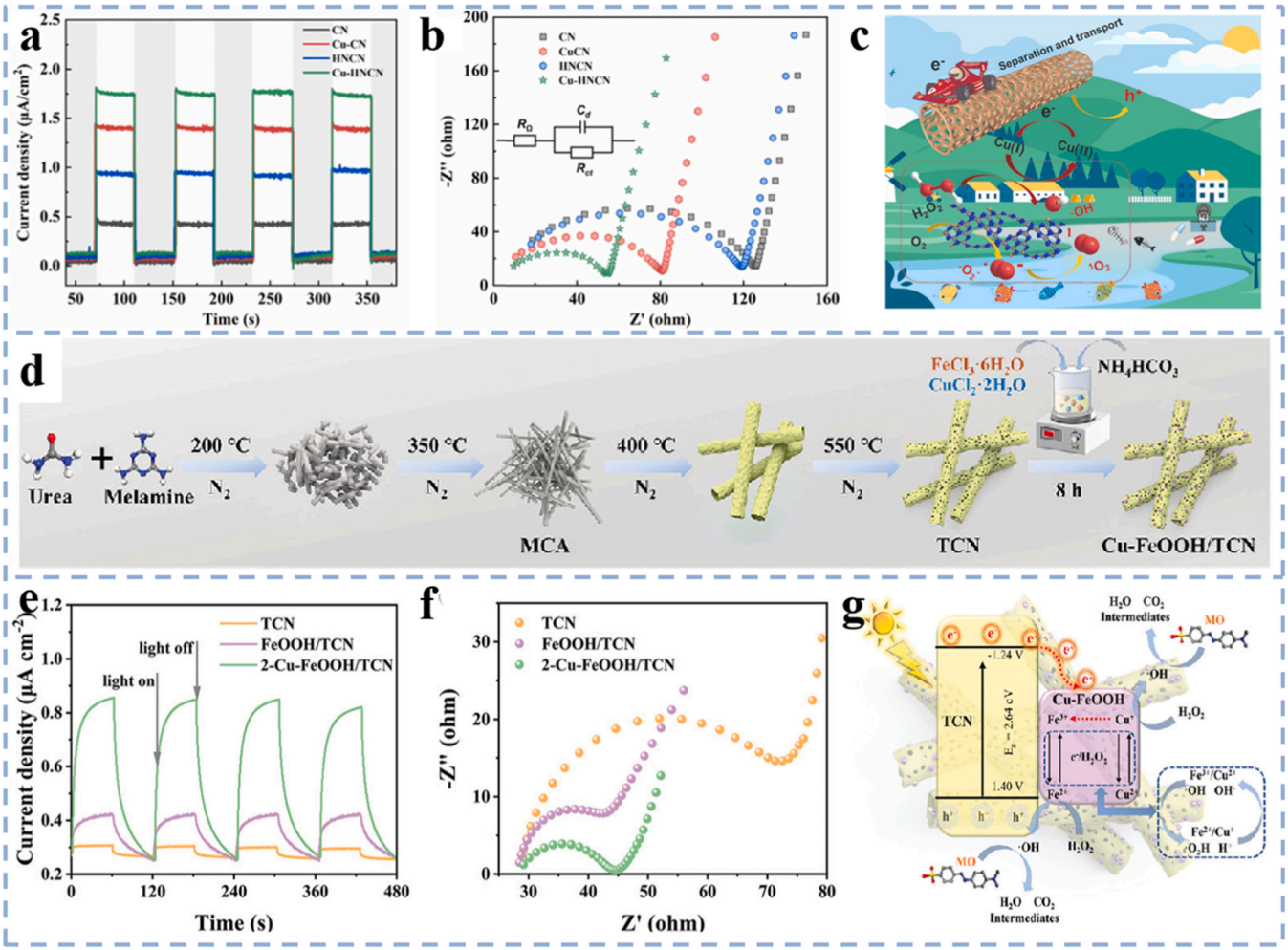

Fig. 8. (a) Transient photocurrent and (b) Nyquist plots of CN, Cu-CN, HNCN, and Cu-HNCN. (c) Reaction mechanisms of tetracycline degradation by the Cu-HNCN/PF system. Reproduced with permission from Ref. [181]. Copyright 2022 Elsevier. (d) Schematic of the synthesis process of Cu-FeOOH/TCN catalysts. (e) Transient photocurrent and (f) Nyquist plots of TCN, FeOOH/TCH, and 2-Cu-FeOOH/TCN. (g) The possible degradation mechanism of methyl orange in Cu-FeOOH/TCN system. Reproduced with permission from Ref. [188]. Copyright 2023 Wiley Online.

separation and transfer of photogenerated electrons in Cu-HNCN, and promoted the generation of $\bullet O_2^-$, •OH, h^+, and $^1O_2$ (Fig. 8c). In addition, 0D quantum dots have small lateral dimensions and abundant surface defects, which can provide abundant active centers for catalysis [179, 185]. However, the self-aggregation phenomenon greatly limits their practical applications [185]. The recent construction of 0D/2D nanocomposites can make quantum dots more dispersed and stable due to the interaction between the two parts, enhancing the photocatalytic activity, such as CuFeO QDs/CNNSs [179], FeOOH/UPCN [186], SA-TCPP/O-CN [187], Fe_2O_3 QDs/g-C_3N_4 [185]. Of course, the construction of 0D/3D nanocomposites can also enhance the photocatalytic activity. For example, Tang et al. constructed Cu-FeOOH/TCN catalyst [188] (Fig. 8d). As shown in Figs. 8e-f, 2-Cu-FeOOH/TCN obtained the highest intensity of photocurrent response reaching 0.85 A cm^{-2}, along with the smallest radius of the impedance, indicating that proper coupling of Cu-FeOOH clusters can effectively inhibit the recombination of photogenerated charges in TCN and greatly enhance the catalytic activity. Specifically, when TCN was exposed to visible light, the photoelectrons were rapidly transferred to Cu-FeOOH clusters, participating in the coversion process of Fe^{3+} to Fe^{2+} and Cu^{2+} to Cu^+, which inhibited the recombination of photogenerated e^--h^+ pairs (Fig. 8g).

Defect engineering is considered as an effective modification strategy to construct highly efficient photocatalysts. Defects can serve as adsorption sites to trap excited electrons and even tune the bandgap of encapsulated transition-metal catalysts to enhance catalytic performance [183]. Defect engineering mainly includes anion vacancy defects (oxygen vacancy and nitrogen vacancy) and cation vacancy defects [189–191]. Generally, there are more studies on anion defects. Oxygen vacancies (V_o) can elongate the O-O bonds in H_2O_2, promoting conversion of H_2O_2 to •OH, and can enhance the photoresponsiveness and carrier capture ability [192,193]. The introduction of nitrogen vacancies (V_n) can adjust the electronic structure and energy band positions to enhance light absorption and photogenerated charge separation capabilities [180,182]. Taking a specific example, Wu et al. [192] prepared OVs-FeOOH/rGO catalysts with controllable oxygen vacancy concentration by precisely adjusting the redox pH conditions, and found that an appropriate amount of oxygen vacancies would act as a high-speed transport channel for electron transfer, effectively inhibiting the e^--h^+ recombination and significantly accelerating the Fe^{3+}/Fe^{2+} redox cycle, leading to the excellent photo-Fenton performance of OVs-FeOOH/rGO (Fig. 9a). In addition, constructing coordinatively unsaturated metal centers to form defect sites as Lewis acid centers can also enhance the PF activity [194–196]. Hu et al. prepared a MXene/MIL-100(Fe) catalyst by growing MIL-100(Fe) on iron protoporphyrin-modified MXene [194]. As shown in Fig. 9b-c, the H_2O_2 generation rate of MXene/MIL-100(Fe) was 12 times higher than that of MIL-100(Fe), while the thiacloprid degradation efficiency was 21-60 times greater in comparison to numerous PF catalysts reported in H_2O_2-free systems. The main reason was that iron protoporphyrin could imitate hemin to capture O_2, and Schottky junction effectively promoted carrier separation, which greatly facilitated the $2e^-$ reduction of O_2 to H_2O_2. Meanwhile, the photogenerated electrons promoted the redox cycle of Fe^{3+}/Fe^{2+}, which facilitated the generation of •OH (Fig. 9d).

The construction of a heterojunction structure facilitates charge separation, thereby reducing the possibility of recombination of excited electrons and holes, thereby affecting the catalytic activity. In recent years, there have been many studies on Z-scheme heterojunction encapsulated transition-metal catalysts for PF degradation of pollutants, and scholars have prepared ternary CuO/CDs/g-C_3N_4 catalysts with Z-scheme heterostructure by inserting 0D carbon dots (CDs) into PF catalysts and constructing CDs interfacial electron transfer bridge assisted dual charge transfer pathways [197]. Another example is that Ju et al. in situ deposited MIL-101(Fe)/g-C_3N_4 with Z-scheme heterostructure on hydrophilic carbon cloth substrate to form MCC catalyst [198]. The three-phase system completely degraded methyl orange within 130 minutes and exhibited no performance decline after 10 cycles. The main reason was that the catalytic reaction occured at the gas (oxygen)-liquid (pollutant solution)-solid (catalyst) interface, and the

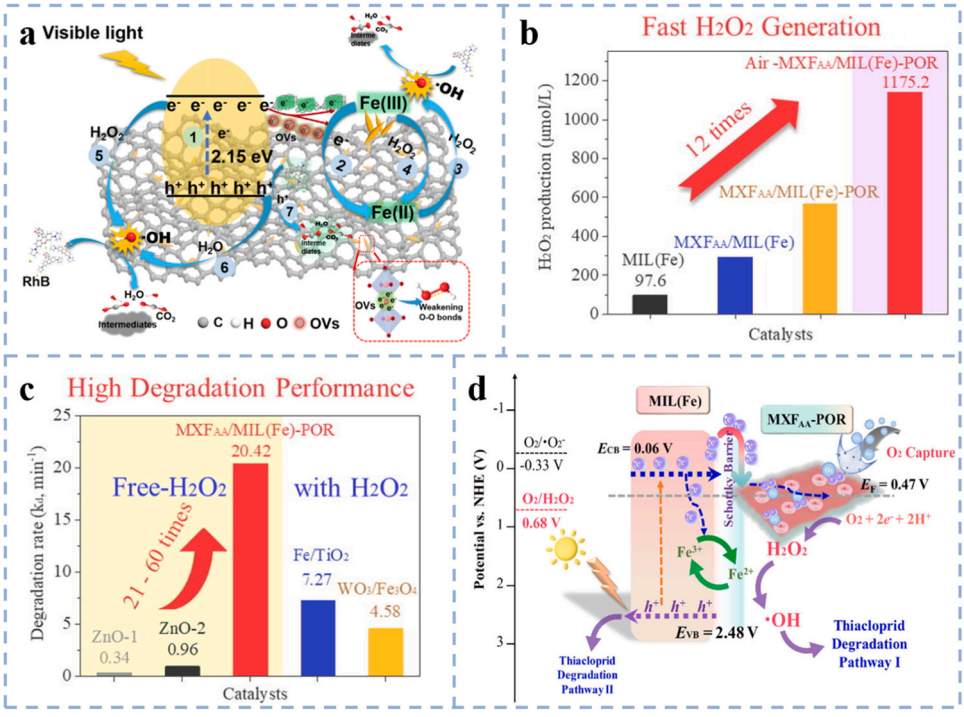

Fig. 9. (a) Possible mechanism for rhodamine B degradation in OVs-FeOOH/rGO/PF system. Reproduced with permission from Ref. [192]. Copyright 2022 Elsevier. (b) Performance of MIL(Fe) and its composites in the generation of H_2O_2. (c) Degradation performance by MXene/MIL-100(Fe) and other reported PF catalysts in H_2O_2-free system. (d) Reaction mechanism for thiacloprid degradation in MXF_{AA}/MIL(Fe)-POR/PF system. Reproduced with permission from Ref. [194]. Copyright 2022 Elsevier.

hydrophilic side of the MCC catalyst played a key role in contacting pollutants, while the hydrophobic side facilitated the transfer of O_2 from air to the catalyst surface, promoting the generation and activation of H_2O_2 (Fig. 10a-b).

In addition, coupling with other technologies will also enhance the PF catalytic performance. Synergizing the photothermal effect with PF to degrade organic pollutants is one of the recent hotspots. Shi et al. prepared core-shell magnetic $CuFe_2O_4$@MIL-100(Fe, Cu) MOFs catalysts with binary homologous bimetallic heterojunctions via two-step hydrothermal method, and found that higher temperature in PF system could effectively lead to higher methylene blue degradation [199]. The photothermally enhanced catalysis might be due to the conversion of light energy into heat by the $CuFe_2O_4$ core, thus accelerating the production and split of photogenerated e^--h^+ and improving the cycles of Fe^{3+}/Fe^{2+} and Cu^{2+}/Cu^+ (Fig. 11a). Moreover, applying catalysts in slurry reactors can also facilitate the pollutant elimination. Li et al. combined submerged magnetic separation membrane photocatalytic reactor (SMSMPR) with TiO_2-graphene oxide-Fe_3O_4 catalyst for amoxicillin degradation and exhibited excellent PF catalytic performance and stability (Fig. 11b) [200]. The significant enhancement was attributed to the efficient transfer of excited electrons from TiO_2 to graphene oxide, which accelerated the cycle of Fe^{3+}/Fe^{2+} and improved the PF catalytic activity (Fig. 11c). Additionally, the implementation of backwash and magnetic separation in SMSMPR improved the recyclability and separation, promoting the practical application of this method.

4.1.3. *Electro-Fenton process*

Heterogeneous electro-Fenton (HEF) is an effective and green technique for the degradation of organic contaminants. The mechanism of action is: 1) H_2O_2 isgenerated in situ by $2e^-$ oxygen reduction reaction (ORR) on the cathode surface ($O_2 \rightarrow {}^*O_2 \rightarrow {}^*H_2O_2 \rightarrow H_2O_2$); 2) H_2O_2 reacts with reduced metal catalysts to generate •OH to degrade pollutants ($H_2O_2 \rightarrow {}^*H_2O_2 \rightarrow {}^*OH \rightarrow$•OH) [201,202]. However, low H_2O_2 production efficiency and high metal leaching limit its application in practical water bodies [202–205]. To overcome this limitation and improve the catalytic efficiency of HEF, research efforts in the following three aspects are generally made: 1) developing encapsulated transition-metal catalysts; 2) functionalizing the cathode electrode; 3) coupling with other technologies.

Encapsulated transition-metal nanoparticles have been studied to act directly as HEF catalysts due to their sustained high catalytic activity, stability, and reusability. Generally, the popular catalysts for HEF systems mainly include Fe elements, such as FeNC@C [206], FeO_x/NHPC [207], and FeS_2/C [208]. FeS_2/C catalysts with core-shell structure was successfully synthesized by simultaneously carbonizing and vulcanizing Fe-MOF precursors [208]. The catalyst exhibited remarkable performance, completely degrading fluoxetine within 60 min under neutral conditions with much lower iron leaching than the FeS_2-EF system (1.5 mg/L vs. 8 mg/L). Compared with encapsulated single transition-metal catalysts, encapsulated catalysts containing two or more transition-metals are considered promising due to synergistic effects and faster electron transfer between multivalent metals, such as FeCo/NPC [209], Cu–Fe–Fe_3C@NDB [203].

Although the directly added encapsulated transition-metal catalyst shows good catalytic performance in the HEF system, there are still some problems, such as low electron transfer ability and unsatisfactory recycling performance [201]. Applying the functionalized cathode to the HEF system is able to overcome the above problems to some degree and could selectively promote the $2e^-$ ORR reaction to generate H_2O_2, favorably reducing or even avoiding the $4e^-$ ORR reaction [210]. Furthermore, the occurrence of O_2 reduction to •OH via $3e^-$ ORR pathway can effectively overcome the rate-limiting steps of electron transfer caused by the catalyst regeneration, thereby quickly removing organic pollutants [202,210,211]. For instance, Xiao et al. innovatively designed FeCo alloy encapsulated by carbon aerogel as working electrodes, which amazingly completely removed ciprofloxacin within 5 min and maintained high degradation efficiency after 50 cycles [210]. Furthermore, the efficiency of $2e^-$ ORR relies on three crucial parameters: catalyst selectivity, O_2 transport efficiency, and charge movement rate [212]. However, regardless of encapsulated transition-metal catalyst, the ORR efficiency is primarily constrained by O_2 transfer efficiency when the selectivity and charge transfer efficiency of the encapsulated transition-metal catalyst reach to a certain extent [213]. Expanding the three-phase interface can effectively promote gas consumption reactions. Geng et al. successfully prepared the sandwiches enriched with three-phase interface by coating FeO_x/activated carbon hydrophilic catalysts on both sides of hydrophobic substrate, and found that it could achieve effective degradation of pollutants by simultaneously enhancing O_2 and pollutant transport [214]. This was because the rapid gaseous O_2 transfer process caused the generation of •OH up to 536.4 μmol/L, which was more than 9 times of the hydrophilic electrode with dissolved oxygen transfer limitation. Meanwhile, the sandwich electrode had more active sites for effective tetracycline adsorption, which was 3.7 times more than hydrophobic electrode with tetracycline transfer limitation (Fig. 12a-b). Using gas diffusion electrodes (GDE) also enables effective improvement in the O_2 transfer and utilization [215,216]. As the catalyst layer of GDE, the applications of Fe^0 confined inside the CNTs cavity (Fe^0-in-CNTs) and outside the CNTs wall (Fe^0-out-CNTs) to degrade phenol in HEF system were explored by Su et al. [216], and it was found that Fe^0-in-CNTs not only exhibited lower iron leaching but also obtained much higher H_2O_2 yield and phenol removal rate than Fe^0-out-CNTs (Fig. 12c).

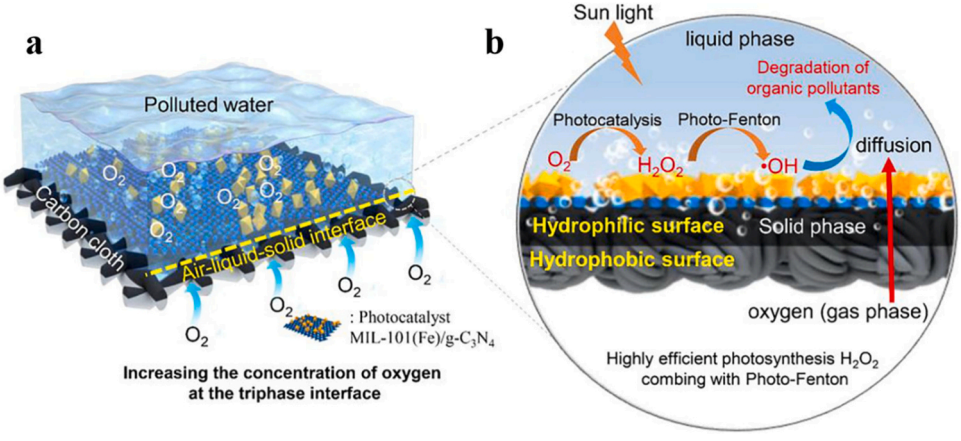

Fig. 10. (a) Illustration of the three-phase interface. (b) Mechanism of methyl orange degradation at three-phase interface in the PF system. Reproduced with permission from Ref. [198]. Copyright 2022 Elsevier.

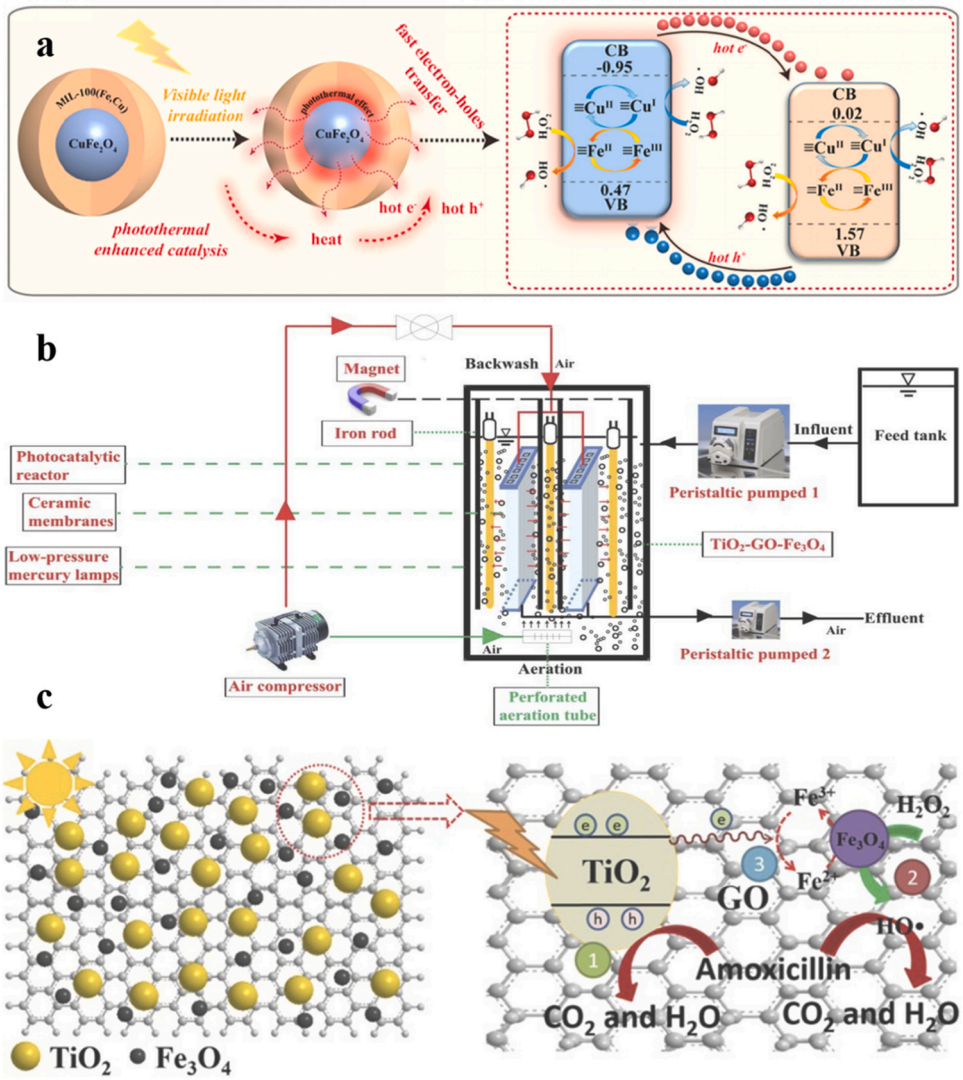

Fig. 11. (a) The PF reaction mechanism of $CuFe_2O_4$@MIL-100(Fe, Cu) MOFs under visible light irradiation. Reproduced with permission from Ref. [199]. Copyright 2021 Elsevier. (b) Schematic dragram of SMSMPR. (c) Mechanism of amoxicillin degradation by TiO_2-graphene oxide-Fe_3O_4 with SMSMPR. Reproduced with permission from Ref. [200]. Copyright 2019 Elsevier.

In addition, coupling with other processes or technologies can also improve encapsulated transition-metal based HEF catalytic performance. The degradation of organic contaminants using the photo-electro-Fenton system is one of the recent hot topics [217–220]. Xin et al. used $CuFeO_2$-NO/PBC as cathode catalyst of composite GDE, and showed excellent degradation performance towards tetracycline in photo-electro-Fenton system [217]. The main reason was that the electrons and photogenerated electrons on the GDE cathode participated in the reduction of Fe^{3+} to Fe^{2+} and Cu^{2+} to Cu^{+}, which promoted the production of •OH and $•O_2^-$ (Fig. 13a). Another is the combination of the flow-through system and encapsulated transition-metal based HEF system, which can effectively enhance the convection, expose reaction sites, accelerate the mass transfer rate of target pollutant, thus accelerating the degradation of pollutants [221–225]. For example, Zhang et al. prepared 0D/2D/3D Co-CNT/$Ti_3C_2T_X$ nanomembrane cathode through vacuum filtration and thermal treatment, and designed high-efficiency flow-through HEF systems, which presented outstanding performance in the catalytic degradation of tetracycline (Fig. 13b) [221].

4.2. Photocatalysis

Photocatalysis is considered as an environmentally friendly, sustainable and effective advanced oxidation process. Common photocatalysts, such as TiO_2 [226,227], ZnO [228,229], g-C_3N_4 [230,231], are constrained by low quantum efficiency, low visible-light utilization and facile recombination of e^--h^+ pair [18,232–236]. Therefore, the focus of photocatalytic removal of pollutants is to find photocatalyst with appropriate gap width, reduce the recombination rate of e^--h^+ pair, enhance the absorption efficiency of visible light and improve stability. Encapsulated transition-metal photocatalyst provides a feasible solution to the above issues. This section will focus on how to modify encapsulated transition-metal photocatalysts to improve their photocatalytic activity and will discuss from the following aspects: heterojunction structure, morphological control, doping, and coupling with other processes.

The preparation of heterojunction structure encapsulated transition-metal photocatalysts is an effective strategy to impart good photocatalytic performance by combining the outstanding advantages of each component. P-n heterojunction encapsulated catalyst can provide additional electric fields to accelerate the migration of e^--h^+ in the heterojnction, thus improving photocatalytic performance [237–240]. The CT-g-ZnTAPc catalyst broke the traditional photocatalytic limitations, whose p-n heterojunction had a tight matched band structure [238]. When exposed to visible light, only ZnTAPc and Cu_2O were

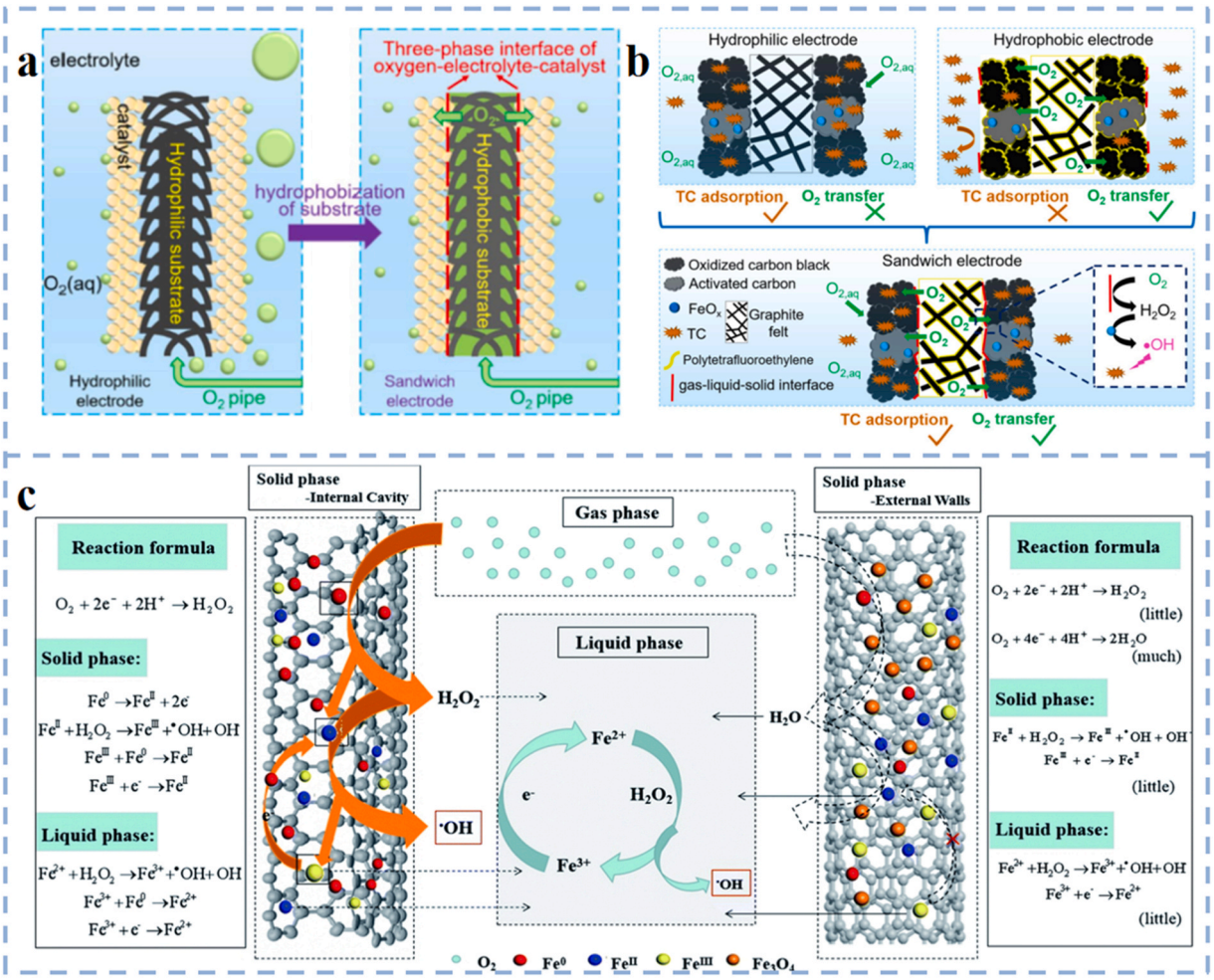

Fig. 12. (a) Schematic of introduction of three-phase interface. (b) The degradation mechanism of tetracycline in the HEF system. Reproduced with permission from Ref. [214]. Copyright 2022 Elsevier. (f) Schematic of the HEF reaction for the ORR process and pollutant removal with Fe^0-in/out-CNTs. Reproduced with permission from Ref. [216]. Copyright 2019 The Royal Society of Chemistry.

excited, resulting in the generation of photogenerated electrons. A portion of these electrons was stored in TiO_2 via reduction of Ti^{4+} to Ti^{3+}. Subsequently, these stored electrons were released and used for the reduction of Cr(VI) in the dark (Fig. 14a-b). Z-scheme heterojunction with electron transfer pattern similar to the natural photosynthesis has been a hotspot of photocatalytic research in recent years because it improves photocatalytic activity by overcoming the inherent defects of conventional heterojunctions with sacrificed redox ability [234,237, 239–241]. For example, Liu et al. found that KCNNT@CdS showed high activity in the degradation of tetracycline due to its Z-scheme heterojunction between KCNN and TiO_2 as well as type II heterojunction between TiO_2 and CdS (Fig. 14c) [236]. Emerging Van Der Waals (VDW) heterojunction opens up new ways in the application of pollutant degradation, which is mainly assembled through VDW interaction without considering the laminar spacing and versatility that exit in the growth of conventional covalently bonded semiconductor heterostructures [239,242,243]. For example, Zhou et al. found that the strong coordination relationship existed between Mo_2C and g-C_3N_4, and the VDW induced electron transfer from g-C_3N_4 nanosheets to Mo_2C and created an internal electric field, which promoted the separation of photogenerated e^--h^+ (Fig. 14d) [242].

Morphology control is one of the most effective strategies for improving the catalytic performance of encapsulated transition-metal photocatalyst. The construction of encapsulated transition-metal photocatalysts with core-shell/yolk-shell structures or hollow tubular structure can expand their specific surface area, increase the reaction sites, shorten the diffusion paths, and thus enhance the photocatalytic activity [239,244,245]. Hasanvandian et al. explored the use of V_2O_5/ultra-wrinkled g-C_3N_4 encapsulated on spinel $CuCo_2O_4$ with a hierarchical hollow sphere morphology to degrade levofloxacin with the advantages of graded hollow balls and Z-scheme system [246]. The hollow nano-structure could capture light in a long period of time, while double Z-scheme heterojunction could promote the e^--h^+ separation (Fig. 15a). In addition, it is believed that the decreasing thickness of the encapsulated transition-metal photocatalyst shell is conducive to significantly shortening the migration distance of photogenerated carriers and inhibit the recombination of e^--h^+ [247].

Doping is a common method for the modification of encapsulated transition-metal photocatalyst. Doping can change the work function through the surface electronic transfer and improve the electric field in the interface, which is conducive to the interfacial carrier transport [232,239,248]. Fu et al. [248] found that the doping of Fe/Pd into g-C_3N_4 could efficiently inhibit the aggregation and oxidation of Fe nanoparticles, and the formation of Fe-Pd galvanic couple promoted the degradation of doxorubicin. Embedding the single atom catalyst Fe into the porous CN_x network could also suppress the agglomeration of Fe nanoparticles, and the hyperdispersed activity center and the CN_x network will accelerate the separation and conversion of photogenerated carriers and improve photocatalytic activity (Fig. 15b) [249]. In addition, Yang et al. doped 1% Fe-N-C nanotube into g-C_3N_4 and found that it could efficiently impede the production of reactive oxygen species at neutral pH, reduce the e^--h^+ recombination rate, and improve

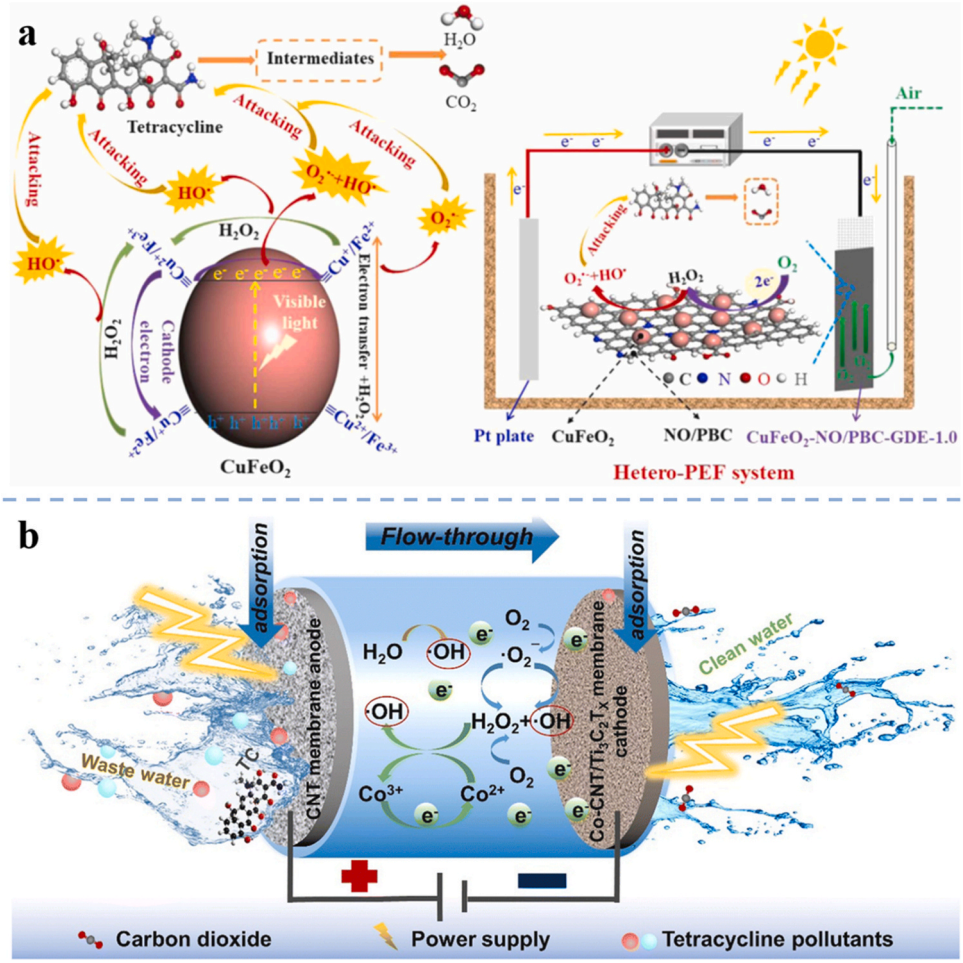

Fig. 13. (a) The mechanism for tetracycline degradation in the heterogeneous photo-electro-Fenton system. Reproduced with permission from Ref. [217]. Copyright 2022 Elsevier. (b) Schematic of the flow-through HEF system with Co-CNT/$Ti_3C_2T_X$ membrane. Reproduced with permission from Ref. [221]. Copyright 2022 The Royal Society of Chemistry.

photocatalytic performance, which was ascribed to the occurrence of $4e^-$ ORR reactions at the Fe-N-C active sites [250].

Apart from organic pollutant degradation and mineralization, additional benefits such as H_2 generation or CO_2 reduction might be acquired from the encapsulated transition-metal based photocatalytic process [103,251,252]. For example, Cao et al. prepared RuO_2@TiO_2@Pt hollow spheres by depositing Pt and RuO_2 nanoparticles on the inner and outer surfaces of TiO_2, and found that RuO_2 enhanced the movement and accumulation of photogenerated holes in TiO_2 cavities, while Pt boosted the movement and accumulation of photogenerated electrons, which synergistically contributed to the degradation of organic matter and the generation of H_2 (Fig. 16a) [103]. Additionally, other processes could be combined to further improve the encapsulated transition-metal based photocatalytic performance. For example, in the C_3N_4-MoS_2/3D graphene flow-through photocatalytic system for ampicillin removal (Fig. 16b) [253], it has been demonstrated that the effective interfacial contact of 3D graphene in the flow-through design and excellent adsorption properties led to the rapid consumption of h^+ via ampicillin oxidation, which inhibited e^--h^+ recombination and improved the photocatalytic performance (Fig. 16c).

4.3. Persulfate activation

In recent years, sulfate radical-based AOPs have been widely studied for the degradation of organic pollutants, and it can solve several major restrictions in Fenton reactions because $•SO_4^-$ possesses a much longer lifetime than •OH and a similar redox potential to •OH. Development of catalysts with desirable catalytic activity and high stability towards persulfate (PS) activation is of great significance in sulfate radical-based AOPs. The encapsulated transition-metal catalyst with spatial confinement function can effectively inhibit the leaching of active transition-metal core, improve catalytic activity, enhance stability and recyclability, and therefore is becoming a rising star in sulfate radical-based AOPs.

Strong metal-support interactions (SMSI) can greatly enhance the catalytic activity and selectivity of encapsulated transition-metal catalysts, mainly because the change in the chemical state of the metal induced by interfacial charge transfer plays a major role in activating the reactants and influencing the catalyst performance. One of its most typical examples is the application of single-atom catalysts [254–256]. The catalytic activity and selectivity can be modulated by adjusting the interaction between the transition-metal atoms and the supports, which also intuitively reveals the structure-activity relationship from the atomic scale [257]. In recent years, there have been many studies on single-atom catalysts for pollutant removal, but their supports are mostly carbon-based nanomaterials, especially graphene and heteroatom-doped sp^2 carbon materials, which is mainly due to the fact that the strong electronic coupling between transition-metal atoms and carbon-based nanomaterials facilitates the electron transfer, which then enhances the catalytic activity and selectivity of the catalysts [258,259]. To date, many studies on the removal of pollutants by N co-doped carbon encapsulated transition-metal (TM-N-C) induced PMS activation

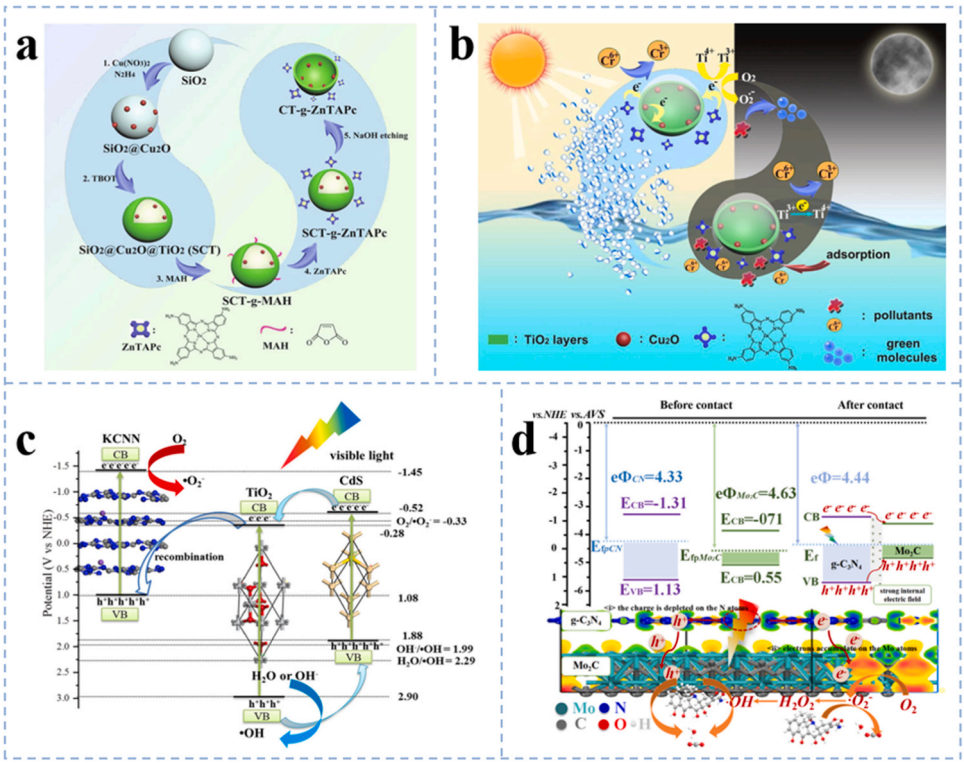

Fig. 14. (a) The synthesis of CT-g-ZnTAPc. (b) Likely reaction mechanism of the "day" and "night" catalyst CT-g-ZnTAPc. Reproduced with permission from Ref. [238]. Copyright 2020 Elsevier. (c) The photoinduced charge carriers of KCNNT@CdS. Reproduced with permission from Ref. [236]. Copyright 2022 Elsevier. (d) The mechanism of the 2D/2D Mo_2C nanosheets/g-C_3N_4 nanosheets VDW heterojunction system. Reproduced with permission from Ref. [242]. Copyright 2021 Elsevier.

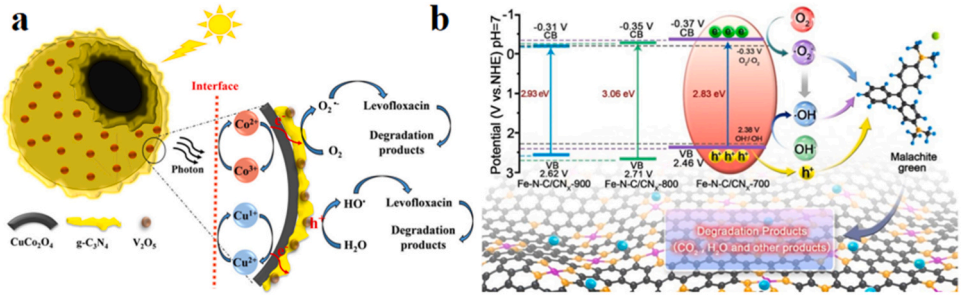

Fig. 15. (a) Degradation of levofloxacin via the use of V_2O_5/ultra-wrinkled g-C_3N_4 encapsulated on spinel $CuCo_2O_4$ with a hierarchical hollow sphere morphology under visible-light irradiation. Reproduced with permission from Ref. [246]. Copyright 2022 Elsevier. (b) Degradation of malachite green using Fe-N-C/CN_x-700 under visible-light irradiation. Reproduced with permission from Ref. [249]. Copyright 2022 Elsevier.

have been reported, and the removal of pollutants by these catalysts is mainly related to their TM-N_x active sites, including CoN_4 [254,256, 260], FeN_4 [261], etc. Most of them degrade pollutants via non-radical pathways ($^1O_2$, direct electron transfer) [260,262,263], and a few of them degrade pollutants via high-valent transition-metal induction [264,265] or combined radical and non-radical pathways [256,261, 266]. For example, studies on Co-NC [57], Co-SA [263], Co-N-C [260], Fe-SACs [267] mainly degraded pollutants through 100% selective generation of $^1O_2$, whose mechanisms could be summarized as follows: 1) PMS spontaneously decomposed to OH* and SO_4* by bonding with TM-N_4 sites to help produce oxygen-containing intermediates, and then oxygen-containing intermediates were adsorbed on TM-N_4 sites to generate $^1O_2$ by direct removal of H (PMS→PMS*→SO_4*+OH*→O*→$^1O_2$); 2) Single atom embedded in carbon skeleton could prevent agglomeration, increase the active sites, and reduce the leaching of transition metal ions. When x<4, the adsorption capacity of TM-N_x activity center towards PMS is enhanced [255]; When x>4, the energy of PMS adsorption and HSO_4^- desorption can be balanced, which prompts the degradation reaction to proceed at low temperature [268].

Transition metal-carbon composite material is considered as one of the most promising encapsulated catalysts in persulfate activation, which is called chainmail catalyst, because robust and flexible carbon materials allow facile incorporation of transition-metal catalysts and can protect the inner metal from harsh reaction environment [73,269,270]. Heteroatom doping serves as one of the effective strategies to enhance persulfate activation and pollutant degradation when encapsulated transition-metal nanoparticle catalysts were used. For instance, Liu et al. fabricated MoO_2-loaded iron-carbon nanocomposite (Fe/Mo-CNs) and found that doping Mo element reduced the reaction energy barrier of PMS activation, promoted the cycle of Fe^{2+}/Fe^{3+} and the generation of Fe(IV), consequently leading to a remarkable degradation efficiency of around 95% within 8 h towards bisphenol S (Fig. 17a) [34]. Nitrogen doping is the most common non-metallic element doping due to its

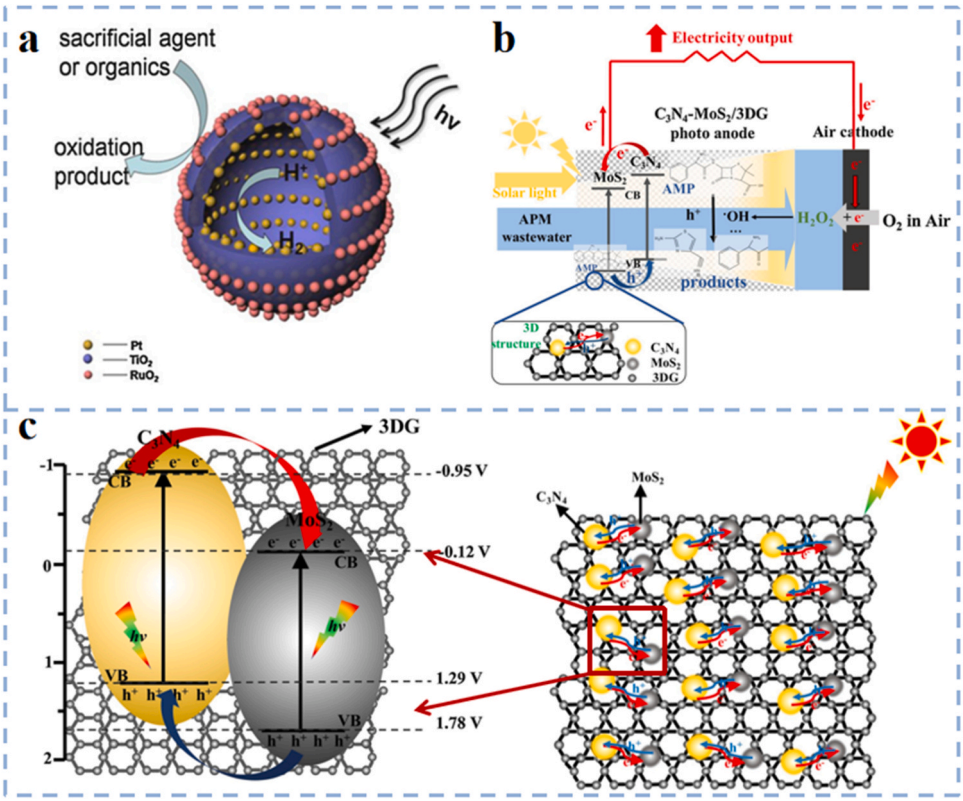

Fig. 16. (a) Mechanism of pollutant degradation and H_2 production over RuO_2@TiO_2@Pt hollow spheres. Reproduced with permission from Ref. [103]. Copyright 2016 Elsevier. (b) Schematic of ampicillin removal using C_3N_4-MoS_2/3D graphene flow-through photocatalytic system. (c) Illustration of charge transfer via the heterojunction mechanism on the C_3N_4-MoS_2/3D graphene composite. Reproduced with permission from Ref. [253]. Copyright 2022 Elsevier.

similar atomic radius and electronnegativity to carbon. Nitrogen doping can trigger obvious bond disorders and lattice distortion, promoting the oxidation reaction reaction. In addition, the doping of sulfur or phosphorus can reduce the energy gap to increase the electron transfer efficiency, while the doping of electron-deficient boron will regulate the electronic structure of the encapsulated catalyst and thus affect the catalytic activity [71,72,271,272]. For example, Yao's group explored the PS activation for dye degradation by metal nanocrystals (Fe, Co, or Ni) encapsulated in N-doped carbon nanotubes [72] as well as Fe nanoparticles encapsulated in B, N-codoped carbon nanotubes [71]. Results revealed that the synergy between the metal nanocrystals and heteroatom-doped carbon contributed to the excellent catalytic performance (Fig. 17b-c).

Defect engineering is another effective strategy to modulate the electronic structure and active centers in encapsulated transition-metal catalysts. V_o, the most common anion defect in encapsulated transition-metal catalysts, can help electron-deficient transition metals to extract electrons from pollutants [189,273–276]. Recent reports generally reveal that V_o-containing encapsulated transition-metal catalysts induce PMS activation to degrade organic pollutants mainly attributed to $^1O_2$ [189,273,274]. For example, Wu et al. used Fe-Co LDH catalyst containing V_o to activate PMS for bisphenol A degradation, and found that bisphenol A was completely degraded in the presence of O_2 within 10 min [274]. As shown in Fig. 18a, V_o on Fe-Co LDH enriched a large number of electrons and generated an internal electron-rich electric field, which promoted the formation of $^1O_2$. And due to the natural affinity of V_o towards O atoms, $^1O_2$ was localized near V_o and promoted the accumulation of O_2, which in turn accelerated the nano-confined electron recycling process in the reaction and promoted the decomposition of bisphenol A. Meanwhile, the introduction of quantum dots into lattice V_o can adjust the transition metal-oxygen bonds covalency, thereby influencing the PMS activation [277,278]. In the Co (II)-FCQDs/FNS/PMS/metronidazole system, the formation of octahedral Co(II) species within the lattice V_o significantly enhanced the charge transfer along the Co-O-Fe bond, resulting in an accelerated recycling process of Fe^{2+}/Fe^{3+} and Co^{2+}/Co^{3+} (Fig. 18b) [277]. V_n is also a common anionic defect [190,279,280]. In LMCN/PMS/tetracycline or sulfamethoxazole systems, V_n on LMCN could capture electrons from the neighboring carbon, prompting the oxidation of tetracycline via direct electron transfer or formation of surface complexes with sulfamethoxazole (Fig. 18c) [279]. Furthermore, sulfur vacancy (S_v) can modulate the surface electronic structure and geometry of encapsulated transition-metal catalyst, thereby improving the catalytic activity [281–284].

Morphology control can enhance the catalytic activity of ensupsulated transition-metal catalyst by increasing the number of active sites. Nanoreactors are one of the most commonly used methods for functionalizing transition-metal catalysts in recent years, and the common nanoreactors are mainly yolk-shell structures [101,106,285,286], core-shell structures [287], and mesoporous structures [288]. The nanoreactor creates a tailored microenvironment that offers the necessary driving force for pollutant adsorption and degradation. Moreover, active sites can be strategically positioned within core or incorporated in the voids of the nanoreactor, thereby enhancing stability and maximizing the exposure of the active centers [101,155,287–289]. For example, Zhang et al. developed MOF-derived Co-Fe N-doped graphite carbon@glutaraldehyde crosslinked chitosan (CoFe/NC@GCS) micro-nanoreactor with good synergistic effects between adsorption and PMS activation. They found that sulfamethoxazole and PMS were adsorbed by active moieties of chitosan on CoFe/NC@GCS micro-nanoreactor, and the -NH_2 and -OH moieties surrounding Co-Fe/NC formed an electron-rich microenvironment and facilitated the rapid pre-adsorption PMS to Co-Fe/NC, which shortened the radical and non-radical pathways, and accelerated the activation of PMS as well as

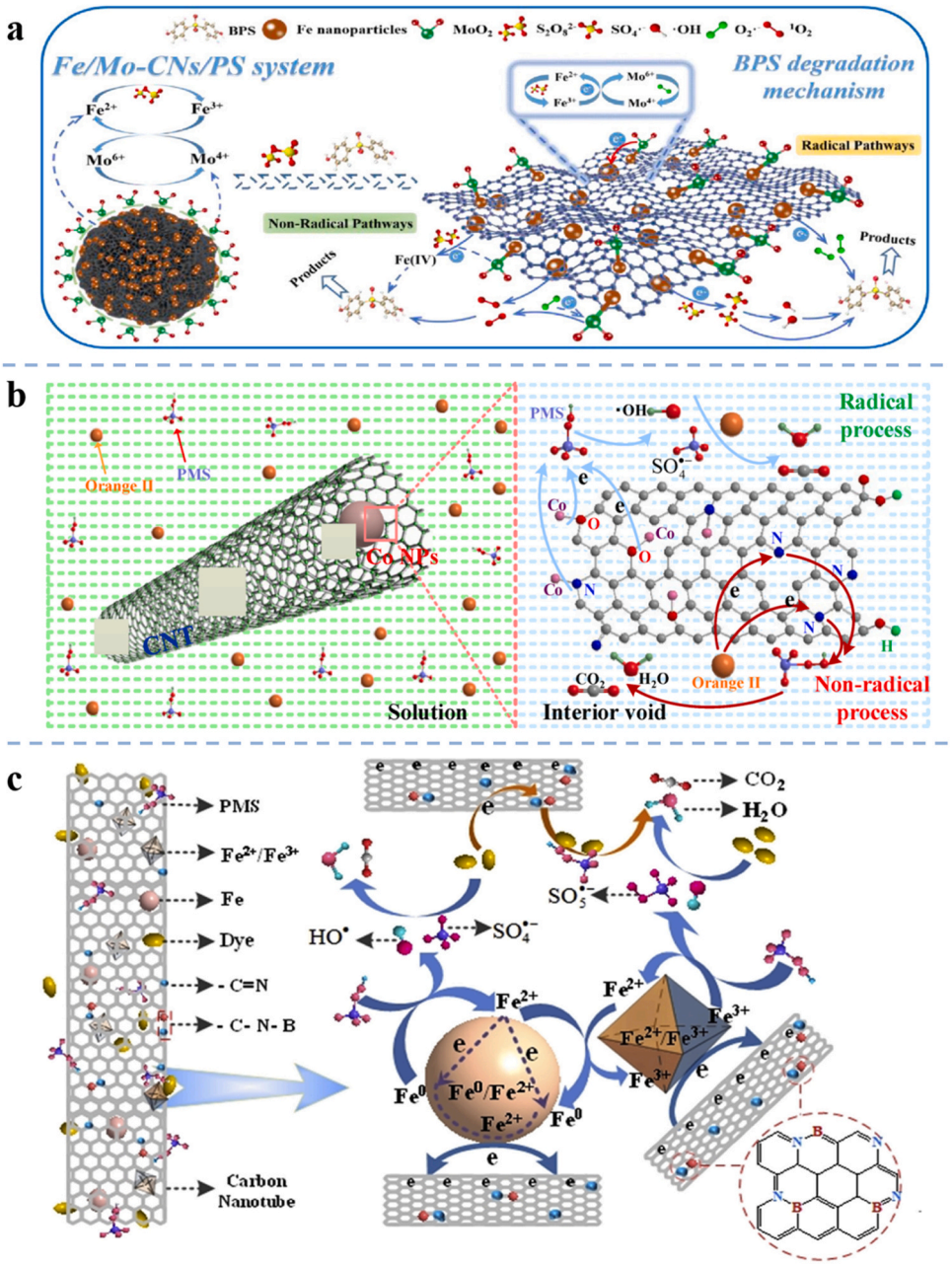

Fig. 17. (a) Mechanism for bisphenol S degradation in the Fe/Mo-CNs/PS system. Reproduced with permission from Ref. [34]. Copyright 2022 Elsevier. (b) Mechanism for dye degradation in the Co@N-C/PMS system. Reproduced with permission from Ref. [72]. Copyright 2016 Elsevier. (c) Mechanism for dye degradation in the Fe@C-BN/PMS system. Reproduced with permission from Ref. [71]. Copyright 2016 Elsevier.

the conversion of $Co^0 \rightarrow Co^{2+} \rightleftharpoons Co^{3+}$ and $Fe^0 \rightarrow Fe^{2+} \rightleftharpoons Fe^{3+}$, thereby promoting the degradation of sulfamethoxazole (Fig. 19a-b) [286]. Hierarchical nanovesicles are a relatively novel nanoreactor. In contrast to conventional core-shell catalysts, the $FeCu_{1.5}O_3$ was embedded within hollow zeolite spheres, and these zeolite sphere units were arranged into layered nanovesicles. A great number of $^1O_2$ was generated via PMS activation because of the synergy between the bimetallic redox pair and the hierarchical nano-vesicle structure, which presented an outstanding removal performance towards bisphenol A [290]. The hollow multi-shell structure provides ample void space that can effectively capture pollutants on the active sites, which can better exert multiple nano-confinement functions and lead to a significant acceleration of reaction kinetics and improvement in the catalytic performance, and the common catalysts include NiO with hollow multi-shell structure (HoMS) (Fig. 19c-h) [291], Co_3O_4 HoMSs [84,292], multishelled Co-P [293], etc.

In addition, the self-assembly of nanocrystals into 2D structured superlattices is one of the effective methods for functionalization of encapsulated transition-metal catalysts. In the system of 2D $FeSe_{2+x}$@C NCSLs/PMS/diatrizoic acid, the 2D layered structure of $FeSe_{2+x}$@C NCSLs played a crucial role in enabling efficient mass transfer and maximizing the exposure of active centers. The tightly ordered superlattice structure further enhanced the stability of the catalyst. Moreover, the presence of unsaturated selenium optimized the electronic structure of the iron active centers and promoted the Fe^{2+}/Fe^{3+} conversion, and enhance the catalytic activity (Fig. 19i-j) [294].

In addition, coupling with other technologies will also improve the ability of PS activation to catalyze the degradation of pollutants. Photo-assisted PS activation is a recent research hotspot in the degradation of pollutants. The strategy of consuming photogenerated electrons by PS molecules is considered to be an effective way to simultaneously inhibit

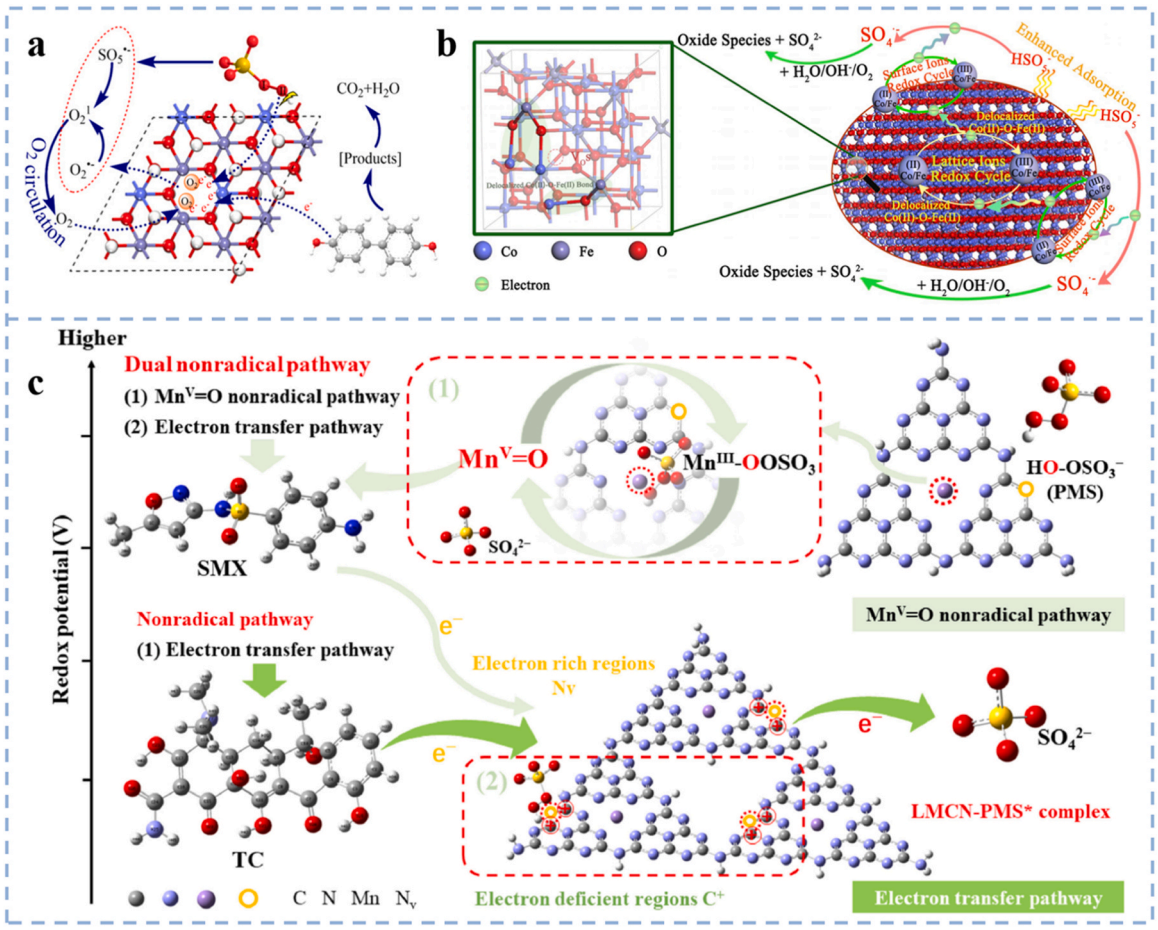

Fig. 18. (a) Illustration of the non-radical oxidation of bisphenol A in the 200Fe–Co LDH/PMS system. Reproduced with permission from Ref. [274]. Copyright 2021 American Chemical Society. (b) The mechanism of Co(II)-FCQDs/FNS for PMS activation. Reproduced with permission from Ref. [277]. Copyright 2022 Elsevier. (c) Degradation mechanism of tetracycline and sulfamethoxazole in the LMCN/PMS system. Reproduced with permission from Ref. [279]. Copyright 2023 Elsevier.

charge carrier recombination and activate PS [190,295,296]. For example, $FeCoO_x$/CN-V_n [280] and $NiCo_2O_4$/g-C_3N_4-N_{vac} [296] were used in PS activation to degrade pollutant, and the mechanism could be summarized as the following aspects: 1) V_n as an anion defect could cause the redistribution of electron density in g-C_3N_4 and provide a large number of unpaired electrons for PS activation; 2) V_n provided abundant photogenerated electrons, accelerating the cycle of Fe^{3+}/Fe^{2+} and Co^{3+}/Co^{2+}, Ni^{3+}/Ni^{2+} and Co^{3+}/Co^{2+}, promoted the generation of $\bullet SO_4^-$ and •OH; 3) The embedding of bimetallic nanoparticles in g-C_3N_4 could prevent agglomeration, increase active sites, and reduce leaching (Fig. 20a-b). Furthermore, flow-through design nanohybrid filter can be rationally employed in electro-PMS activation to achieve ultrafast removal of pollutants [75,297,298]. Jin et al. [60] found that iron single-atom (Fe-SA) functionalized charged Mxene filters (Fe-SA/$Mo_2TiC_2T_x$) could completely degrade sulfamethoxazole in one-way mode because Fe-SA anchored to Mo vacancies could form covalent bonds (Fe-O_6) with the surrounding O atoms to promote the production of $\bullet SO_4^-$ in the presence of an electric field, which facilitated the degradation of sulfamethoxazole.

4.4. Other applications

Recently, peracetic acid (PAA, $CH_3C(O)OOH$) activation has attracted much attention in wastewater treatment. Compared with persulfate activation, PAA activation not only provides disinfection performance but also minimizes the generation of harmful by-products. Meanwhile, PAA activation can address the issue that the efficiency of •OH-based AOPs may be limited in complex aqueous matrices containing •OH radical scavengers such as carbonate/bicarbonate anions and natural organic matter. However, PAA activation cannot efficiently mineralize organic pollutants due to its high selectivity and relatively low oxidation potential [299]. In previous studies, many strategies such as ultraviolet activation, heat activation, ultrasound activation, and alkali activation have been used for PAA activation to degrade organic pollutant [299,300]. Recent studies have focused on PAA activation to degrade pollutant by encapsulated transition-metal nanoparticle catalysts, because nano-confined domain effect can encapsulate short-lived ROS and reactants within the critical diffusion range length [61,301–303]. A typical example was the Co_3O_4-in-CNT and Co_3O_4-out-CNT prepared by Liu et al. [61], who found that the nano-confinement of the Co_3O_4 site greatly promoted PAA activation, and the bisphenol A degradation efficiency in Co_3O_4-in-CNT/PAA after 10 cycles showed almost no decrease compared to Co_3O_4-out-CNT/PAA (95% vs. 70%), which was mainly due to the fact that the Co leached from the latter was much higher than that from the former (52.5 μg/L vs. 0.5 μg/L). Additionally, they demonstrated that confinement of Co_3O_4 in the cavity of CNT was helpful to promote PAA activation to degrade bisphenol A in terms of reactant enrichment, electron-metal-carrier interaction effect, and mass transfer effect (Fig. 21a-d).

Periodate (PI)-based AOPs have also attracted increasing attention due to their ability to remove certain persistent organic pollutants. Compared with H_2O_2 and persulfate activation, PI activation has better thermal stability and is convenient for transportation and storage [59,304,305]. However, similar to PS activation and PAA activation, PI activation alone cannot effectively mineralize organic matter. To date, many studies on PI activation have been reported, such as ultraviolet

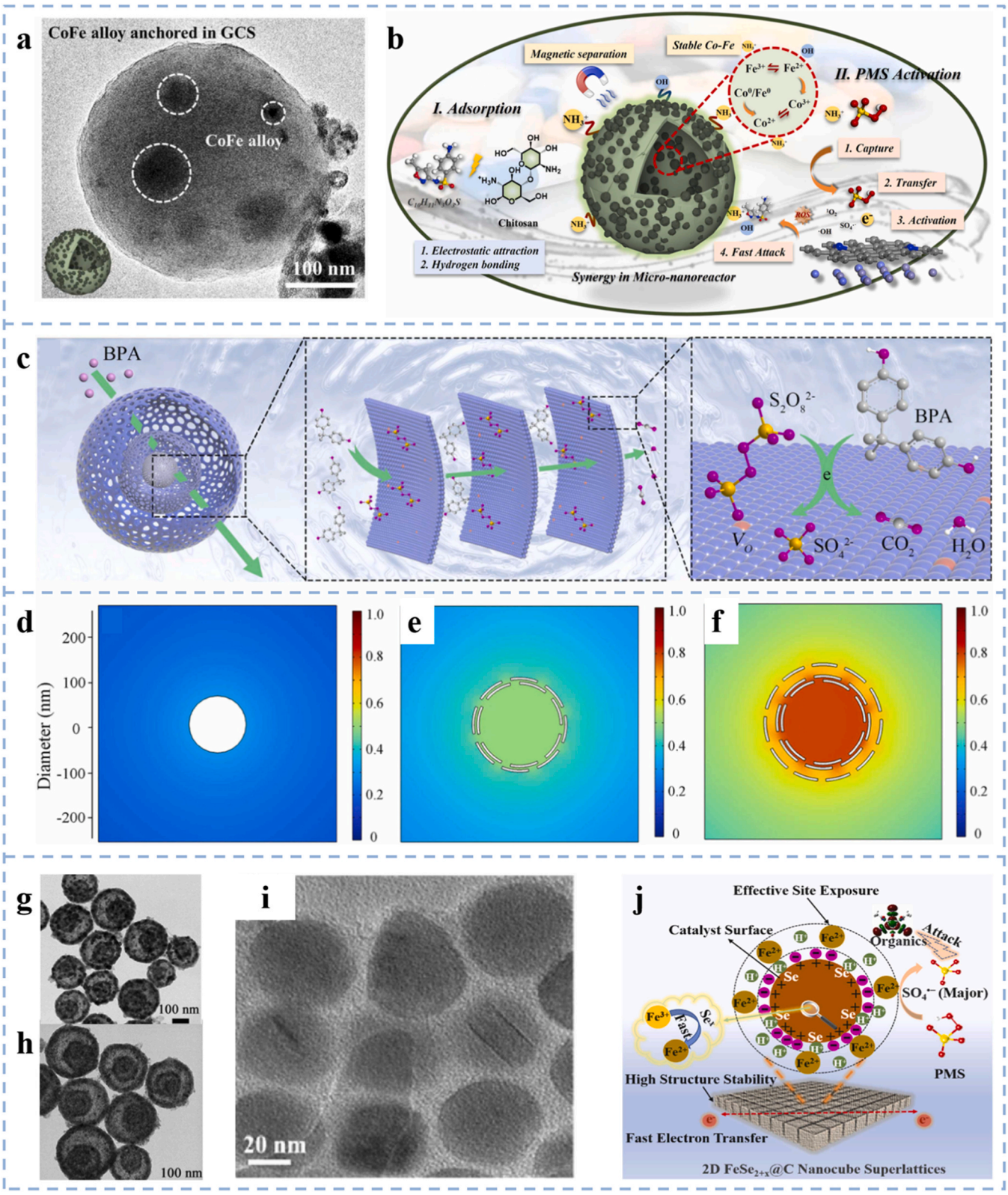

Fig. 19. (a) TEM image of CoFe/NC@GCS micro-nano reactor. (b) Degradation mechanism of sulfamethoxazole with Co-Fe/NC$^{0.7}$@GCS micro-nanoreactor. Reproduced with permission from Ref. [155]. Copyright 2022 Elsevier. (c) The mechanism of the NiO HoMS/persulfate/bisphenol A system. The FEM simulated concentration gradient distribution of bisphenol A and its degradation intermediates over (d) NiO nanoparticle, (e) two-shelled and (f) three-shelled NiO HoMS nanospheres. The TEM images of (g) two-shelled and (h) three-shelled NiO HoMS. Reproduced with permission from Ref. [291]. Copyright 2023 Elsevier. (i) TEM image of $FeSe_{2+x}$@C NCSLs. (j) Degradation mechanism of diatrizoic acid by 2D $FeSe_{2+x}$@C-3 nanocube superlattice. Reproduced with permission from Ref. [294]. Copyright 2023 Elsevier.

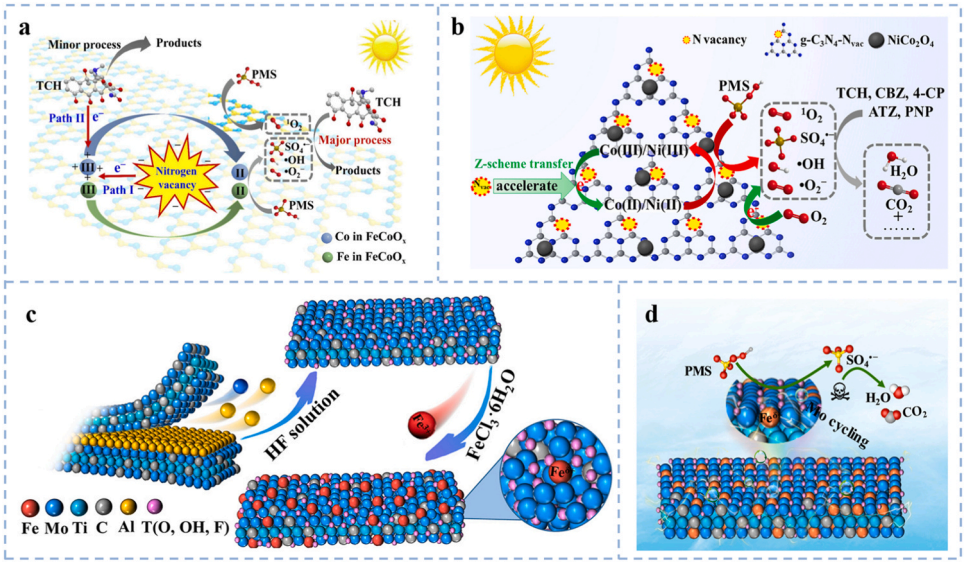

Fig. 20. (a) Schematic of dual-path electron transfer to $FeCoO_x$/CN-V_n for PMS activation. Reproduced with permission from Ref. [280]. Copyright 2022 Elsevier. (b) Schematic of tetracycline hydrochloride degradation over 15% $NiCo_2O_4$/g-C_3N_4-N_{vac} in PMS/vis system. Reproduced with permission from Ref. [296]. Copyright 2021 Elsevier. (c) Preparation of the Fe-SA/$Mo_2TiC_2T_x$ filter. (d) Schematic of sulfamethoxazole degradation by Fe-SA/$Mo_2TiC_2T_x$ filter via electro-PMS activation. Reproduced with permission from Ref. [60]. Copyright 2022 American Chemical Society.

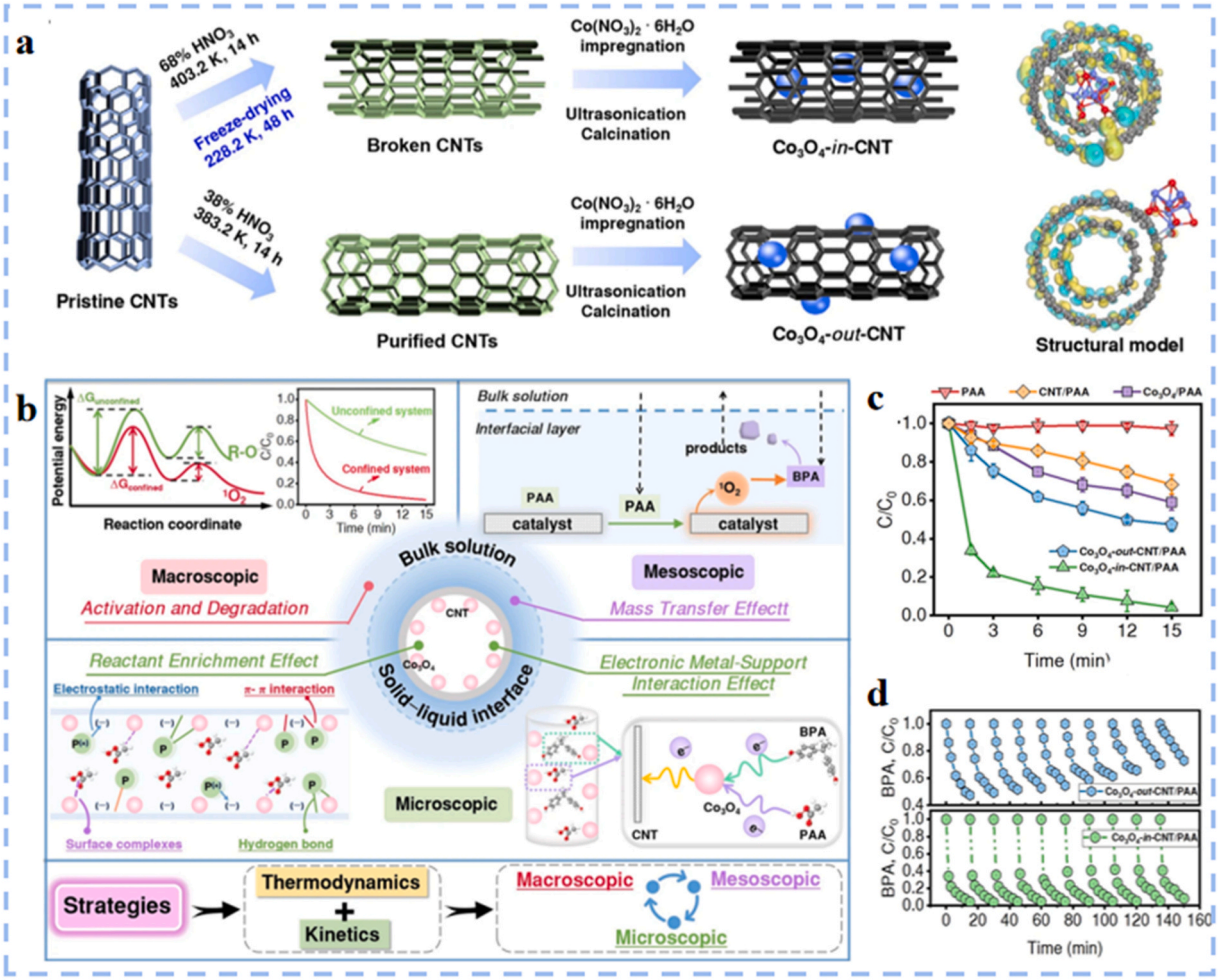

Fig. 21. (a) Synthetic process of the Co_3O_4-in-CNT and Co_3O_4-out-CNT. (b) Strategies to elucidate the internal principle of Fenton-like reaction from macroscopic, mesoscopic and microscopic dimensions. (c) Removal of BPA in various reaction systems. (d) Cyclic test of nanometer catalyst. Reproduced with permission from Ref. [61]. Copyright 2023 Nature.

activation, ultrasonic activation, and heterogeneous activation by encapsulated transition-metal nanoparticle catalysts, etc. [306]. For example, Guo et al. [305] synthesized Fe_2O_3-in-CNT and Fe_2O_3-out-CNT by wet chemical method and applied them for the first time in an electrochemically mediated PI activation system to degrade BPA. They found that the BPA degradation efficiency of the E/Fe_2O_3-in-CNT/PI system was 86.4%, which was about 1.3 times that of the E/Fe_2O_3-out-CNT/PI system (66.3%). And under the long-term continuous operation (48 h) in the single-pass mode, the BPA removal efficiency of the Fe_2O_3-in-CNT functional filter only decreased slightly, whereas the E/Fe_2O_3-out-CNT/PI decreased by 35.5%, which may be due to the fact that Fe_2O_3 was confined within the CNT cavity in the E/Fe_2O_3-in-CNT/PI system to minimize corrosion and leaching.

5. Conclusion and perspectives

In conclusion, recent progress in the applications of encapsulated transition-metal nanoparticles in AOPs for removal of organic contaminants and the associated reaction mechanisms have been reviewed in this article along with the overview of structure and composition types, and various synthetic methods of encapsulated transition-metal nanoparticle catalysts. Encapsulated transition-metal nanoparticle catalysts have been increasingly used in AOPs for environmental remediation and have exhibited excellent performance because of their unique properties and advantages, such as the strong interaction between the transition-metal core and the carbon shells enabling the promotion of electron transfer and enhancement of catalytic activity, the capability of encapsulated shell to protect the active transition-metal core and the ability to induce confined catalytic behaviors, and tunable surface functional groups and pore environment for selective adsorption and mass transfer, etc. It is believed that, in the future, encapsulated transition-metal nanoparticle catalysts will continue to shine in the field of water/wastewater treatment.

Although tremendous progress has been made in encapsulated transition-metal nanoparticle catalysts for AOPs, further efforts are still required. Particularly, attention should be given to the following aspects:

1) Further development of synthesis strategies. The exploration of promising synthesis strategies for encapsulated transition-metal nanoparticle catalysts needs long-term research input. High cost, low productivity, and complex synthesis process are the main problems hindering the development of encapsulated transition-metal nanoparticle catalysts. Although there are many methods for the preparation of encapsulated transition-metal nanoparticle catalysts in the existing literature, simple, green and efficient methods are few. Therefore, further development of simple and green synthesis strategies to reduce cost and increase yield is essential. There is no doubt that the emergence of new synthesis strategies will bring new vitality to the encapsulated transition-metal nanoparticle catalysts in AOPs to remove pollutants.

2) Precise synthesis. At present, most research focuses on the preparation methods of encapsulated transition-metal nanoparticle catalysts or the excellent performance in AOPs. However, the performance of encapsulated transition-metal nanoparticle catalysts is strongly influenced by their size, shape, composition, crystallinity and thickness of the encapsulation layer, and there are limited studies on the synthesis that can precisely control these factors. As mentioned above, the independent and precise control of reaction parameters during the preparation process can better regulate the structure of encapsulated transition-metal catalysts. In order to better apply the catalysts in practical applications, precise synthesis is particularly important because it can optimize the activity, stability and selectivity of the catalysts in practical applications.

3) The underlying mechanisms for pollutant removal by encapsulated transition-metal nanoparticle catalysts should be further explored as well as insight into the structure-activity relationship of encapsulated transition-metal catalysts. Although one of the purposes of synthesising encapsulated transition-metal catalysts is to establish close interaction between the active metal core and the encapsulated layer, the reaction mechanism and the relationship between the structure and performance in degrading pollutants in AOPs are still unclear in many cases, and there is still a lot of controversy about how encapsulated catalysts enhance the catalytic activity, stability and selectivity to degrade pollutants in water. In recent years, although more and more studies have used DFT calculation to elucidate the phenomena, the effort is still not enough. A combination of experimental studies, theory/modelling calculations and in-situ measurements will be conducive to better understanding of the reaction mechanism and benefit the design and fabrication of more promising encapsulated transition-metal catalysts for removal of organic pollutants.

4) There is still a long way to go for encapsulated transition-metal nanoparticle catalyst towards organic pollutant removal to develop into a “practical technology” from “promising technology”. This is primarily reflected in the following several aspects: i) To date, a majority of the relevant studies were conducted via the use of simulated water with simple composition under laboratory conditions with the reaction parameters (e.g., temperature, pH, pollutant concentration) kept unchanged. Although the laboratory data are of great value in demonstrating feasibility, the simulated water prepared from deionized water and well-controlled laboratory conditions could not represent the complication of practical scenarios with mutiple substances coexisted and reaction parameters varied. The coexisting substances and varying reaction parameters might impair the treatment performance of encapsulated transition-metal nanoparticle catalyst and even make them ineffective. To verify whether the encapsulated transition-metal catalysts is still effective under practical conditions, testing using real waters under actual scenarios is recommended, and if decline occurs, the underlying reasons should be figured out. ii) The encapsulated transition-metal catalysts used in current studies are generally prepared from laboratory-scale synthesis, and the quantity of catalysts is difficult to meet the requirements for industrialization. Meanwhile, the pollutant removal experiments are generally conducted using laboratory-scale device instead of pilot-scale or large-scale devices. Therefore, how to scale up the production of encapsulated transition-metal catalysts and the subsequent reaction process requires more research input. iii) Among AOPs using encapsulated transition-metal nanoparticle catalysts, most of the current literature focuses on the degradation of dye and antibiotic contaminants. To broaden the application scenarios, a wider range of persistent organic pollutants can be selected for future studies.

5) Environmental risks. Due to the complexity of environmental factors, the environmental risk of the encapsulated transition-metal catalyst should be investigated prior to large-scale application, as such confirmation is important to ensure environmental safety. When the encapsulated transition-metal catalyst is used in AOPs to remove pollutants from the aqueous environment, a small amount of metal leaching may be released into the water, causing secondary contamination. Although the nano-confined domain effect of encapsulated transition-metals inhibits the leaching of metals, it cannot completely prevent the leaching of metals. Common semiconductors such as TiO_2, CuO, etc. are usually considered toxic substances, and iron oxide particles including Fe_2O_3 and Fe_3O_4 are considered non-toxic or low-toxic substances. Meanwhile, when using encapsulated transition-metal catalysts to degrade pollutants, intermediates with higher biotoxicity than the original pollutant may be produced. In most cases, pollutants are not fully mineralized but partially oxidized to unharmful CO_2, H_2O and inorganic ions, which may increase the complexity of water bodies and may threaten the health of humans, organisms and ecosystems to some extent. Therefore, the environmental risks of encapsulated transition-metal nanoparticle catalysts should be studied more systematically and comprehensively to guarantee human health and environmental safety.

Declaration of Competing Interest

The authors declare that they have no known competing financial interests or personal relationships that could have appeared to influence the work reported in this paper.

Data Availability

Data will be made available on request.

Acknowledgements

This study was financially supported by the National Natural Science Foundation of China (22276048), the Research and Development Plan of Key Areas in Hunan Province (2022SK2066), the Natural Science Foundation of Hunan Province (2021JJ30125), and the Scientific Research Project of Hunan Provincial Education Department (20K032).

Appendix A. Supporting information

Supplementary data associated with this article can be found in the online version at doi:10.1016/j.apcatb.2023.123401.

References

[1] W.X. Li, J. Cao, W.P. Xiong, Z.H. Yang, S.W. Sun, M.Y. Jia, Z.Y. Xu, In-situ growing of metal-organic frameworks on three-dimensional iron network as an efficient adsorbent for antibiotics removal, Chem. Eng. J. 392 (2020), 124844.
[2] C. Zhang, C. Lai, G. Zeng, D. Huang, C. Yang, Y. Wang, Y. Zhou, M. Cheng, Efficacy of carbonaceous nanocomposites for sorbing ionizable antibiotic sulfamethazine from aqueous solution, Water Res 95 (2016) 103–112.
[3] Z. Lu, Q. Yang, T. Hu, J. Wang, W. Tang, FeIIAlIII layered double hydroxide modified carbon-felt cathode for efficient electrochemical reduction of bromate, Chem. Eng. J. 446 (2022), 137356.
[4] J. Du, T.D. Waite, J. Feng, Y. Lei, W. Tang, Coupled electrochemical methods for nitrogen and phosphorus recovery from wastewater: a review, Environ. Chem. Lett. 21 (2023) 885–909.
[5] E.D. Brown, G.D. Wright, Antibacterial drug discovery in the resistance era, Nature 529 (2016) 336–343.
[6] J. Zhang, S. Qiu, H. Feng, T. Hu, Y. Wu, T. Luo, W. Tang, D. Wang, Efficient degradation of tetracycline using core–shell Fe@Fe2O3-CeO2 composite as novel heterogeneous electro-Fenton catalyst, Chem. Eng. J. 428 (2022), 131403.
[7] Y. Yang, X. Zhang, J. Jiang, J. Han, W. Li, X. Li, K.M. Yee Leung, S.A. Snyder, P.J. J. Alvarez, Which micropollutants in water environments deserve more attention globally? Environ. Sci. Technol. 56 (2022) 13–29.
[8] J.L.P. Van Oorschot, P.H. Van Leeuwen, Inhibition of photosynthesis in intact plants of biotypes resistant or susceptible to atrazine and cross-resistance to other herbicides, Weed Res. 28 (1988) 223–230.
[9] Z. Wang, X. Sun, S. Ru, J. Wang, J. Xiong, L. Yang, L. Hao, J. Zhang, X. Zhang, Effects of co-exposure of the triazine herbicides atrazine, prometryn and terbutryn on Phaeodactylum tricornutum photosynthesis and nutritional value, Sci. Total Environ. 807 (2022), 150609.
[10] L. Yang, H. Li, Y. Zhang, N. Jiao, Environmental risk assessment of triazine herbicides in the Bohai Sea and the Yellow Sea and their toxicity to phytoplankton at environmental concentrations, Environ. Int. 133 (2019), 105175.
[11] S. Singh, V. Kumar, A. Chauhan, S. Datta, A.B. Wani, N. Singh, J. Singh, Toxicity, degradation and analysis of the herbicide atrazine, Environ. Chem. Lett. 16 (2018) 211–237.
[12] J. Zhang, D. Wang, F. Zhao, J. Feng, H. Feng, J. Luo, W. Tang, Ferrate modified carbon felt as excellent heterogeneous electro-Fenton cathode for chloramphenicol degradation, Water Res 227 (2022), 119324.
[13] B. Berendsen, L. Stolker, J. de Jong, M. Nielen, E. Tserendorj, R. Sodnomdarjaa, A. Cannavan, C. Elliott, Evidence of natural occurrence of the banned antibiotic chloramphenicol in herbs and grass, Anal. Bioanal. Chem. 397 (2010) 1955–1963.
[14] Z. Alam, T. Coyle, GATA2 mutation in twins with transient aplastic anemia after chloramphenicol exposure; a follow up to nagao and mauer 1969, Blood 136 (2020) 4–5.
[15] W. Jin, J. Feng, W. Xing, W. Tang, Significantly enhanced electrocatalytic reduction of chloramphenicol from water mediated by Fe–F–N Co-doped carbon materials, ACS EST Water 3 (2023) 1385–1394.
[16] J. Wang, R. Zhuan, Degradation of antibiotics by advanced oxidation processes: An overview, Sci. Total Environ. 701 (2020), 135023.
[17] D. Ma, H. Yi, C. Lai, X. Liu, X. Huo, Z. An, L. Li, Y. Fu, B. Li, M. Zhang, L. Qin, S. Liu, L. Yang, Critical review of advanced oxidation processes in organic wastewater treatment, Chemosphere 275 (2021), 130104.
[18] Y. Yang, X. Li, C. Zhou, W. Xiong, G. Zeng, D. Huang, C. Zhang, W. Wang, B. Song, X. Tang, X. Li, H. Guo, Recent advances in application of graphitic carbon nitride-based catalysts for degrading organic contaminants in water through advanced oxidation processes beyond photocatalysis: A critical review, Water Res 184 (2020), 116200.
[19] J. Du, T.D. Waite, P.M. Biesheuvel, W. Tang, Recent advances and prospects in electrochemical coupling technologies for metal recovery from water, J. Hazard. Mater. 442 (2023), 130023.
[20] J. Lee, U. von Gunten, J.-H. Kim, Persulfate-based advanced oxidation: critical assessment of opportunities and roadblocks, Environ. Sci. Technol. 54 (2020) 3064–3081.
[21] J. Wang, S. Wang, Reactive species in advanced oxidation processes: formation, identification and reaction mechanism, Chem. Eng. J. 401 (2020), 126158.
[22] U. Ushani, X. Lu, J. Wang, Z. Zhang, J. Dai, Y. Tan, S. Wang, W. Li, C. Niu, T. Cai, N. Wang, G. Zhen, Sulfate radicals-based advanced oxidation technology in various environmental remediation: a state-of-the–art review, Chem. Eng. J. 402 (2020), 126232.
[23] S. Li, Y. Yang, H. Zheng, Y. Zheng, T. Jing, J. Ma, J. Nan, Y.K. Leong, J.-S. Chang, Advanced oxidation process based on hydroxyl and sulfate radicals to degrade refractory organic pollutants in landfill leachate, Chemosphere 297 (2022), 134214.
[24] X. Duan, H. Sun, Z. Shao, S. Wang, Nonradical reactions in environmental remediation processes: uncertainty and challenges, Appl. Catal. B-Environ. 224 (2018) 973–982.
[25] M. Kohantorabi, G. Moussavi, S. Giannakis, A review of the innovations in metal- and carbon-based catalysts explored for heterogeneous peroxymonosulfate (PMS) activation, with focus on radical vs. non-radical degradation pathways of organic contaminants, Chem. Eng. J. 411 (2021), 127957.
[26] H. Fu, H. Luo, Q. Lin, Q. Zhong, Z. Huang, Y. Wang, L. Wu, Transformation to nonradical pathway for the activation of peroxydisulfate after doping S into Fe3C-encapsulated N/S-codoped carbon nanotubes, Chem. Eng. J. 409 (2021), 128201.
[27] G. Lama, J. Meijide, A. Sanromán, M. Pazos, Heterogeneous advanced oxidation processes: current approaches for wastewater treatment, Catalysts 12 (2022) 344.
[28] A. Mirzaei, Z. Chen, F. Haghighat, L. Yerushalmi, Removal of pharmaceuticals from water by homo/heterogonous Fenton-type processes – a review, Chemosphere 174 (2017) 665–688.
[29] M.M. Bello, A.A. Abdul Raman, A. Asghar, A review on approaches for addressing the limitations of Fenton oxidation for recalcitrant wastewater treatment, Process. Saf. Environ. Prot. 126 (2019) 119–140.
[30] A. Kumar, A. Rana, G. Sharma, M. Naushad, P. Dhiman, A. Kumari, F.J. Stadler, Recent advances in nano-Fenton catalytic degradation of emerging pharmaceutical contaminants, J. Mol. Liq. 290 (2019), 111177.
[31] C. Lai, X. Shi, L. Li, M. Cheng, X. Liu, S. Liu, B. Li, H. Yi, L. Qin, M. Zhang, N. An, Enhancing iron redox cycling for promoting heterogeneous Fenton performance: A review, Sci. Total Environ. 775 (2021), 145850.
[32] Y. Zhu, R. Zhu, Y. Xi, J. Zhu, G. Zhu, H. He, Strategies for enhancing the heterogeneous Fenton catalytic reactivity: a review, Appl. Catal. B-Environ. 255 (2019), 117739.
[33] Y. Liu, M. Cheng, Z. Liu, G. Zeng, H. Zhong, M. Chen, C. Zhou, W. Xiong, B. Shao, B. Song, Heterogeneous Fenton-like catalyst for treatment of rhamnolipid-solubilized hexadecane wastewater, Chemosphere 236 (2019), 124387.
[34] Z. Liu, S. Pan, F. Xu, Z. Wang, C. Zhao, X. Xu, B. Gao, Q. Li, Revealing the fundamental role of MoO2 in promoting efficient and stable activation of persulfate by iron carbon based catalysts: Efficient Fe2+/Fe3+ cycling to generate reactive species, Water Res 225 (2022), 119142.
[35] F. Lu, D. Astruc, Nanocatalysts and other nanomaterials for water remediation from organic pollutants, Coord. Chem. Rev. 408 (2020).
[36] J. Radjenovic, D.L. Sedlak, Challenges and opportunities for electrochemical processes as next-generation technologies for the treatment of contaminated water, Environ. Sci. Technol. 49 (2015) 11292–11302.
[37] B.C. Hodges, E.L. Cates, J.H. Kim, Challenges and prospects of advanced oxidation water treatment processes using catalytic nanomaterials, Nat. Nanotechnol. 13 (2018) 642–650.
[38] J. Deng, D. Deng, X. Bao, Robust catalysis on 2D materials encapsulating metals: concept, application, and perspective, Adv. Mater. 29 (2017) 1606967.
[39] L. Yu, D. Deng, X. Bao, Chain mail for catalysts, Angew. Chem. Int. Ed. Engl. 59 (2020) 15294–15297.
[40] C. Gao, F. Lyu, Y. Yin, Encapsulated metal nanoparticles for catalysis, Chem. Rev. 121 (2021) 834–881.
[41] N. Wang, Q.M. Sun, J.H. Yu, Ultrasmall metal nanoparticles confined within crystalline nanoporous materials: a fascinating class of nanocatalysts, Adv. Mater. 31 (2019) 1803966.
[42] T.W. van Deelen, C.H. Mejia, K.P. de Jong, Control of metal-support interactions in heterogeneous catalysts to enhance activity and selectivity, Nat. Catal. 2 (2019) 955–970.
[43] Y. Wu, X. Chen, Y. Han, D. Yue, X. Cao, Y. Zhao, X. Qian, Highly efficient utilization of nano-Fe(0) embedded in mesoporous carbon for activation of peroxydisulfate, Environ. Sci. Technol. 53 (2019) 9081–9090.
[44] S. Zhang, J.J. Yi, J.R. Chen, Z.L. Yin, T. Tang, W.X. Wei, S.S. Cao, H. Xu, Spatially confined Fe2O3 in hierarchical SiO2@TiO2 hollow sphere exhibiting superior photocatalytic efficiency for degrading antibiotics, Chem. Eng. J. 380 (2020), 122583.
[45] D. Thanh Tran, T. Kshetri, N. Dinh Chuong, J. Gautam, H. Van Hien, L. Huu Tuan, N.H. Kim, J.H. Lee, Emerging core-shell nanostructured catalysts of transition metal encapsulated by two-dimensional carbon materials for electrochemical applications, Nano Today 22 (2018) 100–131.

[46] Z.X. Cai, Z.L. Wang, J. Kim, Y. Yamauchi, Hollow functional materials derived from metal-organic frameworks: synthetic strategies, conversion mechanisms, and electrochemical applications, Adv. Mater. 31 (2019), e1804903.
[47] H.-p Feng, L. Tang, G.-m Zeng, J. Tang, Y.-c Deng, M. Yan, Y.-n Liu, Y.-y Zhou, X.-y Ren, S. Chen, Carbon-based core–shell nanostructured materials for electrochemical energy storage, J. Mater. Chem. A 6 (2018) 7310–7337.
[48] D. He, C. Zhang, G. Zeng, Y. Yang, D. Huang, L. Wang, H. Wang, A multifunctional platform by controlling of carbon nitride in the core-shell structure: from design to construction, and catalysis applications, Appl. Catal. B-Environ. 258 (2019), 117957.
[49] D. Xu, H. Lv, B. Liu, Encapsulation of metal nanoparticle catalysts within mesoporous zeolites and their enhanced catalytic performances: a review, Front. Chem. 6 (2018).
[50] H. Tian, X. Li, L. Zeng, J. Gong, Recent advances on the design of group VIII base-metal catalysts with encapsulated structures, ACS Catal. 5 (2015) 4959–4977.
[51] T. Zhao, X. Huang, R. Cui, W. Han, G. Zhang, Z. Tang, Design of confined catalysts and applications in environmental catalysis: original perspectives and further prospects, J. Clean. Prod. 390 (2023), 136125.
[52] P.I. Dosa, C. Erben, V.S. Iyer, K.P.C. Vollhardt, I.M. Wasser, Metal encapsulating carbon nanostructures from oligoalkyne metal complexes, J. Am. Chem. Soc. 121 (1999) 10430–10431.
[53] R. Chalasani, S. Vasudevan, Cyclodextrin-functionalized Fe3O4@TiO2: reusable, magnetic nanoparticles for photocatalytic degradation of endocrine-disrupting chemicals in water supplies, ACS Nano 7 (2013) 4093–4104.
[54] C. Liu, J. Li, J. Qi, J. Wang, R. Luo, J. Shen, X. Sun, W. Han, L. Wang, Yolk–Shell Fe0@SiO2 nanoparticles as nanoreactors for fenton-like catalytic reaction, ACS Appl. Mater. Interfaces 6 (2014) 13167–13173.
[55] Y. Wang, H. Zhao, G. Zhao, Iron-copper bimetallic nanoparticles embedded within ordered mesoporous carbon as effective and stable heterogeneous Fenton catalyst for the degradation of organic contaminants, Appl. Catal. B-Environ. 164 (2015) 396–406.
[56] X. Qian, M. Ren, Y. Zhu, D. Yue, Y. Han, J. Jia, Y. Zhao, Visible light assisted heterogeneous fenton-like degradation of organic pollutant via alpha-FeOOH/mesoporous carbon composites, Environ. Sci. Technol. 51 (2017) 3993–4000.
[57] X. Li, X. Huang, S. Xi, S. Miao, J. Ding, W. Cai, S. Liu, X. Yang, H. Yang, J. Gao, J. Wang, Y. Huang, T. Zhang, B. Liu, Single cobalt atoms anchored on porous N-doped graphene with dual reaction sites for efficient fenton-like catalysis, J. Am. Chem. Soc. 140 (2018) 12469–12475.
[58] K. Liu, M. Yu, H. Wang, J. Wang, W. Liu, M.R. Hoffmann, Multiphase porous electrochemical catalysts derived from iron-based metal–organic framework compounds, Environ. Sci. Technol. 53 (2019) 6474–6482.
[59] Y. Long, J. Dai, S. Zhao, Y. Su, Z. Wang, Z. Zhang, Atomically dispersed cobalt sites on graphene as efficient periodate activators for selective organic pollutant degradation, Environ. Sci. Technol. 55 (2021) 5357–5370.
[60] L. Jin, S. You, N. Ren, B. Ding, Y. Liu, Mo vacancy-mediated activation of peroxymonosulfate for ultrafast micropollutant removal using an electrified MXene filter functionalized with Fe single atoms, Environ. Sci. Technol. 56 (2022) 11750–11759.
[61] T. Liu, S. Xiao, N. Li, J. Chen, X. Zhou, Y. Qian, C.-H. Huang, Y. Zhang, Water decontamination via nonradical process by nanoconfined Fenton-like catalysts, Nat. Commun. 14 (2023) 2881.
[62] A.M. El-Toni, M.A. Habila, J.P. Labis, Z.A. Alothman, M. Alhoshan, A. A. Elzatahry, F. Zhang, Design, synthesis and applications of core–shell, hollow core, and nanorattle multifunctional nanostructures, Nanoscale 8 (2016) 2510–2531.
[63] X. Yin, L. Yang, Q. Gao, Core–shell nanostructured electrocatalysts for water splitting, Nanoscale 12 (2020) 15944–15969.
[64] M. Li, Y. Yang, D. Yu, W. Li, X. Ning, R. Wan, H. Zhu, J. Mao, Recent advances on the construction of encapsulated catalyst for catalytic applications, Nano Res 16 (2023) 3451–3474.
[65] M. Si, F. Lin, H. Ni, S. Wang, Y. Lu, X. Meng, Research progress of yolk–shell structured nanoparticles and their application in catalysis, RSC Adv. 13 (2023) 2140–2154.
[66] S. Das, J. Pérez-Ramírez, J. Gong, N. Dewangan, K. Hidajat, B.C. Gates, S. Kawi, Core–shell structured catalysts for thermocatalytic, photocatalytic, and electrocatalytic conversion of CO_2, Chem. Soc. Rev. 49 (2020) 2937–3004.
[67] W. Zhang, K. Zhu, W. Ren, H. He, H. Liang, Y. Zhai, W. Li, Recent advances in the marriage of catalyst nanoparticles and mesoporous supports, Adv. Mater. Interfaces 9 (2022) 2101528.
[68] J. Du, W. Xing, J. Yu, J. Feng, L. Tang, W. Tang, Synergistic effect of intercalation and EDLC electrosorption of 2D/3D interconnected architectures to boost capacitive deionization for water desalination via MoSe2/mesoporous carbon hollow spheres, Water Res 235 (2023), 119831.
[69] S. Li, J. Gong, Strategies for improving the performance and stability of Ni-based catalysts for reforming reactions, Chem. Soc. Rev. 43 (2014) 7245–7256.
[70] Y. Ma, X. Lv, D. Xiong, X. Zhao, Z. Zhang, Catalytic degradation of ranitidine using novel magnetic Ti3C2-based MXene nanosheets modified with nanoscale zero-valent iron particles, Appl. Catal. B-Environ. 284 (2021), 119720.
[71] Y. Yao, H. Chen, J. Qin, G. Wu, C. Lian, J. Zhang, S. Wang, Iron encapsulated in boron and nitrogen codoped carbon nanotubes as synergistic catalysts for Fenton-like reaction, Water Res 101 (2016) 281–291.
[72] Y. Yao, H. Chen, C. Lian, F. Wei, D. Zhang, G. Wu, B. Chen, S. Wang, Fe, Co, Ni nanocrystals encapsulated in nitrogen-doped carbon nanotubes as Fenton-like catalysts for organic pollutant removal, J. Hazard. Mater. 314 (2016) 129–139.
[73] P. Duan, X. Xu, K. Guo, Q. Yue, B. Gao, Peroxymonosulfate activation on a chainmail catalyst via an electron shuttle mechanism for efficient organic pollutant removal, Appl. Catal. B-Environ. 316 (2022), 121695.
[74] Y. He, H. Qin, Z. Wang, H. Wang, Y. Zhu, C. Zhou, Y. Zeng, Y. Li, P. Xu, G. Zeng, Fe-Mn oxycarbide anchored on N-doped carbon for enhanced Fenton-like catalysis: importance of high-valent metal-oxo species and singlet oxygen, Appl. Catal. B-Environ. 340 (2024), 123204.
[75] S. Li, M. Zhou, H. Wu, G. Song, J. Jing, N. Meng, W. Wang, High-efficiency degradation of carbamazepine by the synergistic electro-activation and bimetals (FeCo@NC) catalytic-activation of peroxymonosulfate, Appl. Catal. B-Environ. 338 (2023), 123064.
[76] C. Chu, J. Yang, X. Zhou, D. Huang, H. Qi, S. Weon, J. Li, M. Elimelech, A. Wang, J.-H. Kim, Cobalt single atoms on tetrapyridomacrocyclic support for efficient peroxymonosulfate activation, Environ. Sci. Technol. 55 (2021) 1242–1250.
[77] Z. Wang, E. Almatrafi, H. Wang, H. Qin, W. Wang, L. Du, S. Chen, G. Zeng, P. Xu, Cobalt single atoms anchored on oxygen-doped tubular carbon nitride for efficient peroxymonosulfate activation: simultaneous coordination structure and morphology modulation, Angew. Chem. Int. Ed. 61 (2022), e202202338.
[78] S. Dong, X. Chen, X. Zhang, G. Cui, Nanostructured transition metal nitrides for energy storage and fuel cells, Coord. Chem. Rev. 257 (2013) 1946–1956.
[79] C. Liu, J. Li, J. Qi, J. Wang, R. Luo, J. Shen, X. Sun, W. Han, L. Wang, Yolk-shell Fe (0)@SiO2 nanoparticles as nanoreactors for fenton-like catalytic reaction, ACS Appl. Mater. Interfaces 6 (2014) 13167–13173.
[80] R. Yang, Q. Peng, B. Yu, Y. Shen, H. Cong, Yolk-shell Fe3O4@MOF-5 nanocomposites as a heterogeneous Fenton-like catalyst for organic dye removal, Sep. Purif. Technol. 267 (2021), 118620.
[81] B.-T. Zhang, Q. Wang, Y. Zhang, Y. Teng, M. Fan, Degradation of ibuprofen in the carbon dots/Fe3O4@carbon sphere pomegranate-like composites activated persulfate system, Sep. Purif. Technol. 242 (2020), 116820.
[82] B. Liu, W. Song, W. Zhang, X. Zhang, S. Pan, H. Wu, Y. Sun, Y. Xu, Fe3O4@CNT as a high-effective and steady chainmail catalyst for tetracycline degradation with peroxydisulfate activation: Performance and mechanism, Sep. Purif. Technol. 273 (2021), 118705.
[83] G.U. Rehman, M. Tahir, P.S. Goh, A.F. Ismail, A. Samavati, A.K. Zulhairun, D. Rezaei, Facile synthesis of GO and g-C3N4 nanosheets encapsulated magnetite ternary nanocomposite for superior photocatalytic degradation of phenol, Environ. Pollut. 253 (2019) 1066–1078.
[84] W. Li, X. He, B. Li, B. Zhang, T. Liu, Y. Hu, J. Ma, Structural tuning of multishelled hollow microspheres for boosted peroxymonosulfate activation and selectivity: Role of surface superoxide radical, Appl. Catal. B-Environ. 305 (2022), 121019.
[85] A. Reinholdt, J. Bendix, Transition metal carbide complexes, Chem. Rev. 122 (2022) 830–902.
[86] H. Wang, J. Li, K. Li, Y. Lin, J. Chen, L. Gao, V. Nicolosi, X. Xiao, J.-M. Lee, Transition metal nitrides for electrochemical energy applications, Chem. Soc. Rev. 50 (2021) 1354–1390.
[87] X. Xu, W. Liu, Y. Kim, J. Cho, Nanostructured transition metal sulfides for lithium ion batteries: Progress and challenges, Nano Today 9 (2014) 604–630.
[88] J.-E. Zhou, J. Chen, Y. Peng, Y. Zheng, A. Zeb, X. Lin, Metal-organic framework-derived transition metal sulfides and their composites for alkali-ion batteries: A review, Coord. Chem. Rev. 472 (2022), 214781.
[89] H. Yu, J. Ji, Q. Yan, M. Xing, Transition metal phosphides for heterogeneous Fenton-like oxidation of contaminants in water, Chem. Eng. J. 449 (2022), 137856.
[90] Y. Pei, Y. Cheng, J. Chen, W. Smith, P. Dong, P.M. Ajayan, M. Ye, J. Shen, Recent developments of transition metal phosphides as catalysts in the energy conversion field, J. Mater. Chem. A 6 (2018) 23220–23243.
[91] X. Li, W. Xing, T. Hu, K. Luo, J. Wang, W. Tang, Recent advances in transition-metal phosphide electrocatalysts: Synthetic approach, improvement strategies and environmental applications, Coordin, Chem. Rev. 473 (2022), 214811.
[92] J. Wang, J. Feng, T.-O. Soyol-Erdene, Z. Wei, W. Tang, Electrodeposited NiCoP on nickel foam as a self-supported cathode for highly selective electrochemical reduction of nitrate to ammonia, Sep. Purif. Technol. 320 (2023), 124155.
[93] Y. Zhu, S. Murali, W. Cai, X. Li, J.W. Suk, J.R. Potts, R.S. Ruoff, Graphene and Graphene Oxide: Synthesis, Properties, and Applications, Adv. Mater. 22 (2010) 3906–3924.
[94] E. Morales-Narváez, L.F. Sgobbi, S.A.S. Machado, A. Merkoçi, Graphene-encapsulated materials: Synthesis, applications and trends, Prog. Mater. Sci. 86 (2017) 1–24.
[95] A.K. Geim, K.S. Novoselov, The rise of graphene, Nat. Mater. 6 (2007) 183–191.
[96] Z. Li, Y. Wu, 2D early transition metal carbides (MXenes) for catalysis, Small 15 (2019) 1804736.
[97] A. Liu, X. Liang, X. Ren, W. Guan, M. Gao, Y. Yang, Q. Yang, L. Gao, Y. Li, T. Ma, Recent progress in mxene-based materials: potential high-performance electrocatalysts, Adv. Funct. Mater. 30 (2020) 2003437.
[98] M. Duan, L. Jiang, B. Shao, C. Feng, H. Yu, H. Guo, H. Chen, W. Tang, Enhanced visible-light photocatalytic degradation activity of Ti3C2/PDIsm via π–π interaction and interfacial charge separation: experimental and theoretical investigations, Appl. Catal. B-Environ. 297 (2021), 120439.
[99] Y. Zhou, Y. Zhang, X. Hu, Novel zero-valent Co–Fe encapsulated in nitrogen-doped porous carbon nanocomposites derived from CoFe2O4@ZIF-67 for boosting 4-chlorophenol removal via coupling peroxymonosulfate, J. Colloid Interface Sci. 575 (2020) 206–219.
[100] Y. Yao, H. Yin, Y. Zhang, F. Wei, H. Hu, Y. Tang, S. Wang, Fe, Cu-coordinated ZIF-derived bimetal encapsulated N-doped carbon nanotube for efficient remediation of various aqueous pollutants, Chem. Eng. J. 426 (2021), 131801.

[101] M. Zhang, C. Xiao, X. Yan, S. Chen, C. Wang, R. Luo, J. Qi, X. Sun, L. Wang, J. Li, Efficient removal of organic pollutants by metal–organic framework derived Co/C yolk–shell nanoreactors: size-exclusion and confinement effect, Environ. Sci. Technol. 54 (2020) 10289–10300.
[102] C. Gao, F. Lyu, Y. Yin, Encapsulated metal nanoparticles for catalysis, Chem. Rev. 121 (2021) 834–881.
[103] B. Cao, G. Li, H. Li, Hollow spherical RuO2@TiO2@Pt bifunctional photocatalyst for coupled H2 production and pollutant degradation, Appl. Catal. B-Environ. 194 (2016) 42–49.
[104] B. Wang, W. Liu, W. Zhang, J. Liu, Nanoparticles@nanoscale metal-organic framework composites as highly efficient heterogeneous catalysts for size- and shape-selective reactions, Nano Res. 10 (2017) 3826–3835.
[105] Z. Zhao, J. Ding, R. Zhu, H. Pang, The synthesis and electrochemical applications of core–shell MOFs and their derivatives, J. Mater. Chem. A 7 (2019) 15519–15540.
[106] T. Zeng, X. Zhang, S. Wang, H. Niu, Y. Cai, Spatial confinement of a Co3O4 catalyst in hollow metal–organic frameworks as a nanoreactor for improved degradation of organic pollutants, Environ. Sci. Technol. 49 (2015) 2350–2357.
[107] G. Li, S. Zhao, Y. Zhang, Z. Tang, Metal–organic frameworks encapsulating active nanoparticles as emerging composites for catalysis: recent progress and perspectives, Adv. Mater. 30 (2018) 1800702.
[108] M. Liu, Z. Xing, Z. Li, W. Zhou, Recent advances in core–shell metal organic frame-based photocatalysts for solar energy conversion, Coordin. Chem. Rev. 446 (2021), 214123.
[109] M. Yoshimura, K. Byrappa, Hydrothermal processing of materials: past, present and future, J. Mater. Sci. 43 (2008) 2085–2103.
[110] D. He, H. Niu, S. He, L. Mao, Y. Cai, Y. Liang, Strengthened Fenton degradation of phenol catalyzed by core/shell Fe–Pd@C nanocomposites derived from mechanochemically synthesized Fe-Metal organic frameworks, Water Res 162 (2019) 151–160.
[111] K.L. Choy, Chemical vapour deposition of coatings, Prog. Mater. Sci. 48 (2003) 57–170.
[112] Y. Zhou, Y. Li, Y. Hou, C. Wang, Y. Yang, J. Shang, X. Cheng, Core-shell catalysts for the elimination of organic contaminants in aqueous solution: a review, Chem. Eng. J. 455 (2023), 140604.
[113] G. Arora, M. Yadav, R. Gaur, R. Gupta, P. Yadav, R. Dixit, R.K. Sharma, Fabrication, functionalization and advanced applications of magnetic hollow materials in confined catalysis and environmental remediation, Nanoscale 13 (2021) 10967–11003.
[114] Q. Cai, F. Wang, Y. Hou, Y. Jia, B. Liao, B. Shen, D. Zhang, Core-shell materials for selective catalytic reducing of NOx with ammonia: Synthesis, anti-poisoning performance, and remaining challenges, Fuel. Process. Technol. 243 (2023), 107675.
[115] Y. Zuo, J. Feng, T.-O. Soyol-Erdene, Z. Wei, T. Hu, Y. Zhang, W. Tang, Recent advances in wood-derived monolithic carbon materials: Synthesis approaches, modification methods and environmental applications, Chem. Eng. J. 463 (2023), 142332.
[116] H. Niu, Y. Zheng, S. Wang, L. Zhao, S. Yang, Y. Cai, Continuous generation of hydroxyl radicals for highly efficient elimination of chlorophenols and phenols catalyzed by heterogeneous Fenton-like catalysts yolk/shell Pd@Fe3O4@metal organic frameworks, J. Hazard. Mater. 346 (2018) 174–183.
[117] Q. Xia, Z. Jiang, D. Li, J. Wang, Z. Yao, Green synthesis of a dendritic Fe3O4 @Feo composite modified with polar C-groups for Fenton-like oxidation of phenol, J. Alloy. Compd. 746 (2018) 453–461.
[118] Y. Liu, F. Wang, B. Sun, P. Xu, L. Zhang, X. Han, Y. Du, In situ growth of nitrogen-doped carbon nanotubes based on hierarchical Ni@C microspheres for high efficiency bisphenol a removal through peroxymonosulfate activation, ACS Appl. Mater. Interfaces 14 (2022) 21371–21382.
[119] M.-M. Chen, H.-Y. Niu, C.-G. Niu, H. Guo, S. Liang, Y.-Y. Yang, Metal-organic framework-derived CuCo/carbon as an efficient magnetic heterogeneous catalyst for persulfate activation and ciprofloxacin degradation, J. Hazard. Mater. 424 (2022), 127196.
[120] Y. Liu, J. Luo, L. Tang, C. Feng, J. Wang, Y. Deng, H. Liu, J. Yu, H. Feng, J. Wang, Origin of the enhanced reusability and electron transfer of the carbon-coated Mn3O4 nanocube for persulfate activation, ACS Catal. 10 (2020) 14857–14870.
[121] Y. Zhou, Y. Zhang, X. Hu, Novel zero-valent Co-Fe encapsulated in nitrogen-doped porous carbon nanocomposites derived from CoFe2O4@ZIF-67 for boosting 4-chlorophenol removal via coupling peroxymonosulfate, J. Colloid Interface Sci. 575 (2020) 206–219.
[122] K. Xiao, F. Liang, J. Liang, W. Xu, Z. Liu, B. Chen, X. Jiang, X. Wu, J. Xu, J. Beiyuan, H. Wang, Magnetic bimetallic Fe, Ce-embedded N-enriched porous biochar for peroxymonosulfate activation in metronidazole degradation: applications, mechanism insight and toxicity evaluation, Chem. Eng. J. 433 (2022), 134387.
[123] X. Sun, H. Qi, S. Mao, Z. Sun, Atrazine removal by peroxymonosulfate activated with magnetic CoFe alloy@N-doped graphitic carbon encapsulated in chitosan carbonized microspheres, Chem. Eng. J. 423 (2021), 130169.
[124] J. Xiao, J. Chen, Z. Ou, J. Lai, T. Yu, Y. Wang, N-doped carbon-coated Fe3N composite as heterogeneous electro-Fenton catalyst for efficient degradation of organics, Chin. J. Catal. 42 (2021) 953–962.
[125] S. Wang, J. Wang, High efficient activation of peroxymonosulfate by Co9S8 anchored in N, S, O co-doped carbon composite for degradation of sulfamethoxazole: Effect of sulfur precursor and sulfur doping content, Chem. Eng. J. 434 (2022), 134824.
[126] S. Wang, J. Wang, Peroxymonosulfate activation by Co9S8@ S and N co-doped biochar for sulfamethoxazole degradation, Chem. Eng. J. 385 (2020), 123933.
[127] L. Chu, Z. Sun, G. Fang, L. Cang, X. Wang, D. Zhou, J. Gao, Highly effective removal of BPA with boron-doped graphene shell wrapped FeS2 nanoparticles in electro-Fenton process: Performance and mechanism, Sep. Purif. Technol. 267 (2021), 118680.
[128] W. Ma, N. Wang, Y. Du, T. Tong, L. Zhang, K.-Y. Andrew Lin, X. Han, One-step synthesis of novel Fe3C@nitrogen-doped carbon nanotubes/graphene nanosheets for catalytic degradation of Bisphenol A in the presence of peroxymonosulfate, Chem. Eng. J. 356 (2019) 1022–1031.
[129] S. Liang, H.-Y. Niu, H. Guo, C.-G. Niu, C. Liang, J.-S. Li, N. Tang, L.-S. Lin, C.-W. Zheng, Incorporating Fe3C into B, N co-doped CNTs: Non-radical-dominated peroxymonosulfate catalytic activation mechanism, Chem. Eng. J. 405 (2021), 126686.
[130] C. Wang, J. Kang, P. Liang, H. Zhang, H. Sun, M.O. Tadé, S. Wang, Ferric carbide nanocrystals encapsulated in nitrogen-doped carbon nanotubes as an outstanding environmental catalyst, Environ. Sci.: Nano 4 (2017) 170–179.
[131] S. Wang, J. Wang, Synergistic effect of PMS activation by Fe0@Fe3O4 anchored on N, S, O co-doped carbon composite for degradation of sulfamethoxazole, Chem. Eng. J. 427 (2022), 131960.
[132] Q. Wang, Y. Jiang, S. Yang, J. Lin, J. Lu, W. Song, S. Zhu, Z. Wang, Selective degradation of parachlorophenol using Fe/Fe3O4@CPPy nanocomposites via the dual nonradical/radical peroxymonosulfate activation mechanisms, Chem. Eng. J. 445 (2022), 136806.
[133] L. Peng, Y. Shang, B. Gao, X. Xu, Co3O4 anchored in N, S heteroatom co-doped porous carbons for degradation of organic contaminant: role of pyridinic N-Co binding and high tolerance of chloride, Appl. Catal. B-Environ. 282 (2021), 119484.
[134] X. Li, Z. Ao, J. Liu, H. Sun, A.I. Rykov, J. Wang, Topotactic transformation of metal–organic frameworks to graphene-encapsulated transition-metal nitrides as efficient Fenton-like catalysts, ACS Nano 10 (2016) 11532–11540.
[135] C. Zhao, L. Meng, H. Chu, J.-F. Wang, T. Wang, Y. Ma, C.-C. Wang, Ultrafast degradation of emerging organic pollutants via activation of peroxymonosulfate over Fe3C/Fe@N-C-x: singlet oxygen evolution and electron-transfer mechanisms, Appl. Catal. B-Environ. 321 (2023), 122034.
[136] X. Li, X. Huang, S. Xi, S. Miao, J. Ding, W. Cai, S. Liu, X. Yang, H. Yang, J. Gao, J. Wang, Y. Huang, T. Zhang, B. Liu, Single cobalt atoms anchored on porous n-doped graphene with dual reaction sites for efficient fenton-like catalysis, J. Am. Chem. Soc. 140 (2018) 12469–12475.
[137] C. Zhang, J. Tang, F. Gao, C. Yu, S. Li, H. Lyu, H. Sun, Tetrahydrofuran aided self-assembly synthesis of nZVI@gBC composite as persulfate activator for degradation of 2,4-dichlorophenol, Chem. Eng. J. 431 (2022), 134063.
[138] H. Niu, Y. Zheng, S. Wang, L. Zhao, S. Yang, Y. Cai, Continuous generation of hydroxyl radicals for highly efficient elimination of chlorophenols and phenols catalyzed by heterogeneous Fenton-like catalysts yolk/shell Pd@Fe3O4@metal organic frameworks, J. Hazard. Mater. 346 (2018) 174–183.
[139] L. Shen, J. Ying, K.I. Ozoemena, C. Janiak, X.-Y. Yang, Confinement effects in individual carbon encapsulated nonprecious metal-based electrocatalysts, Adv. Funct. Mater. 32 (2022) 2110851.
[140] J.H. Jang, A.A. Jeffery, J. Min, N. Jung, S.J. Yoo, Emerging carbon shell-encapsulated metal nanocatalysts for fuel cells and water electrolysis, Nanoscale 13 (2021) 15116–15141.
[141] J.-H. Jang, A.A. Jeffery, J. Min, N. Jung, S.J. Yoo, Emerging carbon shell-encapsulated metal nanocatalysts for fuel cells and water electrolysis, Nanoscale 13 (2021) 15116–15141.
[142] T.J. Park, R.C. Pawar, S. Kang, C.S. Lee, Ultra-thin coating of g-C3N4 on an aligned ZnO nanorod film for rapid charge separation and improved photodegradation performance, RSC Adv. 6 (2016) 89944–89952.
[143] X. Lai, J.E. Halpert, D. Wang, Recent advances in micro-/nano-structured hollow spheres for energy applications: From simple to complex systems, Energy Environ. Sci. 5 (2012) 5604–5618.
[144] S. Zhang, Q. Fan, H. Gao, Y. Huang, X. Liu, J. Li, X. Xu, X. Wang, Retracted article: formation of Fe3O4@MnO2 ball-in-ball hollow spheres as a high performance catalyst with enhanced catalytic performances, J. Mater. Chem. A 4 (2016) 1414–1422.
[145] T. Zeng, M. Yu, H. Zhang, Z. He, X. Zhang, J. Chen, S. Song, In situ synthesis of cobalt ferrites-embedded hollow N-doped carbon as an outstanding catalyst for elimination of organic pollutants, Sci. Total Environ. 593–594 (2017) 286–296.
[146] W. Shi, D. Du, B. Shen, C. Cui, L. Lu, L. Wang, J. Zhang, Synthesis of yolk–shell structured Fe3O4@void@CdS nanoparticles: a general and effective structure design for photo-Fenton reaction, ACS Appl. Mater. Interfaces 8 (2016) 20831–20838.
[147] E. Doustkhah, R. Hassandoost, A. Khataee, R. Luque, M.H.N. Assadi, Hard-templated metal–organic frameworks for advanced applications, Chem. Soc. Rev. 50 (2021) 2927–2953.
[148] H. Su, Q. Tian, C.-A. Hurd Price, L. Xu, K. Qian, J. Liu, Nanoporous core@shell particles: design, preparation, applications in bioadsorption and biocatalysis, Nano Today 31 (2020).
[149] Q. Wang, X. Liu, A. Cai, H. He, G. Zhang, F. Zhang, X. Fan, W. Peng, Y. Li, Atomically Fe doped hollow mesoporous carbon spheres for peroxymonosulfate mediated advanced oxidation processes with a dual activation pathway, J. Mater. Chem. A 10 (2022) 20535–20544.
[150] R. Su, S. Ge, H. Li, Y. Su, Q. Li, W. Zhou, B. Gao, Q. Yue, Synchronous synthesis of Cu2O/Cu/rGO@carbon nanomaterials photocatalysts via the sodium alginate hydrogel template method for visible light photocatalytic degradation, Sci. Total Environ. 693 (2019), 133657.
[151] Y. Zhang, J. Chen, L. Hua, S. Li, X. Zhang, W. Sheng, S. Cao, High photocatalytic activity of hierarchical SiO2@C-doped TiO2 hollow spheres in UV and visible

light towards degradation of rhodamine B, J. Hazard. Mater. 340 (2017) 309–318.
[152] Y. Zhang, J. Chen, H. Tang, Y. Xiao, S. Qiu, S. Li, S. Cao, Hierarchically-structured SiO2-Ag@TiO2 hollow spheres with excellent photocatalytic activity and recyclability, J. Hazard. Mater. 354 (2018) 17–26.
[153] Z. Lyu, M. Xu, J. Wang, A. Li, P. François-Xavier Corvini, Hierarchical nano-vesicles with bimetal-encapsulated for peroxymonosulfate activation: Singlet oxygen-dominated oxidation process, Chem. Eng. J. 433 (2022).
[154] Y. Wang, W. Yang, X. Chen, J. Wang, Y. Zhu, Photocatalytic activity enhancement of core-shell structure g-C3N4@TiO2 via controlled ultrathin g-C3N4 layer, Appl. Catal. B-Environ. 220 (2018) 337–347.
[155] A. Wang, J. Ni, W. Wang, D. Liu, Q. Zhu, B. Xue, C.-C. Chang, J. Ma, Y. Zhao, MOF Derived Co−Fe nitrogen doped graphite carbon@crosslinked magnetic chitosan Micro−nanoreactor for environmental applications: synergy enhancement effect of adsorption−PMS activation, Appl. Catal. B-Environ. 319 (2022), 121926.
[156] N. Wang, T. Zheng, G. Zhang, P. Wang, A review on Fenton-like processes for organic wastewater treatment, J. Environ. Chem. Eng. 4 (2016) 762–787.
[157] Y. Yang, L. Xu, W. Li, W. Fan, S. Song, J. Yang, Adsorption and degradation of sulfadiazine over nanoscale zero-valent iron encapsulated in three-dimensional graphene network through oxygen-driven heterogeneous Fenton-like reactions, Appl. Catal. B-Environ. 259 (2019), 118057.
[158] W. Xie, Z. Huang, F. Zhou, Y. Li, X. Bi, Q. Bian, S. Sun, Heterogeneous fenton-like degradation of amoxicillin using MOF-derived Fe0 embedded in mesoporous carbon as an effective catalyst, J. Clean. Prod. 313 (2021), 127754.
[159] J. Tang, J. Wang, Fenton-like degradation of sulfamethoxazole using Fe-based magnetic nanoparticles embedded into mesoporous carbon hybrid as an efficient catalyst, Chem. Eng. J. 351 (2018) 1085–1094.
[160] J. Wang, C. Liu, J. Qi, J. Li, X. Sun, J. Shen, W. Han, L. Wang, Enhanced heterogeneous Fenton-like systems based on highly dispersed Fe0-Fe2O3 nanoparticles embedded ordered mesoporous carbon composite catalyst, Environ. Pollut. 243 (2018) 1068–1077.
[161] L. Lyu, M. Han, W. Cao, Y. Gao, Q. Zeng, G. Yu, X. Huang, C. Hu, Efficient Fenton-like process for organic pollutant degradation on Cu-doped mesoporous polyimide nanocomposites, Environ. Sci. -Nano 6 (2019) 798–808.
[162] X. Zhang, Z. Yao, Y. Zhou, Z. Zhang, G. Lu, Z. Jiang, Theoretical guidance for the construction of electron-rich reaction microcenters on C–O–Fe bridges for enhanced Fenton-like degradation of tetracycline hydrochloride, Chem. Eng. J. 411 (2021), 128535.
[163] M. Xiang, M. Huang, H. Li, W. Wang, Y. Huang, Z. Lu, C. Wang, R. Si, W. Cao, Nanoscale zero-valent iron/cobalt@mesoporous hydrated silica core–shell particles as a highly active heterogeneous Fenton catalyst for the degradation of tetrabromobisphenol A, Chem. Eng. J. 417 (2021), 129208.
[164] X. Xu, W. Chen, S. Zong, X. Ren, D. Liu, Magnetic clay as catalyst applied to organics degradation in a combined adsorption and Fenton-like process, Chem. Eng. J. 373 (2019) 140–149.
[165] L. Lyu, G. Yu, L. Zhang, C. Hu, Y. Sun, 4-phenoxyphenol-functionalized reduced graphene oxide nanosheets: a metal-free fenton-like catalyst for pollutant destruction, Environ. Sci. Technol. 52 (2018) 747–756.
[166] L. Lyu, L. Zhang, Q. Wang, Y. Nie, C. Hu, Enhanced fenton catalytic efficiency of gamma-Cu-Al2O3 by sigma-Cu2+-ligand complexes from aromatic pollutant degradation, Environ. Sci. Technol. 49 (2015) 8639–8647.
[167] L. Lyu, D. Yan, G. Yu, W. Cao, C. Hu, Efficient destruction of pollutants in water by a dual-reaction-center fenton-like process over carbon nitride compounds-complexed Cu(II)-CuAlO2, Environ. Sci. Technol. 52 (2018) 4294–4304.
[168] M.K. Panjwani, Q. Wang, Y. Ma, Y. Lin, F. Xiao, S. Yang, High degradation efficiency of sulfamethazine with the dual-reaction-center Fe–Mn–SiO2 Fenton-like nanocatalyst in a wide pH range, Environ. Sci. -Nano 8 (2021) 2204–2213.
[169] L. Li, Z. Yin, M. Cheng, L. Qin, S. Liu, H. Yi, M. Zhang, Y. Fu, X. Yang, X. Zhou, G. Zeng, C. Lai, Insights into reactive species generation and organics selective degradation in Fe-based heterogeneous Fenton-like systems: a critical review, Chem. Eng. J. 454 (2023), 140126.
[170] Y. Zhuang, Q. Liu, Y. Kong, C. Shen, H. Hao, D.D. Dionysiou, B. Shi, Enhanced antibiotic removal through a dual-reaction-center Fenton-like process in 3D graphene based hydrogels, Environ. Sci. -Nano 6 (2019) 388–398.
[171] Y. Zhuang, X. Wang, L. Zhang, D.D. Dionysiou, B. Shi, Fe-Chelated polymer templated graphene aerogel with enhanced Fenton-like efficiency for water treatment, Environ. Sci. -Nano 6 (2019) 3232–3241.
[172] X. Zhang, Z. Yao, J. Wang, W. Guo, X. Wu, Z. Jiang, High-capacity NCNT-encapsulated metal NP catalysts on carbonised loofah with dual-reaction centres over C–M bond bridges for Fenton-like degradation of antibiotics, Appl. Catal. B-Environ. 307 (2022), 121205.
[173] X. Zhang, Z.P. Yao, J.K. Wang, W.Q. Guo, X.H. Wu, Z.H. Jiang, High-capacity NCNT-encapsulated metal NP catalysts on carbonised loofah with dual-reaction centres over C-M bond bridges for Fenton-like degradation of antibiotics, Appl. Catal. B-Environ. 307 (2022), 121205.
[174] P. Su, W. Fu, X. Du, G. Song, Y. Tang, M. Zhou, Nanoscale confinement in carbon nanotubes encapsulated zero-valent iron for phenolics degradation by heterogeneous Fenton: Spatial effect and structure–activity relationship, Sep. Purif. Technol. 276 (2021), 119232.
[175] H. Niu, D. He, Y. Yang, H. Lv, Y. Liang, Long-lasting activity of Fe0-C internal microelectrolysis-Fenton system assisted by Fe@C-montmorillonites nanocomposites, Appl. Catal. B-Environ. 256 (2019), 117820.
[176] L. Xu, Y. Yang, W. Li, Y. Tao, Z. Sui, S. Song, J. Yang, Three-dimensional macroporous graphene-wrapped zero-valent copper nanoparticles as efficient micro-electrolysis-promoted Fenton-like catalysts for metronidazole removal, Sci. Total Environ. 658 (2019) 219–233.
[177] Y. Yang, L. Xu, J. Wang, An enhancement of singlet oxygen generation from dissolved oxygen activated by three-dimensional graphene wrapped nZVI-doped amorphous Al species for chloramphenicol removal in the Fenton-like system, Chem. Eng. J. 425 (2021), 131497.
[178] Y. Yang, H. Shen, L. Xu, Three-dimensional graphene anchored nZVI hybrid MnO2 as a dissolved oxygen activated Fenton-like catalyst for efficient mineralization of oxytetracycline, Chem. Eng. J. 464 (2023), 142781.
[179] M. Liu, H. Xia, W. Yang, X. Liu, J. Xiang, X. Wang, L. Hu, F. Lu, Novel Cu-Fe bi-metal oxide quantum dots coupled g-C3N4 nanosheets with H2O2 adsorption-activation trade-off for efficient photo-Fenton catalysis, Appl. Catal. B-Environ. 301 (2022), 120765.
[180] L. Su, P. Wang, X. Ma, J. Wang, S. Zhan, Regulating local electron density of iron single sites by introducing nitrogen vacancies for efficient photo-Fenton process, Angew. Chem. Int. Ed. 60 (2021) 21261–21266.
[181] X. Zhang, B.K. Xu, S.W. Wang, X. Li, C. Wang, Y.H. Xu, R. Zhou, Y. Yu, H.L. Zheng, P. Yu, Y.J. Sun, Carbon nitride nanotubes anchored with high-density CuNx sites for efficient degradation of antibiotic contaminants under photo-Fenton process: performance and mechanism, Appl. Catal. B-Environ. 306 (2022), 121119.
[182] J. Jiang, X. Wang, Y. Liu, Y. Ma, T. Li, Y. Lin, T. Xie, S. Dong, Photo-Fenton degradation of emerging pollutants over Fe-POM nanoparticle/porous and ultrathin g-C3N4 nanosheet with rich nitrogen defect: Degradation mechanism, pathways, and products toxicity assessment, Appl. Catal. B-Environ. 278 (2020), 119349.
[183] Z. Wang, J. You, J. Li, J. Xu, X. Li, H. Zhang, Review on cobalt ferrite as photo-Fenton catalysts for degradation of organic wastewater, Catal. Sci. Technol. 13 (2023) 274–296.
[184] Z. Tong, D. Yang, Y. Sun, Y. Nan, Z. Jiang, Tubular g-C3N4 isotype heterojunction: enhanced visible-light photocatalytic activity through cooperative manipulation of oriented electron and hole transfer, Small 12 (2016) 4093–4101.
[185] J. Xi, H. Xia, X. Ning, Z. Zhang, J. Liu, Z. Mu, S. Zhang, P. Du, X. Lu, Carbon-intercalated 0D/2D hybrid of hematite quantum dots/graphitic carbon nitride nanosheets as superior catalyst for advanced oxidation, Small 15 (2019) 1902744.
[186] W. Shi, W. Sun, Y. Liu, K. Zhang, H. Sun, X. Lin, Y. Hong, F. Guo, A self-sufficient photo-Fenton system with coupling in-situ production H2O2 of ultrathin porous g-C3N4 nanosheets and amorphous FeOOH quantum dots, J. Hazard. Mater. 436 (2022), 129141.
[187] J. Xu, Q. Gao, Z. Wang, Y. Zhu, An all-organic 0D/2D supramolecular porphyrin/g-C3N4 heterojunction assembled via π-π interaction for efficient visible photocatalytic oxidation, Appl. Catal. B-Environ. 291 (2021), 120059.
[188] J. Tang, R. Xu, G. Sui, D. Guo, Z. Zhao, S. Fu, X. Yang, Y. Li, J. Li, Double-shelled porous g-C3N4 nanotubes modified with amorphous Cu-doped FeOOH nanoclusters as 0D/3D non-homogeneous photo-fenton catalysts for effective removal of organic dyes, Small 19 (2023) 2208232.
[189] W. Li, W. Li, K. He, L. Tang, Q. Liu, K. Yang, Y.-D. Chen, X. Zhao, K. Wang, H. Lin, S. Lv, Peroxymonosulfate activation by oxygen vacancies-enriched MXene nano-Co3O4 co-catalyst for efficient degradation of refractory organic matter: Efficiency, mechanism, and stability, J. Hazard. Mater. 432 (2022), 128719.
[190] J. Jiang, Z. Zhao, J. Gao, T. Li, M. Li, D. Zhou, S. Dong, Nitrogen vacancy-modulated peroxymonosulfate nonradical activation for organic contaminant removal via high-valent cobalt-oxo species, Environ. Sci. Technol. 56 (2022) 5611–5619.
[191] X. Zhou, R. Yin, J. Kang, Z. Li, Y. Pan, J. Bai, A.J. Li, R. Qiu, Atomic cation-vacancy modulated peroxymonosulfate nonradical oxidation of sulfamethoxazole via high-valent iron-oxo species, Appl. Catal. B-Environ. 330 (2023), 122640.
[192] X. Wu, T. Liu, W. Ni, H. Yang, H. Huang, S. He, C. Li, H. Ning, W. Wu, Q. Zhao, M. Wu, Engineering controllable oxygen vacancy defects in iron hydroxide oxide immobilized on reduced graphene oxide for boosting visible light-driven photo-Fenton-like oxidation, J. Colloid Interface Sci. 623 (2022) 9–20.
[193] L. Zhang, S. Huo, W. Li, L. Song, W. Fu, J. Li, M. Gao, Improved heterogeneous photo-Fenton-like degradation of ofloxacin through polyvinylpyrrolidone modified CuFeO2 catalyst: performance, DFT calculation and mechanism, Sep. Purif. Technol. 311 (2023), 123261.
[194] Y. Hu, Z. Zhong, M. Lu, Y. Muhammad, S. Jalil Shah, H. He, W. Gong, Y. Ren, X. Yu, Z. Zhao, Z. Zhao, Biomimetic O2-carrying and highly in-situ H2O2 generation using Ti3C2 MXene/MIL-100(Fe) hybrid via Fe-Protoporphyrin bridging for photo-fenton synergistic degradation of thiacloprid, Chem. Eng. J. 450 (2022), 137964.
[195] M. Ahmad, X. Quan, S. Chen, H. Yu, Tuning Lewis acidity of MIL-88B-Fe with mix-valence coordinatively unsaturated iron centers on ultrathin Ti3C2 nanosheets for efficient photo-Fenton reaction, Appl. Catal. B-Environ. 264 (2020), 118534.
[196] W. Zheng, H. Guo, C. Zhu, C. Yue, W. Zhu, F. Liu, Z. Chen, Ultralow-energy-barrier H2O2 dissociation on coordinatively unsaturated metal centers in binary Ce-Fe prussian blue analogue for efficient and stable photo-fenton catalysis, Energy Environ. Mater. N./a (2022), e12476.
[197] X. Wu, Q. Zhao, J. Zhang, S. Li, H. Liu, K. Liu, Y. Li, D. Kong, H. Sun, M. Wu, 0D carbon dots intercalated Z-scheme CuO/g-C3N4 heterojunction with dual charge transfer pathways for synergetic visible-light-driven photo-Fenton-like catalysis, J. Colloid Interface Sci. 634 (2023) 972–982.
[198] Y. Ju, H. Li, Z. Wang, H. Liu, S. Huo, S. Jiang, S. Duan, Y. Yao, X. Lu, F. Chen, Solar-driven on-site H2O2 generation and tandem photo-Fenton reaction on a triphase interface for rapid organic pollutant degradation, Chem. Eng. J. 430 (2022), 133168.
[199] S. Shi, X. Han, J. Liu, X. Lan, J. Feng, Y. Li, W. Zhang, J. Wang, Photothermal-boosted effect of binary CuFe bimetallic magnetic MOF heterojunction for high-

performance photo-Fenton degradation of organic pollutants, Sci. Total Environ. 795 (2021), 148883.
[200] Q. Li, H. Kong, P. Li, J. Shao, Y. He, Photo-Fenton degradation of amoxicillin via magnetic TiO2-graphene oxide-Fe3O4 composite with a submerged magnetic separation membrane photocatalytic reactor (SMSMPR), J. Hazard. Mater. 373 (2019) 437–446.
[201] W. Chen, D. Huang, C. Lai, Y. Fu, W. Chen, H. Ye, H. Yi, B. Li, L. Li, F. Qin, H. Qin, L. Qin, Recent advances in application of heterogeneous electro-Fenton catalysts for degrading organic contaminants in water, Environ. Sci. Pollut. R. 30 (2023) 39431–39450.
[202] M. Li, L. Bai, S. Jiang, M. Sillanpää, Y. Huang, Y. Liu, Electrocatalytic transformation of oxygen to hydroxyl radicals via three-electron pathway using nitrogen-doped carbon nanotube-encapsulated nickel nanocatalysts for effective organic decontamination, J. Hazard. Mater. 452 (2023), 131352.
[203] H. Qi, G. Pan, X. Shi, Z. Sun, Cu–Fe–FeC3@nitrogen-doped biochar microsphere catalyst derived from CuFe2O4@chitosan for the efficient removal of amoxicillin through the heterogeneous electro-Fenton process, Chem. Eng. J. 434 (2022), 134675.
[204] Y. Lin, P. Huo, F. Li, X. Chen, L. Yang, Y. Jiang, Y. Zhang, B.-J. Ni, M. Zhou, A critical review on cathode modification methods for efficient Electro-Fenton degradation of persistent organic pollutants, Chem. Eng. J. 450 (2022), 137948.
[205] T. Hu, L. Tang, H. Feng, J. Zhang, X. Li, Y. Zuo, Z. Lu, W. Tang, Metal-organic frameworks (MOFs) and their derivatives as emerging catalysts for electro-Fenton process in water purification, Coordin, Chem. Rev. 451 (2022), 214277.
[206] J. Hu, S. Wang, J. Yu, W. Nie, J. Sun, S. Wang, Duet Fe3C and FeNx sites for H2O2 generation and activation toward enhanced electro-fenton performance in wastewater treatment, Environ. Sci. Technol. 55 (2021) 1260–1269.
[207] P.K. Cao, X. Quan, K. Zhao, S. Chen, H.T. Yu, J.F. Niu, Selective electrochemical H2O2 generation and activation on a bifunctional catalyst for heterogeneous electro-Fenton catalysis, J. Hazard. Mater. 382 (2020), 121102.
[208] Z. Ye, J.A. Padilla, E. Xuriguera, J.L. Beltran, F. Alcaide, E. Brillas, I. Sirés, A highly stable metal–organic framework-engineered FeS2/C nanocatalyst for heterogeneous electro-fenton treatment: validation in wastewater at Mild pH, Environ. Sci. Technol. 54 (2020) 4664–4674.
[209] T. Hu, F.X. Deng, H.P. Feng, J.J. Zhang, B.B. Shao, C.Y. Feng, W.W. Tang, L. Tang, Fe/Co bimetallic nanoparticles embedded in MOF-derived nitrogen-doped porous carbon rods as efficient heterogeneous electro-Fenton catalysts for degradation of organic pollutants, Appl. Mater. Today 24 (2021), 101161.
[210] F. Xiao, Z. Wang, J. Fan, T. Majima, H. Zhao, G. Zhao, Selective electrocatalytic reduction of oxygen to hydroxyl radicals via 3-electron pathway with FeCo alloy encapsulated carbon aerogel for fast and complete removing pollutants, Angew. Chem. Int. Ed. Engl. 60 (2021) 10375–10383.
[211] X. Shen, F. Xiao, H. Zhao, Y. Chen, C. Fang, R. Xiao, W. Chu, G. Zhao, In situ-formed PdFe nanoalloy and carbon defects in cathode for synergic reduction–oxidation of chlorinated pollutants in electro-fenton process, Environ. Sci. Technol. 54 (2020) 4564–4572.
[212] Q. Zhang, M. Zhou, G. Ren, Y. Li, Y. Li, X. Du, Highly efficient electrosynthesis of hydrogen peroxide on a superhydrophobic three-phase interface by natural air diffusion, Nat. Commun. 11 (2020) 1731.
[213] Y. Zheng, J. He, S. Qiu, D. Yu, Y. Zhu, H. Pang, J. Zhang, Boosting hydrogen peroxide accumulation by a novel air-breathing gas diffusion electrode in electro-Fenton system, Appl. Catal. B-Environ. 316 (2022), 121617.
[214] J. Geng, H. Zhang, Z. Zhang, J. Gao, S. Wang, X. Hu, J. Li, Enhanced electro-Fenton oxidation by introducing three-phase interface with simultaneous optimization of O2 and pollutant transfer for effective tetracycline hydrochloride removal, Chem. Eng. J. 450 (2022), 137891.
[215] Y. Zou, J. Li, Q. Peng, Z. Liu, Q. Fu, L. Zhang, Q. Liao, X. Zhu, Tuning the wettability of advanced mesoporous FeNC catalysts for optimizing the construction of the gas/liquid/solid three-phase interface in air-cathodes, Chem. Eng. J. 450 (2022), 138342.
[216] P. Su, M. Zhou, G. Ren, X. Lu, X. Du, G. Song, A carbon nanotube-confined iron modified cathode with prominent stability and activity for heterogeneous electro-Fenton reactions, J. Mater. Chem. A 7 (2019) 24408–24419.
[217] S.S. Xin, S.Y. Huo, Y.J. Xin, M.C. Gao, Y.H. Wang, W.J. Liu, C.L. Zhang, X.M. Ma, Heterogeneous photo-electro-Fenton degradation of tetracycline through nitrogen/oxygen self-doped porous biochar supported CuFeO2 multifunctional cathode catalyst under visible light, Appl. Catal. B-Environ. 312 (2022), 121442.
[218] Y. Wang, M. Zhao, C. Hou, W. Chen, S. Li, R. Ren, Z. Li, Efficient degradation of perfluorooctanoic acid by solar photo-electro-Fenton like system fabricated by MOFs/carbon nanofibers composite membrane, Chem. Eng. J. 414 (2021), 128940.
[219] J. Zhang, Z. Zhou, Z. Feng, H. Zhao, G. Zhao, Fast generation of hydroxyl radicals by rerouting the electron transfer pathway via constructed chemical channels during the photo-electro-reduction of oxygen, Environ. Sci. Technol. 56 (2022) 1331–1340.
[220] Y. Wang, S. Li, Y. Shao, L. Jing, R. Ren, L. Ma, X. Wang, Z. Li, J. Wang, C. Hou, Energy-efficient mineralization of perfluorooctanoic acid: Biomass energy driven solar photo-electro-fenton catalysis and mechanism study, Chem. Eng. J. 443 (2022), 136514.
[221] P. Zhang, Y. Wang, X. Luo, J. Wang, W. Wang, X. Duan, K. Qi, M. Li, Flow-through heterogeneous electro-Fenton based on Co-CNT/Ti3C2TX membrane for improved tetracycline removal in wide pH ranges, Environ. Sci. -Nano 9 (2022) 4468–4483.
[222] Z. Li, C. Shen, Y. Liu, C. Ma, F. Li, B. Yang, M. Huang, Z. Wang, L. Dong, S. Wolfgang, Carbon nanotube filter functionalized with iron oxychloride for flow-through electro-Fenton, Appl. Catal. B-Environ. 260 (2020), 118204.
[223] D. Guo, S. Jiang, L. Jin, K. Huang, P. Lu, Y. Liu, CNT encapsulated MnOx for an enhanced flow-through electro-Fenton process: the involvement of Mn(iv), J. Mater. Chem. A 10 (2022) 15981–15989.
[224] D. Guo, Y. Liu, H. Ji, C.-C. Wang, B. Chen, C. Shen, F. Li, Y. Wang, P. Lu, W. Liu, Silicate-enhanced heterogeneous flow-through electro-fenton system using iron oxides under nanoconfinement, Environ. Sci. Technol. 55 (2021) 4045–4053.
[225] A. Feng, J. Feng, W. Xing, K. Jiang, W. Tang, Versatile applications of electrochemical flow-through systems in water treatment processes, Chem. Eng. J. 473 (2023), 145400.
[226] S.K. Maeng, K. Cho, B. Jeong, J. Lee, Y. Lee, C. Lee, K.J. Choi, S.W. Hong, Substrate-immobilized electrospun TiO2 nanofibers for photocatalytic degradation of pharmaceuticals: the effects of pH and dissolved organic matter characteristics, Water Res 86 (2015) 25–34.
[227] K. Nagaveni, G. Sivalingam, M.S. Hegde, G. Madras, Photocatalytic degradation of organic compounds over combustion-synthesized nano-TiO2, Environ. Sci. Technol. 38 (2004) 1600–1604.
[228] M. Shekofteh-Gohari, A. Habibi-Yangjeh, M. Abitorabi, A. Rouhi, Magnetically separable nanocomposites based on ZnO and their applications in photocatalytic processes: a review, Crit. Rev. Environ. Sci. Tec. 48 (2018) 806–857.
[229] Y. Fei, N. Han, M. Zhang, F. Yang, X. Yu, L. Shi, A. Khataee, W. Zhang, D. Tao, M. Jiang, Facile preparation of visible light-sensitive layered g-C3N4 for photocatalytic removal of organic pollutants, Chemosphere 307 (2022), 135718.
[230] J. Liang, X. Yang, Y. Wang, P. He, H. Fu, Y. Zhao, Q. Zou, X. An, A review on g-C3N4 incorporated with organics for enhanced photocatalytic water splitting, J. Mater. Chem. A 9 (2021) 12898–12922.
[231] B. He, M. Feng, X. Chen, Y. Cui, D. Zhao, J. Sun, Fabrication of potassium ion decorated 1D/2D g-C3N4/g-C3N4 homojunction enabled by dual-ions synergistic strategy for enhanced photocatalytic activity towards degradation of organic pollutants, Appl. Surf. Sci. 575 (2022), 151695.
[232] D. Wang, Q. Li, W. Miao, Y. Liu, N. Du, S. Mao, One-pot synthesis of ultrafine NiO loaded and Ti3+ in-situ doped TiO2 induced by cyclodextrin for efficient visible-light photodegradation of hydrophobic pollutants, Chem. Eng. J. 402 (2020), 126211.
[233] S. Shanavas, S. Mohana Roopan, A. Priyadharsan, D. Devipriya, S. Jayapandi, R. Acevedo, P.M. Anbarasan, Computationally guided synthesis of (2D/3D/2D) rGO/Fe2O3/g-C3N4 nanostructure with improved charge separation and transportation efficiency for degradation of pharmaceutical molecules, Appl. Catal. B-Environ. 255 (2019), 117758.
[234] Z. Zhang, R. Ji, Q. Sun, J. He, D. Chen, N. Li, H. Li, A. Marcomini, Q. Xu, J. Lu, Enhanced photocatalytic degradation of 2-chlorophenol over Z-scheme heterojunction of CdS-decorated oxygen-doped g-C3N4 under visible-light, Appl. Catal. B-Environ. 324 (2023), 122276.
[235] F. Zhao, Y. Liu, S.B. Hammouda, B. Doshi, N. Guijarro, X. Min, C.-J. Tang, M. Sillanpää, K. Sivula, S. Wang, MIL-101(Fe)/g-C3N4 for enhanced visible-light-driven photocatalysis toward simultaneous reduction of Cr(VI) and oxidation of bisphenol A in aqueous media, Appl. Catal. B-Environ. 272 (2020), 119033.
[236] Y. Liu, J. Tian, L. Wei, Q. Wang, C. Wang, Z. Xing, X. Li, W. Yang, C. Yang, Modified g-C3N4/TiO2/CdS ternary heterojunction nanocomposite as highly visible light active photocatalyst originated from CdS as the electron source of TiO2 to accelerate Z-type heterojunction, Sep. Purif. Technol. 257 (2021), 117976.
[237] J. Low, J. Yu, M. Jaroniec, S. Wageh, A.A. Al-Ghamdi, Heterojunction Photocatalysts, Adv. Mater. 29 (2017) 1601694.
[238] C. Liu, X. Cui, Y.H. Li, Q. Duan, A hybrid hollow spheres Cu2O@TiO2-g-ZnTAPc with spatially separated structure as an efficient and energy-saving day-night photocatalyst for Cr(VI) reduction and organic pollutants removal, Chem. Eng. J. 399 (2020), 125807.
[239] M. Lin, H. Chen, Z. Zhang, X. Wang, Engineering interface structures for heterojunction photocatalysts, Phys. Chem. Chem. Phys. 25 (2023) 4388–4407.
[240] L. Xie, T. Du, J. Wang, Y. Ma, Y. Ni, Z. Liu, L. Zhang, C. Yang, J. Wang, Recent advances on heterojunction-based photocatalysts for the degradation of persistent organic pollutants, Chem. Eng. J. 426 (2021), 130617.
[241] M. Guo, Z. Xing, T. Zhao, Z. Li, S. Yang, W. Zhou, WS2 quantum dots/MoS2@WO3-x core-shell hierarchical dual Z-scheme tandem heterojunctions with wide-spectrum response and enhanced photocatalytic performance, Appl. Catal. B-Environ. 257 (2019), 117913.
[242] Y. Zhou, C. Zhang, D. Huang, W. Wang, Y. Zhai, Q. Liang, Y. Yang, S. Tian, H. Luo, D. Qin, Structure defined 2D Mo2C/2Dg-C3N4 Van der Waals heterojunction: Oriented charge flow in-plane and separation within the interface to collectively promote photocatalytic degradation of pharmaceutical and personal care products, Appl. Catal. B-Environ. 301 (2022), 120749.
[243] X. Chen, W.-g Pan, R.-t Guo, X. Hu, Z.-x Bi, J. Wang, Recent progress on van der Waals heterojunctions applied in photocatalysis, J. Mater. Chem. A 10 (2022) 7604–7625.
[244] J. Li, X. Li, X. Chen, Z. Yin, Y. Li, X. Jiang, In situ construction of yolk-shell zinc ferrite with carbon and nitrogen co-doping for highly efficient solar light harvesting and improved catalytic performance, J. Colloid Interface Sci. 554 (2019) 91–102.
[245] F. Guo, Z. Chen, X. Huang, L. Cao, X. Cheng, W. Shi, L. Chen, Cu3P nanoparticles decorated hollow tubular carbon nitride as a superior photocatalyst for photodegradation of tetracycline under visible light, Sep. Purif. Technol. 275 (2021), 119223.
[246] F. Hasanvandian, A. Shokri, M. Moradi, B. Kakavandi, S. Rahman Setayesh, Encapsulation of spinel CuCo2O4 hollow sphere in V2O5-decorated graphitic carbon nitride as high-efficiency double Z-type nanocomposite for levofloxacin photodegradation, J. Hazard. Mater. 423 (2022), 127090.

[247] M.S. Abdel-Wahed, A.S. El-Kalliny, M.I. Badawy, M.S. Attia, T.A. Gad-Allah, Core double-shell MnFe2O4@rGO@TiO2 superparamagnetic photocatalyst for wastewater treatment under solar light, Chem. Eng. J. 382 (2020), 122936.
[248] H. Fu, R. Wang, Q. Xu, M. Laipan, C. Tang, W. Zhang, L. Ling, Facile construction of Fe/Pd-doped graphite carbon nitride for effective removal of doxorubicin: performance, mechanism and degradation pathways, Appl. Catal. B-Environ. 299 (2021), 120686.
[249] S. Huang, B. Hu, S. Zhao, S. Zhang, M. Wang, Q. Jia, L. He, Z. Zhang, M. Du, Multiple catalytic sites of Fe-Nx and Fe-N-C single atoms embedded N-doped carbon heterostructures for high-efficiency removal of malachite green, Chem. Eng. J. 430 (2022), 132933.
[250] H. Yang, W. Wang, X. Wu, M.S. Siddique, Z. Su, M. Liu, W. Yu, Reducing ROS generation and accelerating the photocatalytic degradation rate of PPCPs at neutral pH by doping Fe-N-C to g-C3N4, Appl. Catal. B-Environ. 301 (2022), 120790.
[251] L. Ren, L. Tong, X. Yi, W. Zhou, D. Wang, L. Liu, J. Ye, Ultrathin graphene encapsulated Cu nanoparticles: A highly stable and efficient catalyst for photocatalytic H2 evolution and degradation of isopropanol, Chem. Eng. J. 390 (2020), 124558.
[252] B. Dai, W. Zhao, W. Wei, J. Cao, G. Yang, S. Li, C. Sun, D.Y.C. Leung, Photocatalytic reduction of CO_2 and degradation of Bisphenol-S by g-C3N4/Cu2O@Cu S-scheme heterojunction: Study on the photocatalytic performance and mechanism insight, Carbon 193 (2022) 272–284.
[253] W. Yang, Y. Wang, Enhanced electron and mass transfer flow-through cell with C3N4-MoS2 supported on three-dimensional graphene photoanode for the removal of antibiotic and antibacterial potencies in ampicillin wastewater, Appl. Catal. B-Environ. 282 (2021), 119574.
[254] Z. Xu, Y. Zhang, F. Wang, Z. Li, W. Gu, Y. Zhang, H. Xie, Co single-atom confined in N-doped hollow carbon sphere with superb stability for rapid degradation of organic pollutants, Chem. Eng. J. 452 (2023), 139229.
[255] F. Li, Z. Lu, T. Li, P. Zhang, C. Hu, Origin of the excellent activity and selectivity of a single-atom copper catalyst with unsaturated Cu-N2 sites via peroxydisulfate activation: Cu(III) as a dominant oxidizing species, Environ. Sci. Technol. 56 (2022) 8765–8775.
[256] M. Yang, Z. Hou, X. Zhang, B. Gao, Y. Li, Y. Shang, Q. Yue, X. Duan, X. Xu, Unveiling the origins of selective oxidation in single-atom catalysis via Co–N4–C intensified radical and nonradical pathways, Environ. Sci. Technol. 56 (2022) 11635–11645.
[257] M. Huang, S. Peng, W. Xiang, C. Wang, X. Wu, J. Mao, T. Zhou, Strong metal-support interaction between carbon nanotubes and Mn-Fe spinel oxide in boosting peroxymonosulfate activation: underneath mechanisms and application, Chem. Eng. J. 429 (2022), 132372.
[258] W. Zhang, M. Li, J. Luo, G. Zhang, L. Lin, F. Sun, M. Li, Z. Dong, X.-Y. Li, Modulating the coordination environment of Co single-atom catalysts through sulphur doping to efficiently enhance peroxymonosulfate activation for degradation of carbamazepine, Chem. Eng. J. 474 (2023), 145377.
[259] Y. Zou, J. Hu, B. Li, L. Lin, Y. Li, F. Liu, X.-Y. Li, Tailoring the coordination environment of cobalt in a single-atom catalyst through phosphorus doping for enhanced activation of peroxymonosulfate and thus efficient degradation of sulfadiazine, Appl. Catal. B-Environ. 312 (2022), 121408.
[260] Y. Yao, C. Wang, X. Yan, H. Zhang, C. Xiao, J. Qi, Z. Zhu, Y. Zhou, X. Sun, X. Duan, J. Li, Rational regulation of Co–N–C coordination for high-efficiency generation of 1O2 toward nearly 100% selective degradation of organic pollutants, Environ. Sci. Technol. 56 (2022) 8833–8843.
[261] Y. Gao, Y. Zhu, T. Li, Z. Chen, Q. Jiang, Z. Zhao, X. Liang, C. Hu, Unraveling the high-activity origin of single-atom iron catalysts for organic pollutant oxidation via peroxymonosulfate activation, Environ. Sci. Technol. 55 (2021) 8318–8328.
[262] Q. Wu, Y. Zhang, H. Liu, H. Liu, J. Tao, M.-H. Cui, Z. Zheng, D. Wen, X. Zhan, FexN produced in pharmaceutical sludge biochar by endogenous Fe and exogenous N doping to enhance peroxymonosulfate activation for levofloxacin degradation, Water Res 224 (2022), 119022.
[263] X. Mi, P. Wang, S. Xu, L. Su, H. Zhong, H. Wang, Y. Li, S. Zhan, Almost 100% peroxymonosulfate conversion to singlet oxygen on single-atom CoN2+2 sites, Angew. Chem. Int. Ed. 60 (2021) 4588–4593.
[264] K. Qian, H. Chen, W. Li, Z. Ao, X. Guan, Single-atom Fe catalyst outperforms its homogeneous counterpart for activating peroxymonosulfate to achieve effective degradation of organic contaminants, Environ. Sci. Technol. 55 (2021).
[265] B. Zhang, X. Li, K. Akiyama, P.A. Bingham, S. Kubuki, Elucidating the mechanistic origin of a spin state-dependent FeNx–C catalyst toward organic contaminant oxidation via peroxymonosulfate activation, Environ. Sci. Technol. 56 (2022) 1321–1330.
[266] N. Li, R. Li, X. Duan, B. Yan, W. Liu, Z. Cheng, G. Chen, La Hou, S. Wang, Correlation of active sites to generated reactive species and degradation routes of organics in peroxymonosulfate activation by co-loaded carbon, Environ. Sci. Technol. 55 (2021) 16163–16174.
[267] Y. Gao, T. Wu, C. Yang, C. Ma, Z. Zhao, Z. Wu, S. Cao, W. Geng, Y. Wang, Y. Yao, Y. Zhang, C. Cheng, Activity trends and mechanisms in peroxymonosulfate-assisted catalytic production of singlet oxygen over atomic metal-N-C catalysts, Angew. Chem. Int. Ed. 60 (2021) 22513–22521.
[268] C. Zhu, Y. Nie, F. Cun, Y. Wang, Z. Tian, F. Liu, Two-step pyrolysis to anchor ultrahigh-density single-atom FeN5 sites on carbon nitride for efficient Fenton-like catalysis near 0 °C, Appl. Catal. B-Environ. 319 (2022), 121900.
[269] H. Yan, C. Lai, S. Liu, D. Wang, X. Zhou, M. Zhang, L. Li, X. Li, F. Xu, J. Nie, Metal-carbon hybrid materials induced persulfate activation: application, mechanism, and tunable reaction pathways, Water Res 234 (2023), 119808.
[270] Y. Wu, X. Chen, Y. Han, D. Yue, X. Cao, Y. Zhao, X. Qian, Highly efficient utilization of nano-Fe(0) embedded in mesoporous carbon for activation of peroxydisulfate, Environ. Sci. Technol. 53 (2019) 9081–9090.
[271] X.-C. Feng, Z.-J. Xiao, H.-T. Shi, B.-Q. Zhou, Y.-M. Wang, H.-Z. Chi, X.-H. Kou, N.-Q. Ren, How nitrogen and sulfur doping modified material structure, transformed oxidation pathways, and improved degradation performance in peroxymonosulfate activation, Environ. Sci. Technol. 56 (2022) 14048–14058.
[272] W. Du, Q. Zhang, Y. Shang, W. Wang, Q. Li, Q. Yue, B. Gao, X. Xu, Sulfate saturated biosorbent-derived Co-S@NC nanoarchitecture as an efficient catalyst for peroxymonosulfate activation, Appl. Catal. B-Environ. 262 (2020), 118302.
[273] Q. Ye, J. Wu, P. Wu, J. Wang, W. Niu, S. Yang, M. Chen, S. Rehman, N. Zhu, Enhancing peroxymonosulfate activation of Fe-Al layered double hydroxide by dissolved organic matter: performance and mechanism, Water Res 185 (2020), 116246.
[274] L. Wu, Z. Sun, Y. Zhen, S. Zhu, C. Yang, J. Lu, Y. Tian, D. Zhong, J. Ma, Oxygen vacancy-induced nonradical degradation of organics: critical trigger of oxygen (O2) in the Fe–Co LDH/peroxymonosulfate system, Environ. Sci. Technol. 55 (2021) 15400–15411.
[275] L. Qin, H. Ye, C. Lai, S. Liu, X. Zhou, F. Qin, D. Ma, B. Long, Y. Sun, L. Tang, M. Yan, W. Chen, W. Chen, L. Xiang, Citrate-regulated synthesis of hydrotalcite-like compounds as peroxymonosulfate activator - investigation of oxygen vacancies and degradation pathways by combining DFT, Appl. Catal. B-Environ. 317 (2022), 121704.
[276] M.-M. Wang, L.-J. Liu, J.-R. Xi, Y. Ding, P.-X. Liu, L. Mao, B.-J. Ni, W.-K. Wang, J. Xu, Lattice doping of Zn boosts oxygen vacancies in Co3O4 Nanocages: improving persulfate activation via forming Surface-Activated complex, Chem. Eng. J. 451 (2023), 138605.
[277] H. Ren, H. Liu, T. Cui, S. Liu, T. Ma, Z. Han, R. Zhou, Boosting the activation of Peroxymonosulfate and the degradation of metronidazole over FeCo2O4 quantum dots anchored on β-FeOOH Nanosheets: inspired from octahedral Co(II) with missing angle, Chem. Eng. J. 431 (2022), 133803.
[278] J. Liang, L. Fu, Activation of peroxymonosulfate (PMS) by Co3O4 quantum dots decorated hierarchical C@Co3O4 for degradation of organic pollutants:kinetics and radical-nonradical cooperation mechanisms, Appl. Surf. Sci. 563 (2021), 150335.
[279] Y. Hu, J. Guo, W. Wang, Y. He, Z. Li, Unveiling different antibiotic degradation mechanisms on dual reaction center catalysts with nitrogen vacancies via peroxymonosulfate activation, Chemosphere 332 (2023), 138788.
[280] J. Jiang, X. Wang, C. Yue, T. Li, M. Li, C. Li, S. Dong, Nitrogen vacancies induce sustainable redox of iron-cobalt bimetals for efficient peroxymonosulfate activation: Dual-path electron transfer, Chem. Eng. J. 427 (2022), 131702.
[281] J. Ye, J. Dai, D. Yang, C. Li, Y. Yan, Y. Wang, Interfacial engineering of vacancy-rich nitrogen-doped FexOy@MoS2 Co-catalytic carbonaceous beads mediated non-radicals for fast catalytic oxidation, J. Hazard. Mater. 421 (2022), 126715.
[282] H. Zhang, C. Zhou, H. Zeng, Z. Shi, H. Wu, L. Deng, Novel sulfur vacancies featured MIL-88A(Fe)@CuS rods activated peroxymonosulfate for coumarin degradation: Different reactive oxygen species generation routes under acidic and alkaline pH, Process. Saf. Environ. Prot. 166 (2022) 11–22.
[283] L. Wu, P. Guo, X. Wang, H. Li, X. Zhang, K. Chen, P. Zhou, The synergy of sulfur vacancies and heterostructure on CoS@FeS nanosheets for boosting the peroxymonosulfate activation, Chem. Eng. J. 446 (2022), 136759.
[284] J. Ye, J. Dai, D. Yang, C. Li, Y. Yan, Y. Wang, 2D/2D confinement graphene-supported bimetallic Sulfides/g-C3N4 composites with abundant sulfur vacancies as highly active catalytic self-cleaning membranes for organic contaminants degradation, Chem. Eng. J. 418 (2021), 129383.
[285] S. Ma, D. Yang, Y. Guan, Y. Yang, Y. Zhu, Y. Zhang, J. Wu, L. Sheng, L. Liu, T. Yao, Maximally exploiting active sites on Yolk@shell nanoreactor: nearly 100% PMS activation efficiency and outstanding performance over full pH range in Fenton-like reaction, Appl. Catal. B-Environ. 316 (2022), 121594.
[286] S. Zhang, H. Gao, X. Xu, R. Cao, H. Yang, X. Xu, J. Li, MOF-derived CoN/N-C@SiO2 yolk-shell nanoreactor with dual active sites for highly efficient catalytic advanced oxidation processes, Chem. Eng. J. 381 (2020), 122670.
[287] S. Pan, X. Guo, X. Lu, R. Li, H. Hu, X. Nie, B. Liu, R. Chen, M. Zhu, S. Hei, X. Zhu, S. Zhang, H. Zhou, Boosting peroxymonosulfate activation by a novel bifunctional core-shell nanoreactor MnFe2O4@HZO for nitrilotris-methylenephosphonic acid removal, Appl. Catal. B-Environ. 330 (2023), 122508.
[288] A.V. Narendra Kumar, W.S. Shin, Yolk-shell Fe2O3@mesoporous hollow carbon sphere hybrid sub-micro reactors for effective degradation of organic contaminants, Chem. Eng. J. 465 (2023), 142922.
[289] X. Yang, X. Xie, S. Li, W. Zhang, X. Zhang, H. Chai, Y. Huang, The POM@MOF hybrid derived hierarchical hollow Mo/Co bimetal oxides nanocages for efficiently activating peroxymonosulfate to degrade levofloxacin, J. Hazard. Mater. 419 (2021), 126360.
[290] Z. Lyu, M. Xu, J. Wang, A. Li, P. François-Xavier, Corvini, Hierarchical nano-vesicles with bimetal-encapsulated for peroxymonosulfate activation: singlet oxygen-dominated oxidation process, Chem. Eng. J. 433 (2022), 133581.
[291] G. Wang, K. Wang, Z. Liu, Y. Feng, S. Yang, Y. Su, X. Qian, P. Jin, J. Wei, Hollow multi-shelled NiO nanoreactor for nanoconfined catalytic degradation of organic pollutants via peroxydisulfate activation, Appl. Catal. B-Environ. 325 (2023), 122359.
[292] P. Li, Y. Lin, S. Zhao, Y. Fu, W. Li, R. Chen, S. Tian, Defect-engineered Co3O4 with porous multishelled hollow architecture enables boosted advanced oxidation processes, Appl. Catal. B-Environ. 298 (2021), 120596.
[293] P. Li, Y. Huang, Q. Huang, R. Chen, J. Li, S. Tian, Cobalt phosphide with porous multishelled hollow structure design realizing promoted ammonia borane

dehydrogenation: Elucidating roles of architectural and electronic effect, Appl. Catal. B-Environ. 313 (2022), 121444.
[294] Q. Zhong, Y. Sun, S. Wu, C. Xu, S. Yang, Y. Liu, D. Sun, B. Yang, Y. Dai, C. Qi, Z. Xu, H. He, S. Li, S. Wang, Uniformed core-shell FeSe2+x@C nanocube superlattices for Fenton-like reaction: Coordinative roles of cation and anion, Appl. Catal. B-Environ. 325 (2023), 122357.
[295] S. Sun, J. Li, H. Ding, B. Zhang, H. Huang, Z. Xu, Y. Tu, D. Chen, X. Duan, Engineered tourmaline/g-C3N4 composites for photocatalytic Fenton-like oxidation: synergy of spontaneous interface polarization and surface iron circulations induced by minerals, Chem. Eng. J. 460 (2023), 141718.
[296] J. Jiang, X. Wang, C. Yue, S. Liu, Y. Lin, T. Xie, S. Dong, Efficient photoactivation of peroxymonosulfate by Z-scheme nitrogen-defect-rich NiCo2O4/g-C3N4 for rapid emerging pollutants degradation, J. Hazard. Mater. 414 (2021), 125528.
[297] W. Zheng, S. You, Y. Yao, L. Jin, Y. Liu, Development of atomic hydrogen-mediated electrocatalytic filtration system for peroxymonosulfate activation towards ultrafast degradation of emerging organic contaminants, Appl. Catal. B-Environ. 298 (2021), 120593.
[298] W. Li, R. Xiao, H. Lin, K. Yang, W. Li, K. He, L.-H. Yang, M. Pu, M. Li, S. Lv, Electro-activation of peroxymonosulfate by a graphene oxide/iron oxide nanoparticle-doped Ti4O7 ceramic membrane: mechanism of singlet oxygen generation in the removal of 1,4-dioxane, J. Hazard. Mater. 424 (2022), 127342.
[299] X.-w Ao, J. Eloranta, C.-H. Huang, D. Santoro, W.-j Sun, Z.-d Lu, C. Li, Peracetic acid-based advanced oxidation processes for decontamination and disinfection of water: a review, Water Res 188 (2021), 116479.
[300] M.F. Gasim, Y. Bao, A.M. Elgarahy, A.I. Osman, Aa.H. Al-Muhtaseb, D.W. Rooney, P.-S. Yap, W.-D. Oh, Peracetic acid activation using heterogeneous catalysts for environmental decontamination: a review, Catal. Commun. 180 (2023), 106702.
[301] J. Xiao, H. Dong, Y. Li, L. Li, D. Chu, S. Xiang, X. Hou, Q. Dong, S. Xiao, Z. Jin, J. Wang, Graphene shell-encapsulated copper-based nanoparticles (G@Cu-NPs) effectively activate peracetic acid for elimination of sulfamethazine in water under neutral condition, J. Hazard. Mater. 441 (2023), 129895.
[302] L. Zhang, J. Chen, Y. Zhang, Z. Yu, R. Ji, X. Zhou, Activation of peracetic acid with cobalt anchored on 2D sandwich-like MXenes (Co@MXenes) for organic contaminant degradation: high efficiency and contribution of acetylperoxyl radicals, Appl. Catal. B-Environ. 297 (2021), 120475.
[303] J. Wu, X. Zheng, Y. Wang, H. Liu, Y. Wu, X. Jin, P. Chen, W. Lv, G. Liu, Activation of peracetic acid via Co3O4 with double-layered hollow structures for the highly efficient removal of sulfonamides: kinetics insights and assessment of practical applications, J. Hazard. Mater. 431 (2022), 128579.
[304] Y. Long, J. Dai, S. Zhao, S. Huang, Z. Zhang, Metal–organic framework-derived magnetic carbon for efficient decontamination of organic pollutants via periodate activation: surface atomic structure and mechanistic considerations, J. Hazard. Mater. 424 (2022), 126786.
[305] D. Guo, Y. Yao, S. You, L. Jin, P. Lu, Y. Liu, Ultrafast degradation of micropollutants in water via electro-periodate activation catalyzed by nanoconfined Fe2O3, Appl. Catal. B-Environ. 309 (2022), 121289.
[306] L. Yang, L. He, Y. Ma, L. Wu, L. Zheng, J. Wang, Y. Chen, Y. Li, Z. Zhang, Periodate-based oxidation focusing on activation, multivariate-controlled performance and mechanisms for water treatment and purification, Sep. Purif. Technol. 289 (2022), 120746.